DOKUZ EYLÜL UNIVERSITY
GRADUATE SCHOOL OF NATURAL AND APPLIED SCIENCES

STRATIGRAPHY, STRUCTURAL FEATURES AND PETROGRAPHY OF THE NEOGENE SEQUENCES IN SOUTH KAVAKLIDERE (MUĞLA)

by
Özlem YILMAZ AKSOY

November, 2020
İZMİR

STRATIGRAPHY, STRUCTURAL FEATURES AND PETROGRAPHY OF THE NEOGENE SEQUENCES IN SOUTH KAVAKLIDERE (MUĞLA)

A Thesis Submitted to the
Graduate School of Natural and Applied Sciences of
Dokuz Eylül University in Partial Fulfillment of the Requirements for the
Degree of Doctor of Philosophy in Geological Engineering, Applied Geology
Program

by
Özlem YILMAZ AKSOY

November, 2020
İZMİR

Ph.D. THESIS EXAMINATION RESULT FORM

We have read the thesis entitled "**STRATIGRAPHY, STRUCTURAL FEATURES AND PETROGRAPHY OF THE NEOGENE SEQUENCES IN SOUTH KAVAKLIDERE (MUĞLA)**" completed by **ÖZLEM YILMAZ AKSOY** under supervision of **PROF.DR. TALİP GÜNGÖR** and we certify that in our opinion it is fully adequate, in scope and in quality, as a thesis for the degree of Doctor of Philosophy.

Prof. Dr. Talip GÜNGÖR

Supervisor

Assist. Prof. Dr. İsmail İŞİNTEK

Thesis Committee Member

Assoc. Prof. Dr. Ufuk MALAYOĞLU

Thesis Committee Member

Prof. Dr. Süha ÖZDEN

Examining Committee Member

Prof. Dr. Mehmet Serkan AKKİRAZ

Examining Committee Member

Prof. Dr. Özgür ÖZÇELİK

Director

Graduate School of Natural and Applied Sciences

ACKNOWLEDGEMENT

Before all, I would like to express my most sincere thanks to my advisor, Talip Güngör, who supported and guided me with endless patience and devotion throughout this long process. He provided me precious scientific knowledge and special help in how to proceed on this way. I am very grateful for his valuable efforts during my entire stage of Ph.D.

I am highly indebted to İsmail İşintek for imparting his knowledge and expertise on travertine type carbonates. He provided me unique scientific guidance in every step of studying the textural features of the travertines. His precision in scientific research will be an example for me throughout my academic career.

I also would like to express my special gratitude to Burhan Erdoğan, who is the advisor of my master thesis, for inspiring me and leading my academic career.

I should also not forget the mention the memory of Orhan Kaya. He was a very special scientist and an instructor whom I owe my inspiration in sedimentology. I remember him with respect and express my gratitude.

I would like to thank my dear friend Hakan Elçi, who encouraged and guided me whener I stumbled. His friendship is always very precious. I also would like to thank Serhan Lider, who encouraged me to pursue an academic career with his valuable advice when I was an undergraduate student.

I am grateful to Mine Sezgül Kayseri Özer for her personal and professional support for my thesis. Her contribution to my thesis with palynology is valuable. She also willingly helped me with field studies and especially the interpretation of the stable isotope results. I am also very grateful to Funda Akgün for very constructive discussions about the palynology and stratigraphy of the study area. I would like to thank Serdar Mayda and Tanju Kaya for their contribution to mammalian fauna in the study area. I should also thank Atike Nazik for ostracod analysis and Yeşim

Büyükmeriç for gastropod analysis. I would also thank to Mete Çetinkaplan for his help during my microscope studies.

This study was funded by the Dokuz Eylül University, Department of Scientific Research Projects (Project Number: 2014 KB FEN 026), I would like to thank for their support.

I am very grateful for a number of people in Muğla Sıtkı Koçman University for supporting me in different ways during my doctoral studies. Therefore, I would like to thank Murat Gül, Sena Akçer Ön, Bora Ön, Esra Çetin, and Mehmet Çam for sharing their knowledge and valuable support. Besides, I would like to special thank Ali Arslan Kaya for giving me the opportunity to begin my Ph.D. He is a visionary and inspiring person.

Last but not least, I would like to express my deepest gratitude to my family for their help and support. They always patiently share all my good and bad times. I would like to thanks my father, Hüseyin, for always believing and trusting me. I am grateful to my mother, Meliha, she always makes me feel that there is nothing more important than me. I am also grateful to my brothers, Emre and Metehan, for always being there for me as a friend. I would like to special thanks to my husband, Murat Ersen Aksoy, for his help while preparing this thesis. Without his support, I would never have handled some situations. He always provides me different perspectives with his passion for science.

Özlem YILMAZ AKSOY

"…The result, therefore, of our present enquiry is, that we find ***no vestige of a beginning, no prospect of an end****."*

James Hutton

Theory of the Earth, 1788

STRATIGRAPHY, STRUCTURAL FEATURES AND PETROGRAPHY OF THE NEOGENE SEQUENCES IN SOUTH KAVAKLIDERE (MUĞLA)

ABSTRACT

The Mio-Pleistocene sequence of the Göktepe area (Southern Aegean, Turkey) is composed of the Turgut, Sekköy, Yatağan, Milet, and Sungur formations and unconformably overlays the tectonic boundary of the Menderes Massif and Lycian Nappes. The fossil evidence of the Turgut Formation indicates a warm, subtropical brackish/freshwater lacustrine environment in the late early to early middle Miocene. However, the fossil record of the middle-late middle Miocene presents a freshwater lacustrine environment under warm temperate climatic conditions. Radiometric data of the travertine type lacustrine carbonates located upper part of the Milet Formation show that the Göktepe travertines were deposited until ~364 ka (Middle Pleistocene).

The carbonate fabrics, facies and components of the Göktepe travertines are classified as micrite fabrics and facies, spar fabrics and facies, zoned algal fabrics and facies, shrub fabrics and facies, biological components, and pores. These facies indicate a littoral and sublittoral shallow lake environment for the Göktepe travertines. The vertical facies changes are related to cyanobacteria variations because of water thickness and chemistry. The $\delta^{18}O$ values of the travertines range between -11.34 ‰ and -7.93 ‰ PDB and $\delta^{13}C$ values change between -4.64 ‰ and 3.65 ‰ PDB. The upwardly decreasing carbon values and increasing on oxygen values may indicate that the climatic conditions are changed from cold-dry conditions to wet-warmer conditions The oscillations in stable isotope values, limited fossil content, deficiency in the variety of fauna and flora, the existence of paleosol levels indicate frequently fluctuation of the lake water due to climatic changes (temperature and rainfall). Our microfacies and stable isotope results contribute to further evidence for the climatic conditions of the MIS 11 interglacial periods for the Aegean region.

Keywords: Göktepe, Mio-Pleistocene, lacustrine environment, travertine, microfacies, stable isotope, paleoclimate

KAVAKLIDERE (MUĞLA) GÜNEYİ NEOJEN İSTİFLERİNİN STRATİGRAFİSİ, YAPISAL ÖZELLİKLERİ VE PETROGRAFİSİ

ÖZ

Göktepe bölgesindeki Miyo-Pleyistosen istifi (Güney Ege, Türkiye) Turgut, Sekköy, Yatağan, Milet ve Sungur formasyonlarından oluşur ve bu istif Menderes Masifi ile Likya Naplarının tektonik dokanağını uyumsuz olarak üstlemektedir. Turgut Formasyonu'nda bulunan fosiller, geç erken - erken orta Miyosen'de ılık, yarı tropical acısu/tatlısu ortamını gösterir. Ancak, orta-geç orta Miyosen linyit çökellerinin fosil içeriği ise ılık, ılıman iklim koşulları altındaki bir tatlı su ortamını işaret etmektedir. Milet Formasyonu'nun en üst seviyesini oluşturan traverten tipi gölsel karbonatların radyometrik verileri, traverten çökeliminin yaklaşık 346 bin yıla (Orta Pleyistosen) kadar devam ettiğini gösterir.

Göktepe travertenlerinin karbonat yapıları, fasiyesleri ve bileşenleri, mikrit yapılar ve fasiyesleri, spar yapılar ve fasiyesleri, çalı yapıları ve fasiyesleri, biyolojik bileşenler ve gözenekler olarak sınıflandırılmıştır. Bu, yapı, fasiyes ve bileşenler çok sığ, sığ göl kenarı ve bağıl olarak derin sığ göl ortamını göstermektedir. Fasiyeslerin düşey yöndeki değişimleri su kalınlığı ve kimyası nedeniyle siyanobakteri miktarı ve çeşitliliği ile ilişkilidir. Travertenlerin $\delta^{18}O$ değerleri binde -11,34 ve -7,93 PDB arasında değişirken, $\delta^{13}C$ değerleri binde -4,64 ve 3,65 PDB arasında değişmektedir. İstifin üst seviyelerinde doğru, azalan karbon ve artan oksijen değerleri, iklim koşullarının soğuk-kurak koşullardan, ılık nemli koşullara doğru değiştiğine işaret etmektedir. Duraylı izotop değerlerindeki salınımlar, sınırlı fosil içeriği, fauna ve floranın fakirliği, paleosol seviyelerinin varlığı iklimsel değişiklikleri (sıcaklık ve yağış) nedeniyle göl su seviyesinin sık sık değiştiğini gösterir. Çalışma, mikrofasiyes analizi ve duraylı izotop değerleri ile MIS 11 döneminde Ege Bölgesi iklim koşulları için yeni kanıtlar sunmaktadır.

Anahtar Kelimeler: Göktepe, Miyo-Pleyistosen, gölsel ortam, traverten, mikrofasiyes, duraylı izotop, paleoiklim

CONTENTS

Page

Ph.D THESIS EXAMINATION RESULT FORM ii
ACKNOWLEDGEMENT iii
ABSTRACT vi
ÖZ vii
LIST OF FIGURES xi
LIST OF TABLES xviii

CHAPTER 1 - INTRODUCTION 1

1.1 Methodology 5
1.1.1 Paleontological Analysis 5
1.1.2 Microfacies Analysis 6
1.1.3 U-Series Dating 8
1.1.4 Stable Isotope Analysis 9

CHAPTER 2 - STRATIGRAPHY 11

2.1 Menderes Massif 11
2.2 Mio-Pleistocene Basin-Fill Succession 13
2.2.1 Turgut Formation 14
2.2.1.1 Gastropods 15
2.2.1.2 Mammalian records 15
2.2.1.3 Sungur Palynomorph Assemblage 17
2.2.1.4 Ostracods 20
2.2.1.5 Mammalian Records 20
2.2.1.6 Çamoluk palynomorph assemblage 21
2.2.2 Sekköy Formation 22
2.2.3 Yatağan Formation 23
2.2.4 Milet Formation 24
2.2.4.1 U Series Dating 25
2.2.4.2 Göktepe Fault 28
2.2.5 Sungur Formation 30

2.3 Paleoenvironmental Evolution 31
2.3.1 Late Early Miocene - Early Middle Miocene (MN 4-5) 31
2.3.2 Middle-Late Middle Miocene (MN 6-7) 33
2.3.3 Middle Pleistocene 34

CHAPTER 3 - MICROFACIES OF THE GÖKTEPE TRAVERTINES 35

3.1 Introduction 35
3.2 Carbonate Fabrics, Facies, and Components of the Göktepe Travertines 37
3.2.1 Micrite Fabrics and Facies 38
3.2.1.1 Clotted Micrite Fabrics and Facies (CMF) 38
3.2.1.2 Microbial Micrite Fabrics and Facies (MMF) 40
3.2.1.3 Encrusted Micrite Fabrics (em) 41
3.2.1.4 Intraclast (i) 42
3.2.2 Spar Fabrics and Facies 42
3.2.2.1 Algal Microspar-Spar Clump Fabrics and Facies (AMCF) 43
3.2.2.2 Encrusted Spar Fabrics (es) and Facies 44
3.2.2.3 Spar Carbonate Fragments and Fragmented Carbonate Facies (FCF) … 46
3.2.2.4 Intra-Frame Spar Fabrics 46
3.2.2.5 Inter Shrub Spar 48
3.2.3 Zoned Algal Fabric and Facies 48
3.2.3.1 Zoned Algal Clump Fabrics and Facies (ZAC) 48
3.2.3.2 Zoned Encrusted Algal Fabrics (ZEA) 49
3.2.4 Shrub Fabrics and Facies 49
3.2.4.1 Micritic quill-feather shrub fabrics and facies (MQFSF) 49
3.2.4.2 Macrophytes Spar Quill Shrub Fabrics and Facies (MCSQSF) 50
3.2.5 Biological Components 51
3.2.6 Cavities and Pores 53
3.2.6.1 Fenestral Pores 53
3.2.6.2 Gas Pores 54
3.2.6.3 Intra Organism Pores 54
3.2.6.4 Intra-Frame Pores 54

3.3 Paleoenvironmental Interpretation 56

CHAPTER 4 - STRATIGRAPHY OF THE GÖKTEPE TRAVERTINES.....59

4.1 Introduction.....59
4.2 Yarılgan Hill Section.....59
4.3 Kepez Hill Section.....62
4.4 Paleoenvironmental Conditions 71
4.5 Lacustrine Depositional Model.....72

CHAPTER 5 -STABLE ISOTOPE ANALYSIS OF THE GÖKTEPE TRAVERTINES 74

5.1 Introduction.....74
5.2 Stable Isotope Values of Göktepe Travertines.....75
5.3 Relation between the Stable Carbon and Oxygen Isotopes.....78
5.4 Correlation between the Stable Isotope Values and Microfacies of the Göktepe Travertines 80
5.4.1 The Yarılgan Hill Section 81
5.4.2 The Kepez Hill Section.....82

CHAPTER 6 - CONCLUSION 85

REFERENCES 89

APPENDICES.....102

LIST OF FIGURES

Page

Figure 1.1 a) Map showing the current geographical position of the Kale-Tavas (KTB), Yatağan (YB), Ören (ÖB), Bozdoğan (BB), and Karacasu (KB) basins. Faults are imported from Okay (2001), Seyitoğlu et al. (2004), and Ocakoğlu et al. (2014)..... 2

Figure 1.2 Stratigraphy and correlation chart of the Yatağan and Kale-Tavas basins in previous and herewith studies 3

Figure 1.3 a. View from the Kepez Hill and Yarılgan Hill where Göktepe travertines were sampled in, b. the birds-eye view of the travertine quarry at the Kepez Hill, c. the close-up view of the area shown with a black arrow in b..... 7

Figure 1.4 The sketch of the measuring reference levels, b. microscopic studies, c. an example of panoramic microscope images (the height of the images is 7 cm) 8

Figure 2.1 Geological map of the Göktepe area.....11

Figure 2.2 Stratigraphic section of the Göktepe area (modified after Atalay, 1980 and Hakyemez, 1989). Mio-Pleistocene sedimentary sequence covers the tectonic boundary of the Menderes Massif and Lycian Nappes along an angular unconformity.....12

Figure 2.3 View from the metamorphic rocks of the Menderes Massif. a) Marble and micashist alternation of the Göktepe Formation. b) White marbles c) Rudist fossils (arrows) in the Mesozoic marbles of the Menderes Massif 13

Figure 2.4 Field views of the Turgut Formation (640920 E, 4146200 N). a) Field photographs showing gray beige colored Turgut Formation. The formation is composed of mudstone, sandstone, and conglomerate (including max. pebble-sized grains) alternation. b) This photo shows the cross-bedding structures in the thickly bedded sandstones 14

Figure 2.5 The lower part of the Turgut Formation exposes in a narrow zone (0636632 E, 4145695 N). a) The fossil location on the Göktepe-Sungur road. b) Cross-section that gives detailed stratigraphy (i. yellowish, thin laminated, calcareus claystone, mudstone; ii. calcareus claystone; iii. green, fractured claystone with fractured gastropod shells and branches, and thin laminated

brownish mudstone at lower levels; iv. yellowish-gray mudstone; v. white claystone, siltstone; and vi. greenish-gray, weakly bounded sandstone. c) Bivalve and gastropod shells in claystone levels. d) SEM photos of gastropods. e) Left lower m1 of *Brachypotherium brachypus*, scale: 2 cm. f) Palynological samples (1. Schizaeceae, 2. Polypodiaceae, 3. *Cathaya*, 4. *Cedrus*, 5. *Pinus diploxylon* type, 6. and 7. *Calamus*, 8. *Engelhardia*, 9. *Carya*, 10. Adoxaceae-*Viburnum*, 11. *Fagus*).....16

Figure 2.6 a) Field view of the coal-bearing levels of the Turgut Formation (0641305 E, 4147993 N) (Personal archive, 2015), b) Type section of the upper levels of the Turgut Formation. c) Compiled measured section of the longwall face in the tunnel and drilling logs of the coal-bearing layers of the Turgut Formation. d) Ostracod images (1.*Heterocypris formalis* (Mandelstam), 1a. External view of the left valve, 1b. External view of carapace, 1c. Dorsal view of carapace. 2. *Heterocypris* ex gr. *gregaria* (Skoksberg), external view of the right valve. 3. Stereomicroscope image of ostracod assemblage. 4. *Heterocypris salina* (Brady) 4a and 4c. Internal view of the right valve, 4b. External view of the right valve. e) Fossil mammal teeth (1, right lower m2 of *Gomphotherium angustidens*; 2. Right lower m2 of *Megalocherus homon*gus; scale: 2 cm). f) Palynomorph assemblages (1. *Cathaya*, 2. *Cedrus*, 3. *Pinus diploxylon* type, 4. Ephedraceae, 5. *Carya*, 6. *Alnus*, 7. *Tilia*, 8. Asteraceae-Asteroideae type, 9. Chenopodiaceae).....19

Figure 2.7 Field photographs shows the different lithologies of Yatağan Formation (0641170 E, 4143241 N). a) View of the fine-grained levels of the formation including fluvial deposits that consist of silt, sand, clay, and marl alternations (outcrop height is approx. 11m). b) photograph shows the orange colored conglomerate levels of the formation.....23

Figure 2.8 Field photographs of the Milet Formation (Kepez Hill). a. Field view from Kepez Hill to Göktepe village. b. and c. Travertine type lacustrine carbonates of the Milet Formation. Triangles show the sample locations for U series dating (samples 7 and 8 were taken from the benches at lower levels) 24

Figure 2.9 Photograph and drawing to show the northern branch of the 2-km-long, NW-SE trending Göktepe Fault. The drag of limestone beds along the fault zone indicates a normal sense of movement. This normal fault put early Miocene - Pleistocene sedimentary units up against a metamorphic basement that is composed of marble and mica-schist 29
Figure 2.10 Asymmetry in the basin fill indicates that the Göktepe Fault was a growth fault. The formations in the hangingwall are several times thicker than those in the footwall.....30
Figure 2.11 Field views of the Sungur Formation. a. The formation has the orange color and horizontal beds, b. The formation is composed of poorly sorted conglomerate including angular grains of Menderes metamorphics in a sandy matrix 31
Figure 2.12 The map showing the extension of the early Miocene Sea (redrawn and modified after De Graciansky, 1972) 33
Figure 3.1 The microscope images of clotted micrite facies under plane-polarized light (PPL). a.and b. clotted micrite fabric and facies from sample 77 and 88, respectively c. clotted clumps in a microspar-spar matrix from sample 75, d. clotted microspar from sample 75, (c: clotted micrite fabrics, s: secondary spar fabrics that precipitated in the pores between clotted micrites, p: empty pore. cc: clotted clumps, and ms: microspar size clotted micrite fabrics) 39
Figure 3.2 The microscope images of very dark-colored, massive microbial micrite facies (yellow arrows) under PPL. a. and c. the layered microbial micrite facies from samples 87 and 58, respectively, b. the microbial micrite between the spar carbonates sample 65, d. very dark microbial micrite fabrics from sample 124.....40
Figure 3.3. The microscopic images of encrusted micrite fabrics (yellow arrows) that surround the reed-like macrophytes under PPL. The images from sample: a. 113, b. 89.2, c.122-c, and d. 137.....41
Figure 3.4 The microscopic images of intraclasts (yellow arrows) under PPL from thin sections of a. sample 69 and b. sample 92 42

Figure 3.5 The microscopic images of algal microspar clumps (amc,black arrows) and algal spar clumps (ams) from a. sample 180 under cross-polarized light (XPL) b. sample 180 (PPL), c. sample 114 (PPL) and d. sample 128 (PPL). Sometimes the pores between these fabrics are filled by microbial micrite fabric or spar calcite cement secondarily 43
Figure 3.6 The microscopic images of the encrusted spar fabrics (es) (yellow arrows) under PPL from a. sample 159, b. sample 51-2, c. sample 126, and d. closeup view from c (yellow rectangle). c: clotted micrite, s: spar calcite cement.44
Figure 3.7 The microscopic images of macrophyte encrusted spar facies under XPL from sample 132. These fabrics are surrounded with thin black microbial micrite fabrics (mm). The white areas (s) are secondary spar cement between the macrophyte encrusted spar fabrics. The big pores may sometimes remain empty (p) 45
Figure 3.8 The microscopic images of thin macrophyte encrusted spar fabrics (yellow arrows) under XPL from sample 72 (a), sample 175 (b and d), and sample 169 (c) 45
Figure 3.9 The microscopic images of the encrusted microspar-spar fabrics (yellow arrows) under PPL from a. sample 92, and b. sample 66.....46
Figure 3.10 The microscopic images of the intra-frame spar fabrics under cross-polarized light (XPL) a. clotted micrite intra-frame spar fabrics from sample 56, b. algal mikrospar clump intra-frame spar fabrics from sample 61, c. and d. encrusted macrophytes intra-frame spar from sample 132, and sample 103, respectively (s: spar calcite cement, p: empty pore) 47
Figure 3.11 The microscopic images of the zoned algal clump fabrics (black arrows) under PPL from sample 80-1.....48
Figure 3.12 The microscopic images of the zoned encrusted algal fabrics (yellow arrows) under PPL from a. sample 54 and b. sample 116.....49
Figure 3.13 The microscopic images of micritic quill-feather shrubs from sample 80-1(a), sample 119 (b), sample 120-2 (c), and sample 121b (d). The micritic shrubs in figure a and figure b are wider and shorter, while others have thinner and taller dendrits. The white areas (s) are spar calcite crystals that

secondarily precipitated the pores between these dendritic shrubs. Yellow arrows show the inter shrub microspar-spar fabrics 50
Figure 3.14 The microscopic images of macrophyte spar quill-feather shrubs a. thin section view of the sample 119 (PPL) and b. sample 61 (XPL).....51
Figure 3.15 The microscopic image of gastropods under plane-polarized light from a.sample 126, b. sample 157, and c.sample 96.....51
Figure 3.16 The microscopic image of ostracods under XPL from a. sample 126, b. sample 135 and c. sample 154.....52
Figure 3.17 The microscopic image of charophytes under PPL from a. sample 62-1, b. sample 51-1, and c. sample 66.....52
Figure 3.18 The microscopic image of macrophytes under PPL from a. sample 169 and b. sample 175 53
Figure 3.19 The undefining macrophytes from sample 197 under XPL 53
Figure 3.20 a. The view from the alternations of porous-non-porous laminas and b. reed-like tubular plants (yellow arrows) 54
Figure 3.21 The microscopic images of pores. a. fenestral pores from sample 33 (PPL), b. Gas pores from sample 117 (PPL), c. inner pores of the gastropods from sample 90 and 118 (XPL), respectively 55
Figure 3.22 The microscopic images of intra frame pores (yellow arrows). a. clotted micrite intra frame pores from sample 77 (PPL), b. algal spar clump intra frame pores from sample 61 (XPL) c. intra frame pores of shrub fabrics from sample 121 (PPL), and d. macrophyte intra-frame pores from sample 132 (XPL) 56
Figure 3.23 The examples of panoramic microscope images under plane-polarized light from a) sample 130, b. sample 93-2, and c. sample 187. CMF: Clotted Micrite Facies, MMF: Microbial Micrite Facies, ZEA: Zoned Encrusted Algal Fabrics, TMC-ES: Thin Macrophyte Encrusted Spar Quill Shrub Facies, AMCF: Algal Microspar Clump Facies. 57
Figure 4.1 a. The measured section of the Yarılgan Hill, b. the view of the Yarılgan Hill and landslides, c. the fractures on the bottom have related the landslides and are seen several parts of the hill. d. examples of beige, pinkish and

brown (from left to right) levels of the sequence shown in the measured section (a) (CM: Clotted Micrite, MM: Microbial Micrite).....60
Figure 4.2 The panoramic microscope images under XPL. The images show the clotted micrite facies and microbial micrite facies with geopetal structures (yellow arrows) and gastropods (gs) from a. sample 191 and b. sample 213.....61
Figure 4.3 The bird-eye view from the 8 benches of the travertine quarry on the Kepez Hill 62
Figure 4.4 The section shows the benches, sample locations and travertines of different colors and textures. Facies, fabrics and the components in related levels of the travertine sequence were also given in columnar section (CM: Clotted Micrite, MM: Microbial Micrite, MC: macrophytes, SQS: Spar Quill Shrub, MQFS: Micritic Quill Feather Shrub, ASC: Algal Spar Clump, AMC: Algal Microspar Clump, FCF: Fragmented Carbonate Facies, ZEA: Zoned Encrusted Algal Fabrics, ZAC: Zoned Algal Clump.....63
Figure 4.5 The view from the first bench sequence of the quarry and sample locations. The bench thickness is 4.20 m. 64
Figure 4.6 The view of the second bench sequence of the quarry. There are two paleosol levels (black arrows) are seen in the bench. The thickness is 6 m. 65
Figure 4.7 The view of the third bench of the quarry and sample locations, paleosol levels (black arrows). The bench thickness is 8 m. 66
Figure 4.8 a. Views from the waste area, b. shows the suitable surfaces (right) that we used for sampling.....67
Figure 4.9 a. The general view from the benchs of 5, 6, and 7, b. closer view from the bench-5 c. closer view from the bench-6 68
Figure 4.10 View from the seventh bench sequence 69
Figure 4.11 View of the eighth bench sequence and sample locations (74-91).....70
Figure 4.12 View from the eastern bench of the Kepez Hill travertine quarry. This bench is at least 15 m in thicknes 70
Figure 4.13 The lacustrine environmental model for the depositon of the travertine sequence (CMF: Clotted Micrite Facies, MMF: Microbial Micrite Facies, AMC: Algal Microspar Clump Facies, MCSQSF: Macrophytes Spar Quill

Shrub Facies, MQFSF: Micritic Quill Feather Shrub Facies, ZAC: Zoned Algal Facies 73
Figure 5.1 The diagram shows the stable isotopes values ($\delta^{18}O/\delta^{13}C$) of the lacustrine carbonate on the Yarılgan Hill section. The number on the blue line with a red circle indicate the sample numbers 76
Figure 5.2 The diagram shows the stable isotopes values ($\delta^{18}O/\delta^{13}C$) of the Kepez Hill section. The number on the blue line with a red circle indicate the sample numbers 77
Figure 5.3 The graphics shows the stable carbon and oxygen isotopes of the Yarılgan Hill. There is no specific correlation..... 79
Figure 5.4 The graphics shows the stable carbon and oxygen isotopes. There is a high negative correlation on the stable isotope values 79
Figure 5.5 The correlation between microfacies and stable isotopes changes of the Yarılgan Hill Section 81
Figure 5.6 The correlation between microfacies and stable isotopes changes of the Kepez Hill Section. The yellow areas show shifting range of the values .. 83

LIST OF TABLES

Page

Table 2.1 U series dating results of the Milet Formation.....26
Table 5.1 The average, median, minimum, and maximum values of the stable isotopes of the Göktepe travertines 76

CHAPTER 1
INTRODUCTION

Sedimentary basins that develop after the closure of an ocean have a key role in understanding the spatial and temporal evolution from compressional to extensional tectonics. The basins in southwest Turkey are optimal places for studying post-collision events following the closure of the Neotethys Ocean. The development of sedimentary basins, such as the Kale-Tavas, Yatağan, and Ören basins preserves the evidence of the transition from compression to extension of the regional tectonism (Seyitoğlu et al., 2004, Sözbilir, 2005). These basins in SW Turkey started to develop immediately after the emplacement of the Lycian Nappes over the Menderes Massif (Gürer & Yılmaz, 2002).

The Menderes Massif and the Lycian Nappes are the main tectonic belts of southwest Turkey in the eastern Mediterranean. The Lycian Nappes were emplaced on the Menderes Massif during the Late Cretaceous-Eocene related to the closure of northern Neotethys Ocean (Şengör & Yılmaz, 1981; Collins & Robertson, 1998; Yılmaz et al., 2000; Gürer & Yılmaz, 2002; Alçiçek & ten Veen, 2008; Gürer et al., 2013). The boundary of these tectonic belts is unconformably covered by the Oligo-Miocene sequences deposited in the Kale-Tavas Basin (Akgün & Sözbilir, 2001; Gürer & Yılmaz, 2002; Seyitoğlu et al., 2004; Sözbilir, 2005; Gürer et al., 2013). Subsequently, N-S striking normal faults dissected the Kale-Tavas Basin into the Ören and Yatağan basins, in the early to middle Miocene (Gürer & Yılmaz, 2002) (Figure 1.1).

The study area is located in the west of the Kale-Tavas Basin, in the south of the Bozdoğan Basin and is currently separated by a mountain range from the Yatağan Basin (Figure 1.1).

Most of the previous studies in this area are related to the paleontology, stratigraphy, and/or structural features of the Kale-Tavas, Yatağan and Ören basins (Becker-Platen 1970; Benda 1971; Ünal, 1988; Seyitoğlu & Scott 1991; Yılmaz et al.,

2000; Akgün & Sözbilir, 2001; Gürer & Yılmaz 2002; Sözbilir, 2005, Özcan et al., 2009, Alçiçek, 2010; Gürer et al., 2013; Kayseri-Özer et al., 2014). The stratigraphy of the Yatağan Basin was documented in detail by Becker-Platen (1970), Atalay (1980), and Hakyemez (1989) (Figure 1.2). These studies have not reached a common explanation yet for the stratigraphy and tectonic evolution of the relevant basins.

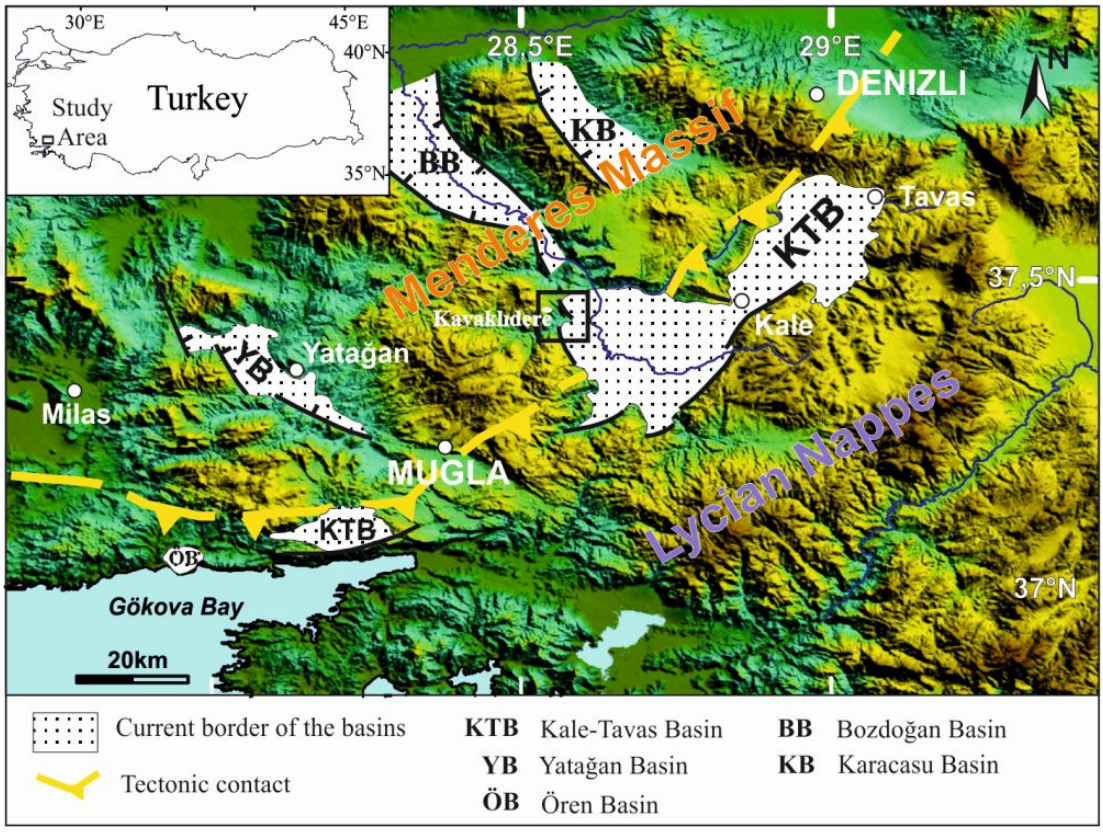


Figure 1.1 a) Map showing the current geographical position of the Kale-Tavas (KTB), Yatağan (YB), Ören (ÖB), Bozdoğan (BB), and Karacasu (KB) basins. Faults are imported from Okay (2001), Seyitoğlu et al. (2004), and Ocakoğlu et al. (2014)

The coal-bearing lacustrine and fluvial deposits in the Yatağan Basin were named as the Muğla Group and divided into the Turgut, Sekköy, Yatağan, and Milet formations from base to top. Due to the rich coal reserves, the Yatağan Basin provides a substantial amount of data to infer the paleoenvironment and paleoclimate during the middle Miocene to Pleistocene (Yılmaz et al, 2020). The Turgut, Eskihisar, Bağyaka, Tınaz, and Bayır sectors are the main coal production locations in the Yatağan Basin. These coal deposits were documented in detail by Nebert (1956), Becker-Platen (1970), Benda (1971), Nakoman (1978), Ünal (1988), Seyitoğlu & Scott (1991),

Nakoman and İnaner (1996), Querol et al. (1999), and Bouchal et al. (2016, 2017). These studies were focused on coal geology, quality or their reserve estimation. Some others are related to the sporomorph contents of the coal layers. Nevertheless, the stratigraphic position of the lignite beds is still matter. Atalay (1980) suggested that the Turgut Formation could be differentiated from the Sekköy Formation with thick coal layers. Bouchal et al. (2016, 2017) confirmed the same stratigraphic position of coal layers described by Atalay (1980). However, Querol et al. (1999) and İnaner et al. (2008) put this main coal seam within the Sekköy Formation (Figure 1.2).

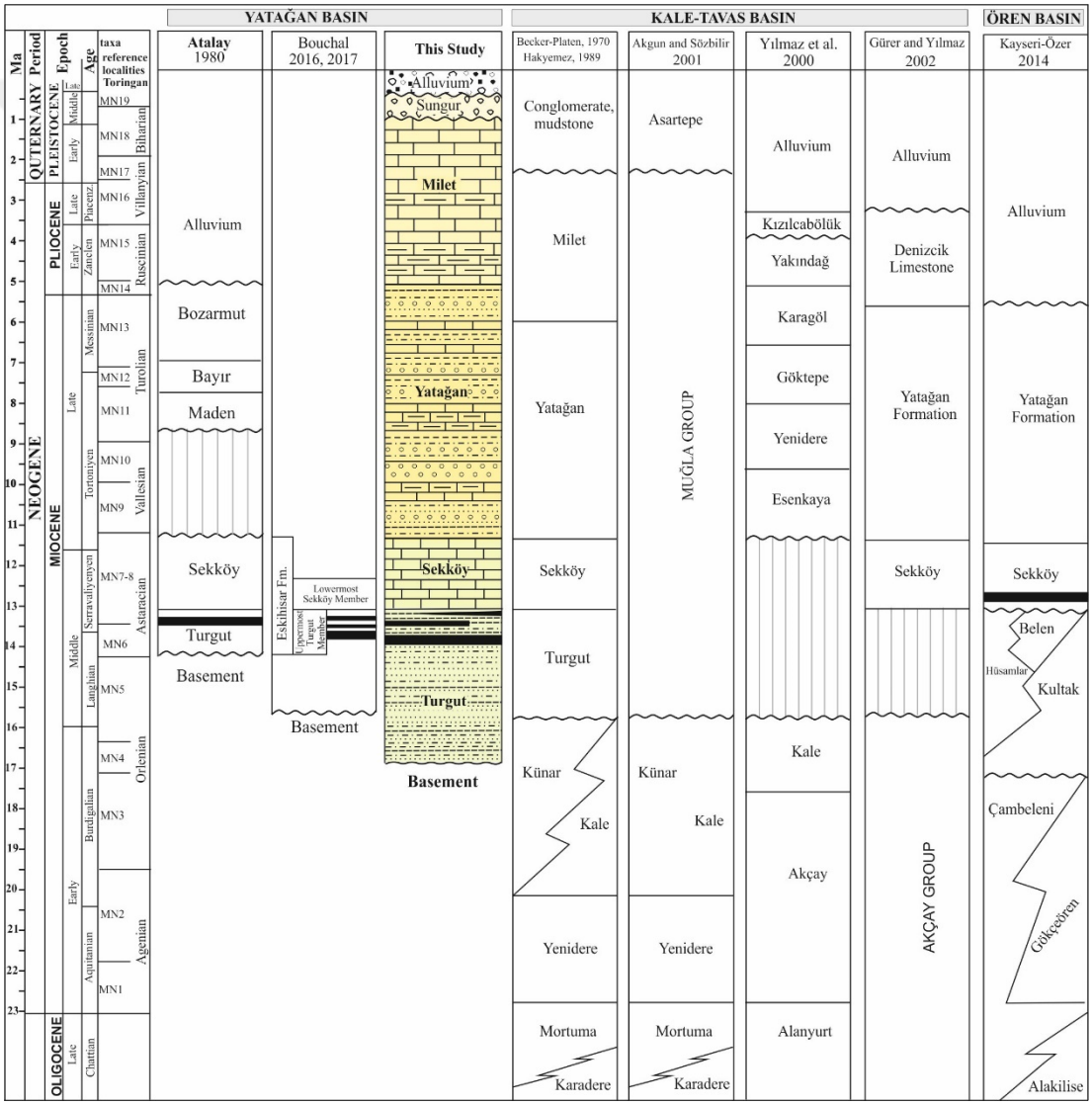


Figure 1.2 Stratigraphy and correlation chart of the Yatağan and Kale-Tavas basins in previous and herewith studies

In this study, we aim to describe the paleontology, stratigraphy, and structural features of the Neogene sequences in the Göktepe area (Figure 1.1). Here, depositional environment and paleoclimate conditions of the area were revealed by new paleontological, petrographical and radiometric data.

Furthermore, a comparative evaluation of the facies changes and stable isotope values of the travertine type lacustrine carbonates of the Milet Formation were also presented in order to assess the paleo-climate and the depositional environment in the Middle Pleistocene.

This thesis consists of five chapters:

Chapter 1 explains the geographical position, general geological setting, and tectonic importance of the study area. This part includes some basic information about the previous studies and gives our main objectives. Finally, this chapter summarizes the structure of the paper and give details about the methodology.

Chapter 2 presents stratigraphy of the Mio-Pleistocene sedimentary sequence of the Göktepe area including our paleontological and radiometric results. In this chapter, the palynomorph assemblages, gastropods, ostracods, and mammalian fossils were described. These fossils allow us to constrain the new age of the Turgut Formation. U series dating for the Milet Formation were provided. Based on our new data, the stratigraphy and tectonic history of the Göktepe area were disscussed.

Chapter 3 focuses on the petrographic and microfacies characteristic of travertine type lacustrine carbonates of the Milet Formation. The carbonate fabrics, facies, and components of the travertines and depositional environment of each facies were described using textural characteristics.

Chapter 4 gives a stratigraphic description of the travertine sequence of the Milet Formation. Field observations, micro and macro features of the travertines were used to describe vertical and horizontal changes of the sequence along the measuring

sections. The depositional environment was interpreted by using these observations and we suggest a lacustrine model for their depositional environment.

Chapter 5 describes stable isotope values from the travertine sequence. The paleoclimate conditions of the Middle Pleistocene were discussed by evaluating these values with microfacies changes.

1.1 Methodology

We studied the basin-fills with measured sections throughout detailed geological mapping at scale of 1/25000. The paleontological analysis was applied to pollen assemblages (palynomorphs), ostracods, gastropods, and mammal bones and teeth collected from the lignite layers and surrounding clay levels of the Turgut Formation. The microfacies analysis, U series dating, and stable isotopes analysis were applied to further investigations on the travertine type lacustrine carbonates of the Milet Formation. The details are given below.

1.1.1 Paleontological Analysis

We measured two sections in the Turgut Formation that are located in Çamoluk and Sungur villages (Figure 2.1). We studied the pollen assemblages of 5 samples from the Sungur location and 38 samples from the lignite seams which were collected from 100 m below the surface in a coal mine and from the drilling cores around Çamoluk village. The pollen analyses were performed by Prof. Dr. Funda Akgün and Assoc. Prof. Dr. Mine Sezgül Kayseri Özer at Dokuz Eylül University (İzmir, Turkey), using standard palynological techniques (e.g., Batten, 1999). The samples were treated with HCl and HF to remove the carbonates and silicate minerals, respectively. The separation of the palynomorphs was carried out centrifugal action, using $ZnCl_2$ as a heavy liquid.

The ostracod analyses were performed by Prof. Dr. Atike Nazik at Çukurova University (Adana, Turkey). Claystone samples of 100 g were disaggregated with 10% H_2O_2 and stored for 24 h. The samples were then washed with pressurized water

through 100- and 150-mm mesh sieves and dried at 50 °C. The ostracod contents of residue materials were examined with a binocular microscope. Scanning Electron Microscope (SEM) images were taken at Muğla Sıtkı Koçman University, on a JSM 7600F Field Emission Scanning Electron Microscope (JEOL, Japan) at an accelerating voltage of 15 kV. The ostracod samples were placed on specimen stubs with double-sided adhesive carbon tape and coated by gold (Emmitech K550, UK).

The gastropods were studied by Prof. Dr. Yeşim Büyükmeriç at Zonguldak Bülent Ecevit University (Turkey). The mammal bones were studied by Prof. Dr. Tümel Tanju Kaya and Assist. Prof. Dr. Serdar Mayda at Ege University, Natural History Museum (EUNHM, Bornova, İzmir, Turkey).

1.1.2 Microfacies Analysis

The uppermost levels of the Milet Formation composed of, nearly horizontal travertine type lacustrine carbonates with a thickness of about 80 m. These travertines create high topographies and nearly flat plateaus surrounding Göktepe village (Figure 1.3). We measured two stratigraphic sections located on the Kepez Hill and the Yarılgan Hill, at the north of the Göktepe village (Figure 1.1, 1.3). A travertine quarry occurs on the Kepez Hill and includes operation steps of open pit that cut the horizontal travertine sequence.

The travertine sequence was systematically sampled (from bottom to top) at approximately every 30 cm of the 80 m thick travertine sequence to determine facies changes both in vertical and horizontal directions. The lower benches at the travertine quarry were densely covered by trees and these benches are far from each other. Therefore, GPS, a tripod, a laser meter, and tape were used to measure in order to determine the vertical distance between the samples and the positions of the benches. The laser meter on a tripod was set at a height of 150 cm on the lower bench and horizontally assigned a reference level in the upper bench. The sample locations were measured according to these reference levels (Figure 1.4a)

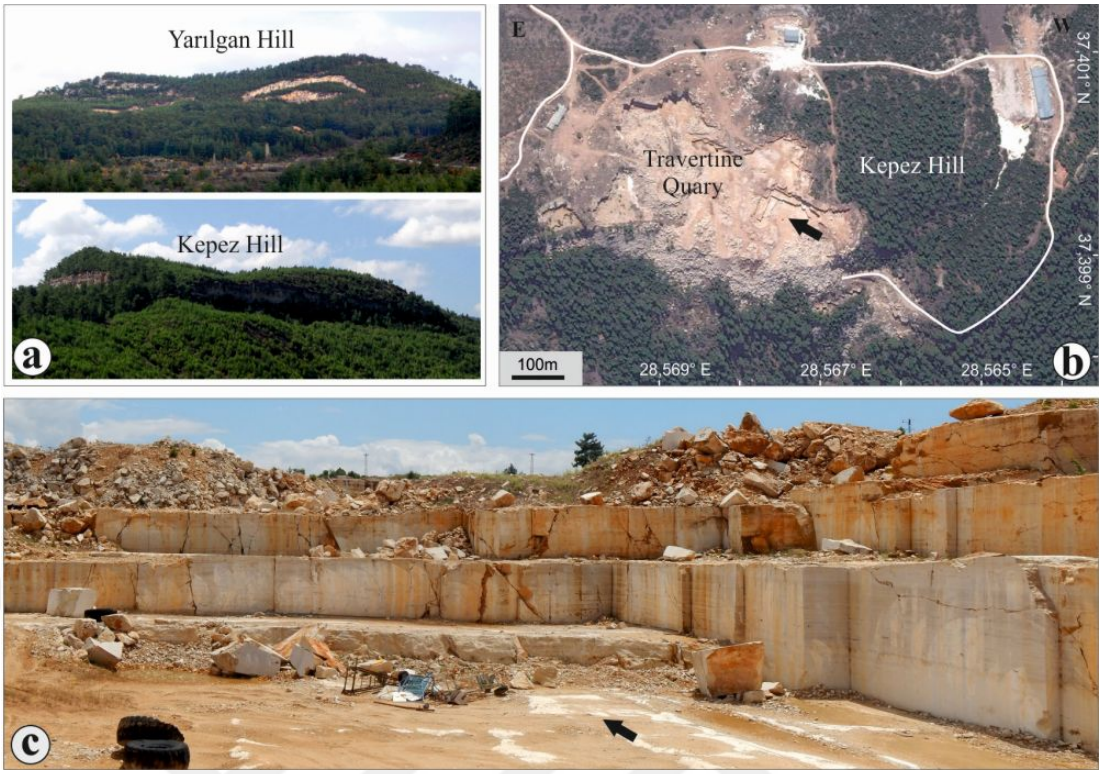


Figure 1.3 a. View from the Kepez Hill and Yarılgan Hill where Göktepe travertines were sampled in, b. the birds-eye view of the travertine quarry at the Kepez Hill, c. the close-up view of the area shown with a black arrow in b (Personal archive, 2014)

146 samples from the Kepez Hill and 30 samples from the Yarılgan Hill were collected and marked the top of each sample. A total of 211 thin sections were prepared by using 6x8 cm sized glasses in Thin Section Laboratory of Dokuz Eylül University. The thin sections were examined wit a Leica, model DM750P research microscope with x1.25, x2.5, x4, and x10 lens sizes. Each thin section was photographed both under cross-polarized (XPL) and parallel-polarized (PPL) light from bottom to top (Figure 1.4b). Then, the microphotographs of thin sections were merged by Photoshop 14 to describe vertical texture changes (Figure 1.4c). The carbonate fabrics and components forming the travertine sequence and vertical microfacies changes were determined. The paleoenvironmental conditions were revealed by evaluating these panoramic images and field observations.

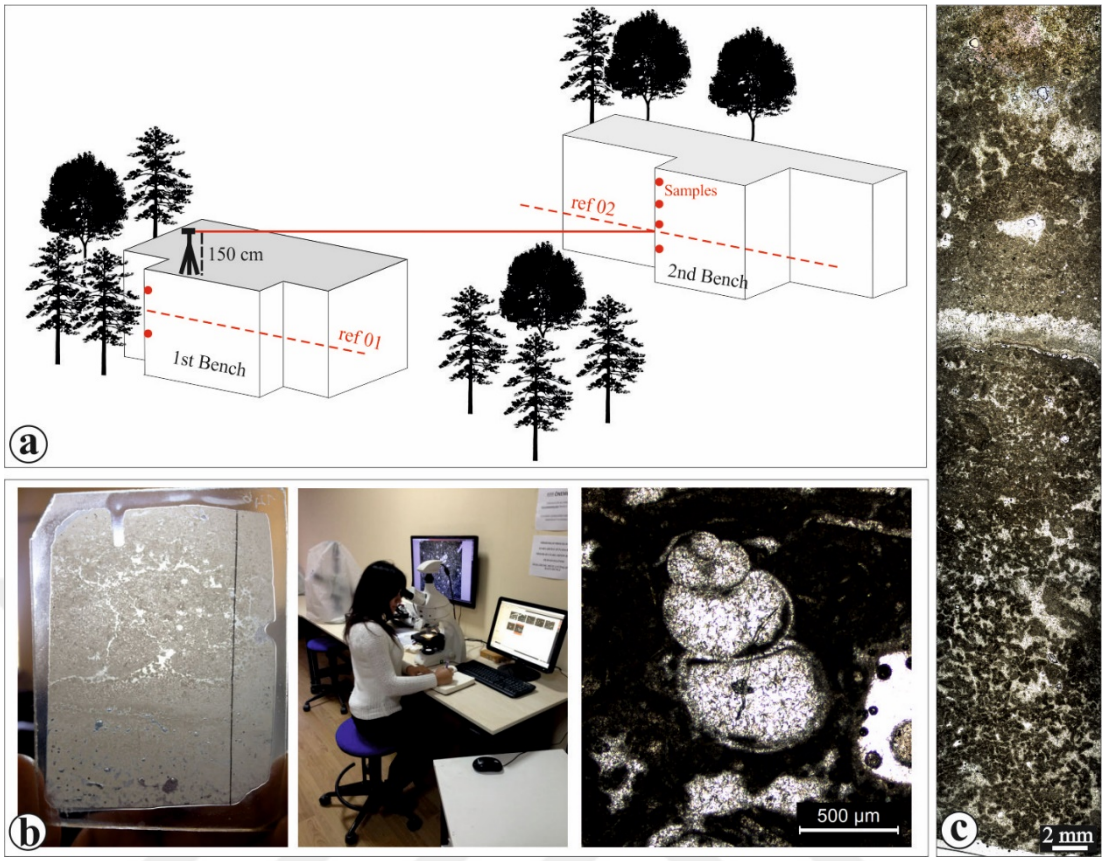


Figure 1.4 The sketch of the measuring reference levels, b. microscopic studies, c. an example of panoramic microscope images (the height of the images is 7 cm) (Personal archive, 2015)

1.1.3 U-Series Dating

U series dating was applied to travertine type lacustrine carbonates of the Milet Formation by eight, micritic, non-porous samples from a quarry located on Kepez Hill (Figure 1.3). The analysis was performed by Bassam Ghalep at the GEOTOP research center of the University of Quebec in Montreal, Canada. The details of the analytical procedure were described by Ghaleb et al. (2019). Briefly, about 1 g of travertine sample was cut using a rotary tool with a diamond disc (Deremel). Then the subsamples were weighed in Teflon beakers, in which an accurately weighed amount of ^{236}U-^{233}U-^{229}Th spike was evaporated at low temperature (~60 °C) to determine U and Th isotopes by isotope dilution technique. The samples were covered with deionized water and dissolved slowly by adding HNO3 (7 M) drop-by-drop. After the total dissolution, about 10 mg of the iron carrier was added and the samples were left overnight in order to ensure spike-sample equilibration. U and Th isotopes were co-

precipitated with $Fe(OH)_3$ by adding ammonium hydroxide to the solution reaching up to pH 8-9. The precipitates were recovered by centrifugation, washed with water and dissolved in HCl (6 M). Chemical separation of U and Th isotopes was done by anion exchange resin (AG1X8, 200-400 mesh). Thorium fractions were recovered with HCl (6 M) while the uranium with iron fractions were eluted with water. Finally, U purification from iron was done using U-Teva resin, the iron being eluted with HNO_3 (3 M), and the uranium with HNO_3 (0.02 M). For the thorium fraction, after evaporation, a purification column of 2 mL of AG1X8 was used in HNO3 (7 M) and eluted with HCl (6 M).

Measurements of U and Th isotopes were performed using a Nu Instrument Multi-Collector via inductively coupled plasma mass spectrometry (MC-ICP-MS). The ^{236}U-^{233}U certified ratio of the spike was used to correct for mass bias for U and Th isotopes. Age calculations and detrital corrections were done using the Isoplot 4.15 software program (Ludwig, 2012).

1.1.4 Stable Isotope Analysis

Totally, 216 hand sample were applied to the stable isotope analysis. Firstly, relevant samples were washed in the sample preparation laboratory of Dokuz Eylül University then about 0.2 g of powder samples were prepared with the help of a small, fine-tipped hand drill (Figure 1.5). To prevent the mixing of secondary calcite crystals, the clean, micritic, and non-porous parts of the samples were selected as much as possible. The prepared samples were sent to the Iso-Analytical laboratory, England to measure the ^{13}C and ^{18}O concentrations. The analysis method used by the laboratory is given below.

Samples were weighed into clean ExetainerTM tubes and then flushed with 99.995 % helium. After flushing, phosphoric acid was added to the samples and they were allowed to react in the acid overnight to allow complete conversion of carbonate to CO_2. Reference and control materials were prepared the same way. The CO_2 gas liberated from samples was then analysed by Continuous Flow-Isotope Ratio Mass

Spectrometry (CF-IRMS). Carbon dioxide was sampled from the ExetainerTM tubes into a continuously flowing He stream using a double holed needle. The CO_2 was resolved on a packed column gas chromatograph and the resultant chromatographic peak carried forward into the ion source of a Europa Scientific 20-20 IRMS where it is ionized and accelerated. Gas species of different mass are separated in a magnetic field then simultaneously measured using a Faraday cup collector array to measure the isotopomers of CO_2 at m/z 44, 45, and 46. The phosphoric acid which had been prepared for isotopic analysis in accordance with Coplen et al. (1983) was injected through the septum into the vials. The reference material used during the analysis of the samples was IA-R022 (Iso-Analytical working standard calcium carbonate). Acid preparations of samples and controls were measured directly against acid preparations of calcium carbonate standard. This procedure removes the need to apply separate corrections for temperature dependent isotope fractionation. The results obtained for the NBS18 and IA-R066 controls are used to check and correct the data as required. 20% of the samples were analysed in duplicate. Results are reported in delta notation versus PDB (Iso Analytical Laboratory Report, 2015).

CHAPTER 2
STRATIGRAPHY

Menderes Massif and Lycian Nappes form the basement of the Mio-Pleistocene sequences in the study area. These sedimentary sequences overlay the Menderes Massif with an angular unconformity (Figure 2.1, 2.2). The Lycian Nappes do not expose at Göktepe village, but they are found around the villages of Yeşimendere, Özlüce near Muğla.

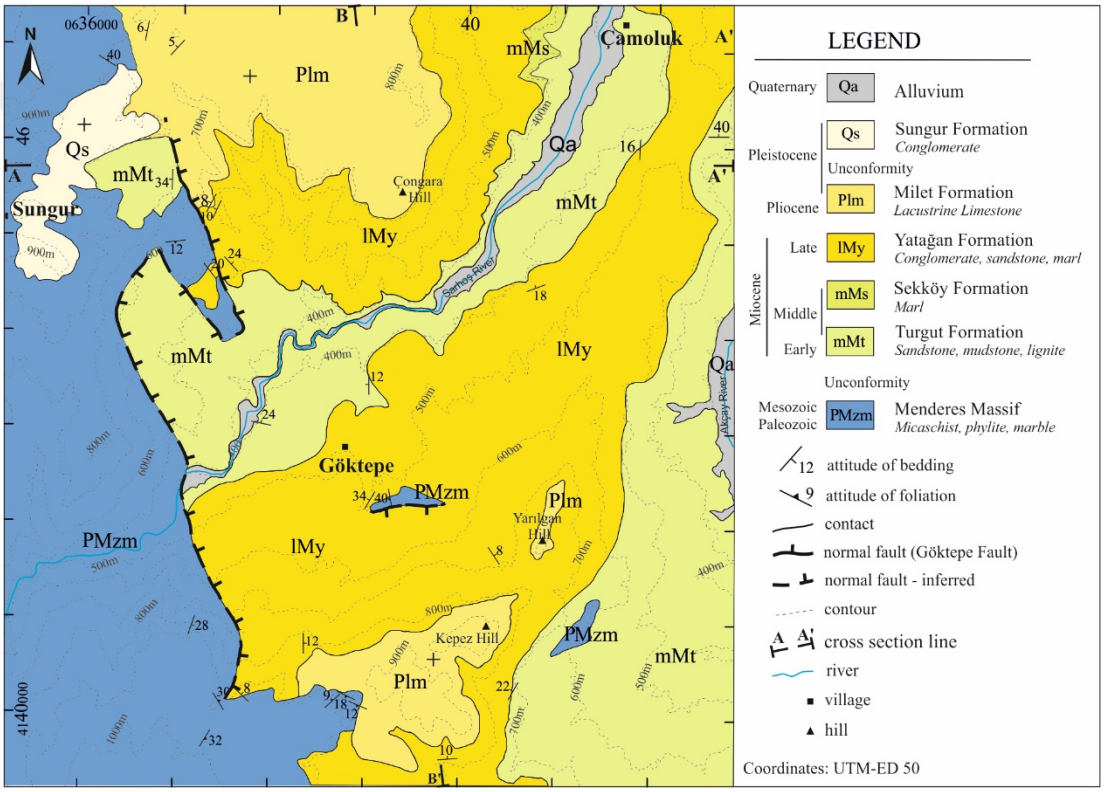


Figure 2.1 Geological map of the Göktepe area (cross-sections are given in appendices)

2.1 Menderes Massif

In the Göktepe area, the Menderes Massif is composed of metamorphic rocks underwent green-schist facies metamorphism and it extends throughout the west of the study area and patches to the souhteast Göktepe representing tops of the buried hills. (Figure 2.1). The Menderes Massif starts with the fusulinid-bearing Permo-Carboniferous Göktepe Formation (Önay, 1949; Erdoğan & Güngör, 2004) which is

made up of dark brown to gray phyllites, schists, quartzites, and marbles (Figure 2.3a). Schists and crinoid bearing light gray marbles are observed around Sungur village (Figure 2.1).

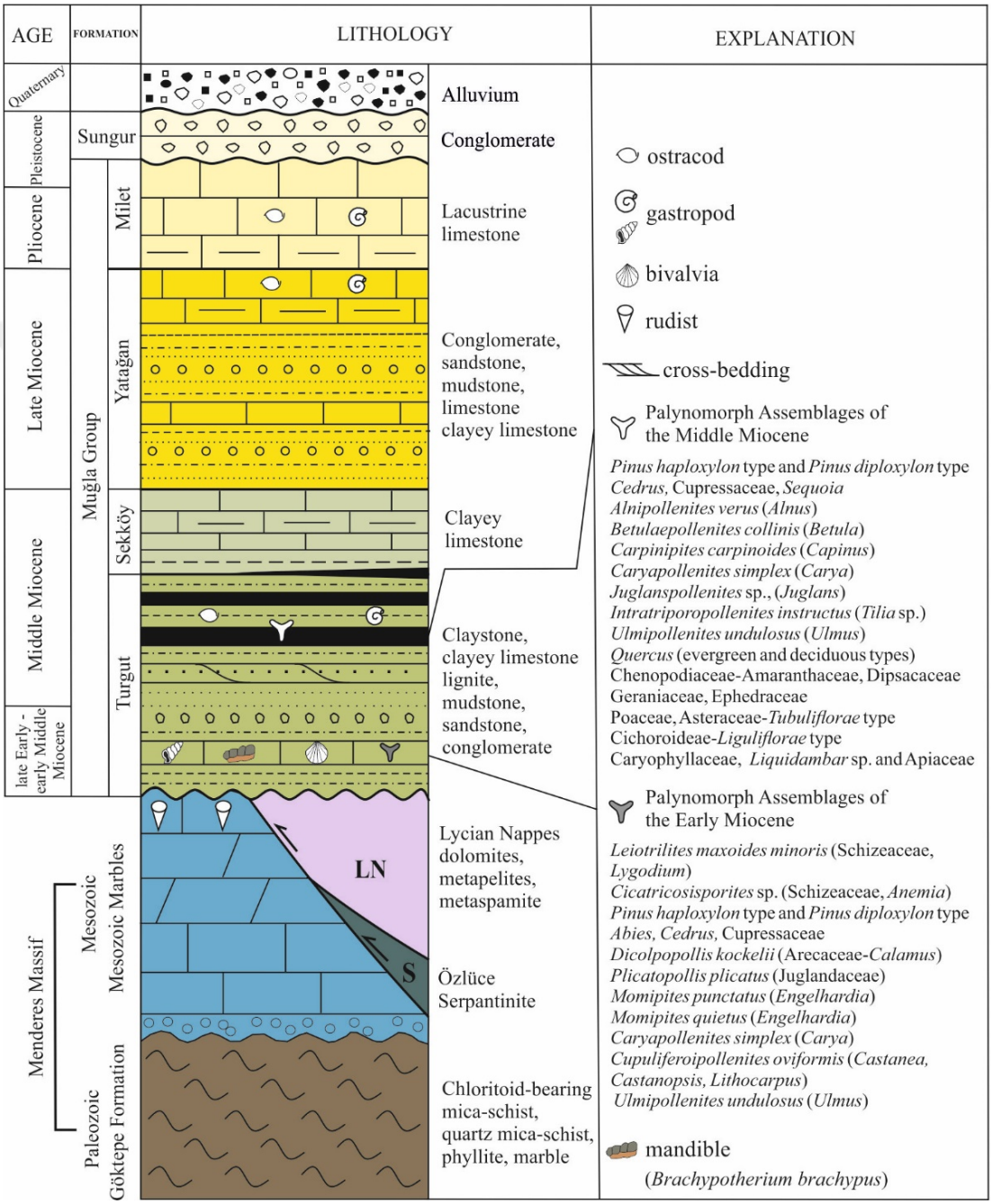


Figure 2.2 Stratigraphic section of the Göktepe area (modified after Atalay, 1980 and Hakyemez, 1989). Mio-Pleistocene sedimentary sequence covers the tectonic boundary of the Menderes Massif and Lycian Nappes along an angular unconformity

The Göktepe Formation is unconformably overlain by a Mesozoic succession which is made up of mainly dark gray to black marbles showing a prominent foliation with varying dip directions (Önay, 1949; Konak et al., 1987; Özer & Sözbilir, 2003; Erdoğan & Güngör, 2004) (Figure 2.3b and 2.3c). Banded and black marbles of the Mesozoic section expose to the north of the Çamoluk and south of Göktepe villages. In the Kepez Hill, these black marbles contain some rudist fragments as well (Figure 2.3c).

The Miocene-Pleistocene fluvial and lacustrine deposits cover the Menderes Massif along an unconformable boundary (Hakyemez, 1989; Akgün & Sözbilir, 2001; Gürer et al., 2013) (Figure 2.2).



Figure 2.3 View from the metamorphic rocks of the Menderes Massif. a) Marble and micashist alternation of the Göktepe Formation. b) White marbles c) Rudist fossils (arrows) in the Mesozoic marbles of the Menderes Massif (Personal archive, 2015)

2.2 Mio-Pleistocene Basin-Fill Succession

The Mio-Pleistocene sequences were named as the Muğla Group which was divided into four different formations (from bottom to top) the Turgut, Sekköy, Yatağan, and Milet formations (Atalay, 1980; Hakyemez, 1989).

2.2.1 Turgut Formation

This formation forms the basal part of the Mio-Pleistocene sequence, and crops out at the lower altitudes of the area, particularly along both sides of the Sarhoş Stream and Akçay River (Figure 2.1). It consists of yellowish-gray and green, thin- to medium-bedded, claystone, mudstone, sandstone, and conglomerate alternations with some thin limestone levels (Figure 2.4). Conglomerate levels include small-scale channel fills. Sandstones show mostly cross-bedding (Figure 2.4b).

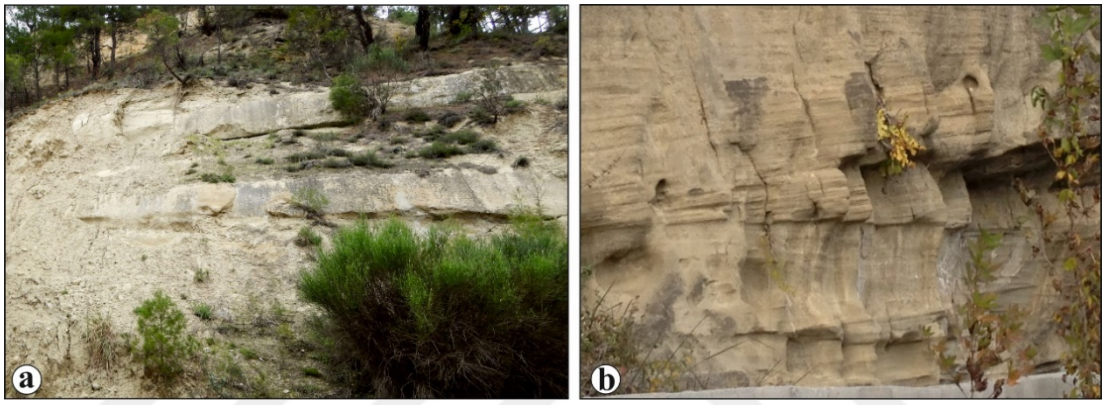


Figure 2.4 Field views of the Turgut Formation (640920 E, 4146200 N). a) Field photographs showing gray beige colored Turgut Formation. The formation is composed of mudstone, sandstone, and conglomerate (including max. pebble-sized grains) alternation. b) This photo shows the cross-bedding structures in the thickly bedded sandstones (Personal archive, 2015)

The lower part of the Turgut Formation is exposed in a small area near Sungur village, along a road-cut and a drainage channel (Figure 2.1 and 2.5a). The detailed section of this outcrop is given in Figure 2.5b. The sequence starts with yellowish-orange, laminated, marl-mudstone, very thin pale green claystone, and thin laminated brownish mudstone. It continues upwards with yellowish beige mudstone, gray claystone, and siltstone. The upper levels of the succession are composed of gray-colored, poorly lithified, medium- to coarse-grained sandstones and matrix-supported, granule- and pebble-sized conglomerates. The sandstones and conglomerate levels show both parallel and cross-bedding. The sequence ends with sandstones >10 m thick. Abundant broken gastropod shells, bivalve fossils, and mammal bones are found in this outcrop (Figure 2.5c, 2.5d, and 2.5e). These mammal bones and gastropods have

been collected and the claystone levels were sampled for palynological analysis (Figure 2.5f). The fossil records are given below.

2.2.1.1 Gastropods

Although the taxonomic revision of *Tinnyea laurea* s.s. is not complete (syn. *Tinnyea escheri* Brongniart, 1822; Harzhauser et al., 2016), we found species that resemble *Tinnyea laurea* (Matheron, 1843) in having opisthocline axial ribs (Figure 2.5d). The thiarid *Tinnyea* is an extinct freshwater genus, common in the Oligocene-Neogene lake systems of the Mediterranean and Paratethys areas (Harzhauser & Mandic, 2008; Harzhauser et al., 2016). *T. escheri* s.l. is a characteristic taxon for freshwater to brackish environments and commonly observed in Thrace and Central Paratethyan Basins (Mikuz & Pavsic, 2000; Harzhauser et al., 2002, 2011, 2016). Thus, our record can be considered indicative of similar environments.

2.2.1.2 Mammalian records

The Sungur locality yielded a rhino mandible fragment referred to *Brachypotherium brachypus* (Figure 2.5e). The material is biometrically larger than *Brachypotherium brachypus* remains from the middle Miocene locality of Paşalar (NW Turkey) (Fortelius, 1990) as well as those from European ones. It is also larger than *B. minor* records from Africa (Geraads & Miller, 2013) and *B. perimense* from middle-late Miocene localities of Siwalik Pakistan. Furthermore, it is quite smaller than *B. goldfussi* from Eppelsheim (MN6-9). The Sungur specimen is morphologically and metrically similar to those from the early middle Miocene (MN5) locality of Kultak (Muğla-Turkey) (Kayseri-Özer et al., 2014).

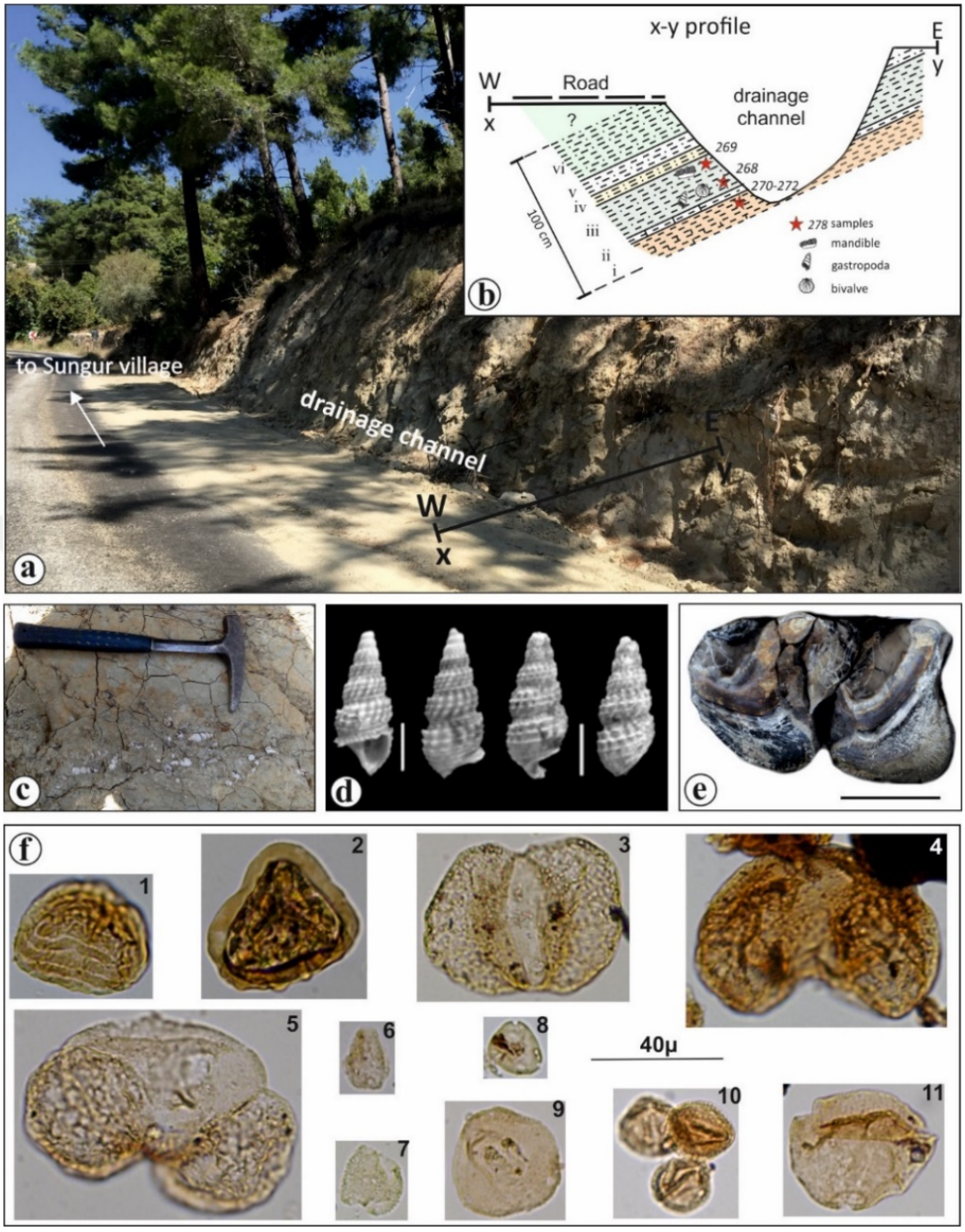


Figure 2.5 The lower part of the Turgut Formation exposes in a narrow zone (0636632 E, 4145695 N). a) The fossil location on the Göktepe-Sungur road. b) Cross-section that gives detailed stratigraphy (i. yellowish, thin laminated, calcareus claystone, mudstone; ii. calcareus claystone; iii. green, fractured claystone with fractured gastropod shells and branches, and thin laminated brownish mudstone at lower levels; iv. yellowish-gray mudstone; v. white claystone, siltstone; and vi. greenish-gray, weakly bounded sandstone. c) Bivalve and gastropod shells in claystone levels. d) SEM photos of gastropods. e) Left lower m1 of *Brachypotherium brachypus*, scale: 2 cm. f) Palynological samples (1. Schizaeceae, 2. Polypodiaceae, 3. *Cathaya*, 4. *Cedrus*, 5. *Pinus diploxylon* type, 6. and 7. *Calamus*, 8. *Engelhardia*, 9. *Carya*, 10. Adoxaceae-*Viburnum*, 11. *Fagus*) (Personal archive, 2015)

2.2.1.3 Sungur Palynomorph Assemblage

The microflora of sedimentary sequence in the lower part of the Turgut Formation is characterized by spores of Pteridophyta *(Verrucatosporites* sp., 1%; *Leiotriletes maxoides minoris (*Schizeaceae, *Lygodium*, 1%), *Polypodiaceoisporites* sp. (Pteridaceae, *Pteris*), *Cicatricosisporites* sp. *(*Schizeaceae, *Anemia*, 1%-4%*)*, *Laevigatosporites* sp. and *Echinatisporis* sp. (*Selaginella*, 1%)). Abundance and variety of the gymnosperms (>50%; Cupressaceae, *Cathaya*, *Abies*, *Cedrus*, and Pinaceae-*Pinus haploxylon* and *diploxylon* types) in this assemblage indicate an existence of middle and high-altitude landscapes around the deposition area. We also identified *Dicolpopollis kockelii* (Arecaceae-*Calamus*, 1%-2%) which is a species of the *Calamus* palm marking tropical and subtropical areas. This genus was recorded from the Oligocene-early Miocene deposits of Turkey (e.g., Nakoman, 1966; Akyol, 1971; Ediger et al., 1990; Akgün & Sözbilir, 2001; Sancay et al., 2006; Akgün et al., 2007, 2013; Batı and Sancay, 2007; Kayseri, 2010; Akkiraz et al., 2011; Kayseri-Özer et al., 2014). *Plicatopollis plicatus* (Juglandaceae) is another biostratigraphical marker in the Anatolian and European palynofloras and its abundance decreases from the Eocene to the Miocene (e.g., Akgün et al., 2007, 2013; Akkiraz et al., 2011; Kayseri-Özer, 2014). In this study, *Dicolpopollis kockelii* and *Plicatopollis plicatus* are infrequent in the samples of the lower part of the Turgut Formation. In addition, some angiosperm species such as *Momipites punctatus* (*Engelhardia*, 1%-4%), *M. quietus* (*Engelhardia*, 1%), *Caryapollenites simplex (Carya*, 1%*), Cupuliferoipollenites oviformis* (*Castanea, Castanopsis, Lithocarpus*, 1%), *Ulmipollenites undulosus* (*Ulmus*, 1%), *Triporopollenites coryloides* (*Corylus*, 1%), *Faguspollenites verus* (*Fagus*, 1%), *Faguspollenites* spp. (*Fagus*, 1%), *Caprifoliipites viburnoides* (Adoxaceae, *Viburnum*, 26%*), Quercoidites* spp. (*Quercus*, 1%), *Acaciapollenites* sp. (*Acacia*, 1%), and *Tricolporopollenites* sp. *(Lonicera*, 1%*)* are also recorded in the Sungur palynoflora (Figure 2.5f). According to this palynofloral composition, the deposition period of the formation ranges from the Burdigalian to the Langhian. The age constraints from the palynological data are coherent with the ages from the mammalian fossils (MN4-5). Palynological findings further indicate that the formation was deposited in a fully lacustrine environment under warm subtropical

climate. Spores and pollen species (*Acrostichum aureum*, *Anemia*, *Nypa*, *Pelliciera*, *Acacia*, *Rhizophora*, *Avicennia*, and *Calamus* palm), and palynomorphs (e.g., *Botroyococcus,* microforaminiferal ligning and Dinoflagellate species) prefer to live in mangrove and back-mangrove paleoenvironments that have brackish conditions due to marine influence (e.g. Gruas-Cavagnetto, 1977; Cavagnetto & Anadón, 1996; Riegel et al.,1999; Plaziat et al., 2001; Akgün, 2002; Akgün et al., 2002; Akkiraz et al., 2008; Kayseri-Özer, 2014). In this study, the existence of palynomorphs in the Sungur palynoflora such as *Botroyococcus*, *Acaciapollenites*, *Dicolpopollis*, and *Cicatricosisporites* that can tolerate brackish conditions implies that this may be a brackish lake.

The upper parts of the formation are made up of claystone, calcareous claystone, and clayey limestone alternations. To the north of Çamoluk village, two levels of lignite appear in this sequece (Figure 2.6a and 2.6c). The thickness of the lignite seams varies along its strike and wedges out. The main lignite seam, which is approximately 2 m thick and contains mammal bones and teeth, grades upward into beige-colored, laminated claystone and dark green claystone with abundant fractured gastropod and ostracods (Figure 2.6b). Dark green claystone levels include some plant remnants. On top of this layer, there are gray-beige, clayey limestone and beige claystone levels with fractured gastropod shells and abundant ostracods. The overlying second seam has been measured from drilling cores and is about 30 cm thick (Figure 2.6c). These coal seams and surrounding clay levels were sampled for palaeontological examinations and provided us the mammal bones.

Two samples (numbers 294 and 295) for ostracod analysis and four samples (numbers 296-299) for palynological analysis were collected from the calcareous claystone and clayey limestone levels of the Turgut Formation around Çamoluk village (Figure 2.6b). Moreover, 2 m-thick lignite level from 100 m below the surface were sampled along the long-wall face in the underground mine. The second thin lignite level and the other clay levels were sampled from the drilling cores (Figure 2.6c).

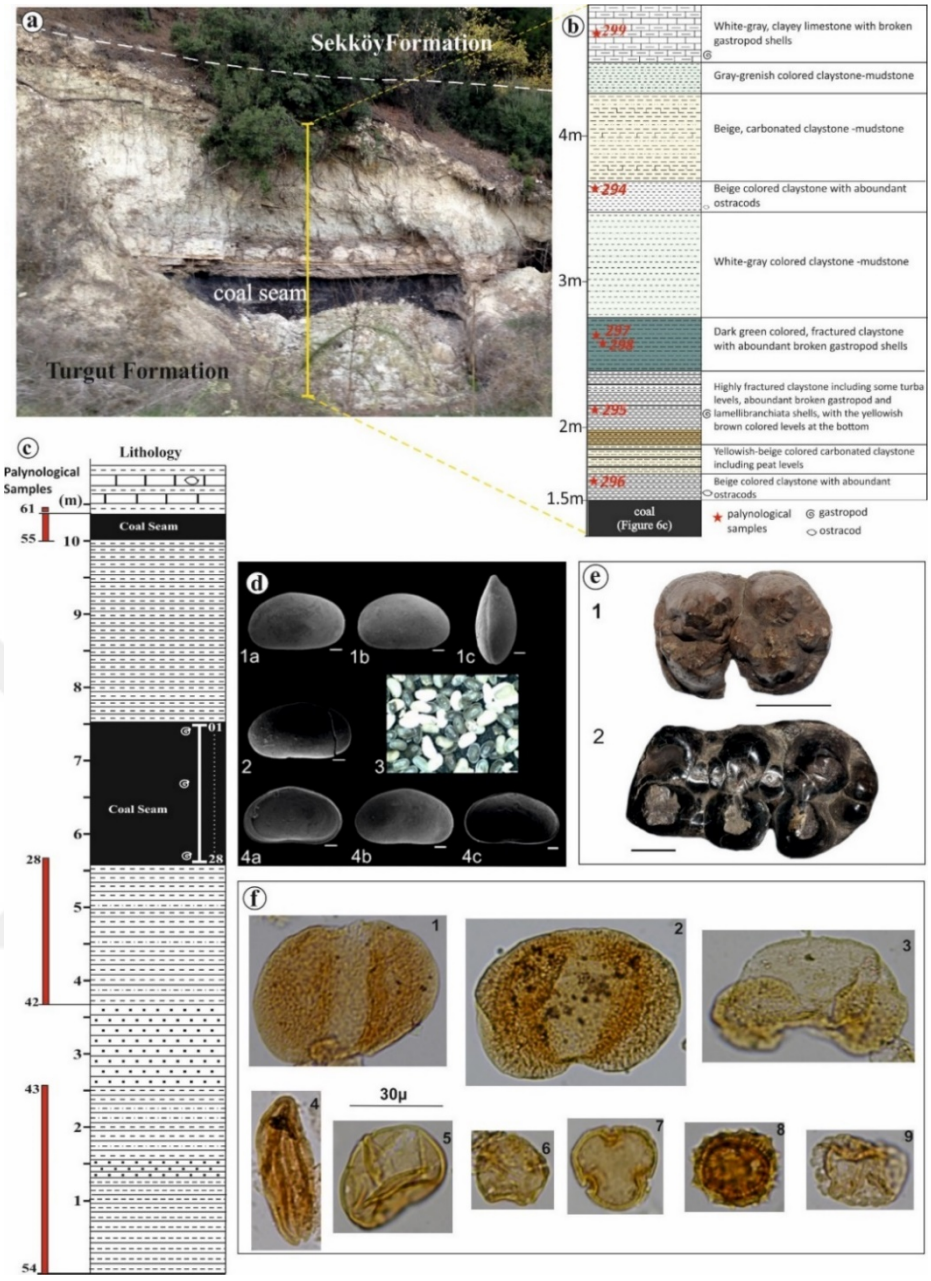


Figure 2.6 a) Field view of the coal-bearing levels of the Turgut Formation (0641305 E, 4147993 N) (Personal archive, 2015), b) Type section of the upper levels of the Turgut Formation. c) Compiled measured section of the longwall face in the tunnel and drilling logs of the coal-bearing layers of the Turgut Formation. d) Ostracod images (1.*Heterocypris formalis* (Mandelstam), 1a. External view of the left valve, 1b. External view of carapace, 1c. Dorsal view of carapace. 2. *Heterocypris* ex gr. *gregaria* (Skoksberg), external view of the right valve. 3. Stereomicroscope image of ostracod assemblage. 4. *Heterocypris salina* (Brady) 4a and 4c. Internal view of the right valve, 4b. External view of the right valve. e) Fossil mammal teeth (1, right lower m2 of *Gomphotherium angustidens*; 2. Right lower m2 of *Megalocherus homon*gus; scale: 2 cm). f) Palynomorph assemblages (1. *Cathaya*, 2. *Cedrus*, 3. *Pinus diploxylon* type, 4. Ephedraceae, 5. *Carya*, 6. *Alnus*, 7. *Tilia*, 8. Asteraceae-Asteroideae type, 9. Chenopodiaceae)

These samples were used for the analysis of palynomorphs and mammals. The fossil findings are described below.

2.2.1.4 Ostracods

The species of the genus *Heterocypris* were found in the samples 294 and 295 (Figure 2.6b and 2.6d). These are as follows: *Heterocypris formalis* (Mandelstam) (Miocene-Pliocene) (Serbia, China, Turkey), *Heterocypris* ex gr. *gregaria* (Skoksberg) (middle Miocene-Pliocene) (Turkey), and *Heterocypris salina* (Brady) (late Miocene-Recent) (Slovakia, Turkey, Romania, Bulgaria, Greek islands, and Iran). Most species of *Heterocypris* are common in freshwater environments, while some prefer oligo- to mesohaline habitats (van Morkhoven, 1963). These populations are characteristic for limnic environment (Freels, 1980; Witt, 2003; Matzke-Karasz & Witt, 2005).

2.2.1.5 Mammalian Records

Despite the small number of specimens, mammal remnants were extremely well preserved. We recorded dental remains of two proboscidean taxa at Çamoluk; a fragmentary astragal of a primitive equid: *Anchitherium* sp. and a single lower molar of a giant suid. For proboscideans, a lower second molar and a portion of an upper tusk can be referred to *Gomphotherium angustidens* that is the most common gomphothere of Europe during the middle Miocene (Figure 2.6e inset 1). Some additional molar fragments that we found, also display the typical morphology of this taxon. This species is known from Anatolia, mainly from the early middle Miocene localities of Bursa-Paşalar (MN5-6), Muğla-Kultak (MN5) and late middle Miocene localities of Muğla-Sarıçay and Çatakbağyaka (MN7/8). Metrically, *G. angustidens* from Çamoluk falls in the size range of *G. angustidens* from the middle Miocene (Astaracian, MN6-8) localities of France and Germany and it is larger than the Paşalar samples though these taxa did not show a tendency towards increasing molar size over time (Tassy, 2014). However, the well-developed posterior cingulum and bunodonty clearly differentiate the Çamoluk specimens from the Orleanian (MN4-5) forms, i.e. Corcoles

(Spain, MN4) and Quinta Grande (Portugal, MN4) (Bergounioux et al., 1953; Mazo, 1977, 1996; Maldonado et al., 1983; Tassy, 1985). The occurrence of a second proboscidean species at Çamoluk is supported by an upper second molar. This specimen is tentatively referred to the amebelodontid genus *Protanancus* based on its generally well-pronounced pseudo-anancoidy, cementodonty and posttrite conules. Besides the Anatolian records from the middle Miocene localities, such as İzmir-Mordoğan, Bursa-Paşalar, and Ankara-Çandır, the Çamoluk specimen mostly resembles the *Protanancus* material from Bulgaria-Vetren which was also dated to the middle Miocene (Markov & Vergiev, 2010).

A second lower molar represents a giant Kubanochoerine suid- and confirms the presence of the enigmatic genus *Megalochoerus* at Çamoluk. The kubanochoerines migrated into Eurasia during the MN 5 and survived until the MN 7/8 (Pickford, 2001). The previous record from Turkey, an upper molar from Ankara-Kazan-İnönü (MN6) was thought to be an M2 of *Kubanochoerus mancharensis* (junior synonym of *Megalochoerus humungous*) (Pickford & Ertürk, 1979; van der Made, 1996) (Figure 2.6e, inset 2). Since the Kubanochoerine suids underwent a rapid increase in size from early to middle Miocene times, they can be used for biochronology (Pickford, 2001; Pickford & Morales, 2003). In light of this, the Çamoluk specimen fits well with the morphologic and metrical features of the Astaracian species *M. humungous* although it has slightly lower range values compared to the youngest records of this taxa, collected from the MN 8 localities (late Astracian) of Pakistan. This could also be interpreted as a sign of an older age than MN 8 for Çamoluk. The fragmentary astragal of anchithere remains from Çamoluk is morphologically identical to the Turkish and European middle Miocene *Anchitherium* samples but distinguished from the early Miocene forms by its relatively larger size.

2.2.1.6 Çamoluk palynomorph assemblage

Palynological data were obtained from 38 samples of lignite and claystone levels of the Turgut Formation (Figures 2.6c and 2.6f). Spores are various but infrequent, except for *Laevigatisporites haardti* (Pteridophyta). Also, gymnosperm pollen

(Pinaceae, *Pinus haploxylon* and *diploxylon* types, *Cathaya* sp., *Glyptostrobus/Taxodium/Cryptomeria* sp., *Podocarpus* sp., *Cedrus* sp., *Sequoia* sp., and Cupressaceae, 5%-60%) are abundant in all samples. The woody angiosperm plants are represented by *Alnipollenites verus* (*Alnus*, 1%-3%), *Betulaepollenites collinis (Betula*, 1%*), Carpinipites carpinoides* (*Capinus*, 1%), *Caryapollenites simplex* (*Carya*, 1%-5%), *Juglanspollenites* sp. (*Juglans*, 1%), *Intratriporopollenites instructus* (*Tilia*, 1%), *Ulmipollenites undulosus* (*Ulmus*, 1%-2%), *Quercus* evergreen and deciduous types, 1%-3%, and *Caprifoliipites sambucoides* (Adoxaceae-*Sambucus*, 1%), *Lonicerapollis* sp. (*Caprifoliaceae-Lonicera* sp. , 1%), *Faguspollenites verus* (Fagaceae-*Fagus*, 1%), *Aceripollenites* sp. (*Acer*, 1%). In contrast to the lower part of the Turgut Formation, herbaceous pollen (e.g., Chenopodiaceae-Amaranthaceae, Dipsacaceae, Geraniaceae, Ephedraceae, Poaceae, Asteraceae-Tubuliflorae type, Cichoroideae-Liguliflorae type, Caryophyllaceae, *Liquidambar* sp., and Apiaceae, 5%-10%) are various and abundant in the Çamoluk palynoflora. This palynomorph association of the Turgut Formation resembles the middle-late middle Miocene palynomorphs associations recorded in other sites of Anatolia (e.g., Kırşehir (Akgün et al., 1995), Büyük Menderes Graben (Akgün & Akyol, 1999), Konya-Ilgın (Karayiğit et al., 1999), Soma (Erdei et al., 2002), Western Anatolia (Akgün et al., 2007), and Çorum and Sivas (Kayseri & Akgün, 2008). Based on our palynofloral data, the Turgut Formation was deposited under a warm temperate climate during the middle-late middle Miocene (Akgün et al., 2007; Kayseri-Özer et al., 2014).

The Turgut Formation is conformably overlain by the Sekköy Formation (Atalay, 1980; Hakyemez, 1989).

2.2.2 Sekköy Formation

The Sekköy Formation is poorly exposed in the west of Çamoluk village with elevations of about 400 m (Figure 2.1). The formation is composed of lignite free deposits such as gastropod-bearing, lacustrine clayey limestones, and limestones. There are no lignite layers observed. The lignite layers are located in the upper part of

the Turgut Formation and these coal layers gradationally pass upward to the lacustrine deposits of the Sekköy Formation (Figure 2.6a).

The Sekköy Formation is conformably overlain by the Yatağan Formation (Figure 2.1 and 2.2).

2.2.3 Yatağan Formation

The Yatağan Formation exposes well along the hillslopes of the Çongara, Yarılgan, and Kepez hills, about 400 m above sea level (a.s.l.) (Figure 2.7). This formation has a distinct orange-red color and is characterized by an alternation of conglomerate, sandstone, siltstone, and mudstone alternation with some clayey limestone and limestone lenses (Figure 2.7). It starts with matrix-supported, poorly sorted conglomerates, which contain sub-rounded, sub-angular clasts and alternate with medium-to coarse-grained cross-bedded sandstones. These fluvial clastics change upwards to lacustrine limestones.

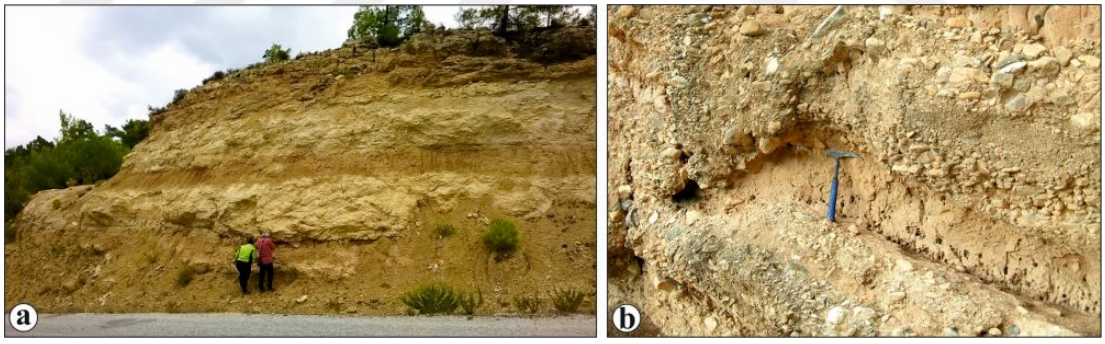


Figure 2.7 Field photographs shows the different lithologies of Yatağan Formation (0641170 E, 4143241 N). a) View of the fine-grained levels of the formation including fluvial deposits that consist of silt, sand, clay, and marl alternations (outcrop height is approx. 11 m). b) photograph shows the orange colored conglomerate levels of the formation (Personal archive, 2015)

The age of the Yatağan Formation is Turolian (upper Miocene) based on vertebrate fossils described by Atalay (1980) and Hakyemez (1989). The Yatağan Formation is conformably overlain by the Milet Formation.

2.2.4 Milet Formation

The Milet Formation was described by Becker-Platen (1970) as the Milet beds and revised by Hakyemez (1989) who put it in the Milet Formation. In the study area and further east towards the town of Kale (Denizli), the Milet Formation is exposed on top of plateaus around Göktepe village (Figure 2.8).



Figure 2.8 Field photographs of the Milet Formation (Kepez Hill). a. Field view from Kepez Hill to Göktepe village. b. and c. Travertine type lacustrine carbonates of the Milet Formation. Triangles show the sample locations for U series dating (samples 7 and 8 were taken from the benches at lower levels) (Personal archive, 2015)

This formation is composed of yellowish cream claystone, marl, and travertine-type lacustrine limestones. The lower parts of the formation are graded vertically into the orange-colored conglomerates of the Yatağan Formation and pass through upward travertine-type lacustrine limestones. The thickness of the travertine is approximately 80 m and it includes plant remains, gastropods and ostracods. The Milet Formation is almost horizontal in the south of the study area, but it shallowly dips to the NW (5-10^{o}) north of Göktepe village.

Atalay (1980) suggested the age of the Milet Formation as upper Miocene (Turolian)–Pliocene according to vertebrate fossils from Bozarmut village (Muğla). Hakyemez (1989) also stated the age of the formation as Pliocene because the Milet Formation stratigraphically lies on top of sequences that contain Turolian mammal fossils. In this study, U-series dating was used to determine the age of the travertine-type lacustrine limestones of the Milet Formation at the uppermost part of the formation. These results were first presented by Yılmaz et al. (2016). The radiometric dating results show a Middle Pleistocene age for travertines. The dating details are given below.

2.2.4.1 U Series Dating

The basis of U-series dating is that the $CaCO_3$ phase incorporates only uranium (soluble in oxidizing conditions), not ^{230}Th (insoluble) during the precipitation. The uranium then produces the authigenic ^{230}Th by radioactive decay and the activity ratio of $^{230}Th/U$ increases from zero at time of precipitation until reaching the secular equilibrium value around 500-600 ka. If the radioactive system remains closed (no loss or gain of any U and Th isotopes except by radioactivity) then the activity ratio of $^{230}Th/U$ allows calculation of the time since the precipitation of the carbonate phases.

Stratigraphically, the ages of our samples taken from the uppermost levels of the sequence must be younger than those from the bottom. However, the results are incompatible with the stratigraphy (Table 2.1).

Table 2.1 U series dating results of the Milet Formation

No	Sample No	Depth (m)	^{238}U ppb	±	^{232}Th ppb	±	^{234}U/ ^{238}U	±	^{230}Th/ ^{238}U	±	^{230}Th/ ^{232}Th	±	Calculated Age (ka)	±	Corrected Age (ka)	±
1	31	0	269.6533	1.1178	36.8952	0.1989	1.1552	0.0046	1.2187	0.0062	27.2212	0.2157	660.642	208.165	659.008	302.898
2	100	10	500.2964	1.6345	99.2053	0.5479	1.2591	0.0053	1.3242	0.0045	20.4088	0.1311	412.043	21.847	407.576	49.450
3	96	12	578.2602	2.6088	126.2914	0.7374	1.0267	0.0039	1.0347	0.0098	14.4791	0.1681	626.523	329.080	618.916	450.035
4	71	24	238.8013	1.6988	453.7210	6.5519	1.0653	0.0082	1.0879	0.0078	1.7499	0.0277	593.702	259.120	538.797	2249.599
5	62	30	535.9998	1.9015	179.0017	1.3190	1.0460	0.0042	1.0355	0.0040	9.4761	0.0797	399.761	25.644	389.269	62.890
6	45	36.5	729.7777	3.0307	270.3427	2.5858	1.0199	0.0049	1.0299	0.0073	8.4972	0.0998	Older than 600 ka	n.d.	Older than 600 ka	n.d.
7	157	57	714.4085	3.3484	41.2162	0.2128	1.0640	0.0044	1.0402	0.0065	55.1063	0.4795	346.162	19.108	343.372	19.934
8	123	70.5	148.2832	0.8005	2.6312	0.0136	1.0940	0.0065	1.0931	0.0067	188.2735	1.6321	380.554	30.516	378.758	30.541

There may be several potential reasons for this inversion in the stratigraphic order. The first one is that our travertine samples have incorporated variable amounts of detrital contamination. This is indicated by the presence of variable amounts of ^{232}Th (and all other thorium isotopes). In such a case, the measured ^{230}Th in our samples corresponds to the sum of authigenic ^{230}Th that is produced by incorporation with both uranium and the non-authigenic ^{230}Th related to detrital contamination. Thus, we should subtract the amount of detrital ^{230}Th from the total ^{230}Th before calculating the age of a sample. We used an average crustal correction model similar to the one used by Ludwig & Paces (2002) to obtain the corrected ages that are given in the Table 2.1. Specifically, ^{232}Th was used as an index and typical crustal Th/U was used for detrital component. The activity ratio values used are $^{232}Th/^{238}U = 1.21 \pm 50\%$, $^{230}Th/^{238}U = 1 \pm 10\%$ and $^{234}U/^{238}U = 1 \pm 10\%$. We believe that with such assigned errors for the detritus component the detrital correction should correct our sample results in a manner that covers most of the natural detritus observed on the earth's surface.

As seen in the Table 2.1 the corrected ages are incompatible with the stratigraphic order yet, therefore indicating that detrital contamination is not the primary cause for the incompatibility with the stratigraphic order and another process should be evoked. As mentioned above, U series dating is based on the assumption of a closed radioactive system (no loss or gain of any U and Th isotopes except by radioactivity). We think that this condition is not met in our samples, thus preventing the obtaining of reliable ages. In fact, our samples show clear evidence that a recrystallization process has occurred. This indicates a potential opening of the radioactive system and this opening will essentially affect the uranium isotopes that can be transferred without necessarily fractionation of ^{234}U-^{238}U. Deschamps et al. (2004) observed a disequilibrium of $^{234}U/^{238}U$ in Mesozoic limestone formations in the eastern Paris Basin and they suggested a discrete uranium mobility/transfer as a result of pressure dissolution structures (stylolites or dissolution of seams). The uranium mobility/transfer mechanism can be evoked to induce the slight disequilibrium observed in our samples. On the other hand, and given the old ages of the travertines, the U series activity ratios should be near the secular equilibrium (limit of the method: 500-600ka). Thus, any small mobility or transfer of uranium will result in huge differences in the calculated

ages due to exponential character of the radioactivity phenomena. The precision of the dating decreases with increasing age (Geyh & Schleicher, 1990 and references therein).

Whatever the process responsible for the disequilibrium observed in our samples and given the limited number of analyzed samples, we suggest that from a theoretical point of view the samples that lost a part of their uranium will yield calculated ages older than the true age, while those that gained uranium will yield a younger age than the true one. From this perspective, one can consider that the youngest calculated age (~346 ± 19 ka) can be considered as a minimum age for this formation.

Consequently, the lacustrine carbonates of the Milet Formation were deposited in the Middle Pleistocene, most likely until ~346ka. We consider that the travertine type carbonates of Milet Formation might have been deposited during Marine Isotopic Stage 11 (MIS 11). MIS 11 (424 - 374 ka) was the warmest and longest interglacial period in the past 500ka (Howard, 1997). Loutre & Berger (2003) suggests that the MIS 11 and especially 405 - 340 ka before present could be a good analog for future climate.

2.2.4.2 Göktepe Fault

The Göktepe fault is a 6-km-long fault that extends along the western part of the study area. The fault is an eastward dipping high angle normal fault that strikes towards the northwest (Figures 2.1). The Göktepe normal fault is divided into two segments; each of them is approximately 2 km long and extends toward the north. These branches separate the Mio-Pleistocene sedimentary units from the metamorphic basement. This fault shows a growth fault geometry because the thickness of the sequence on the hanging wall block is distinctly thicker than those on the footwall block.

The Millet Formation is highly inclined due to fault dragging to the north of Göktepe village. However, the uppermost levels of the Milet Formation overlap the Göktepe Fault (Figure 2.9). Field observations show that the limestone beds in the

upper part of the formation are undisturbed at elevations of ~800 m. This location is shown with a red square in Figure 2.1. The U series dating results of the uppermost levels of the travertine-type-lacustrine carbonates (Milet Formation) yield a minimum radiometric age of ~346ka B.P. (Middle Pleistocene). Since these carbonates overlapped the Göktepe fault, it may imply that this fault has been inactive since at least ~346ka (Figure 2.10).

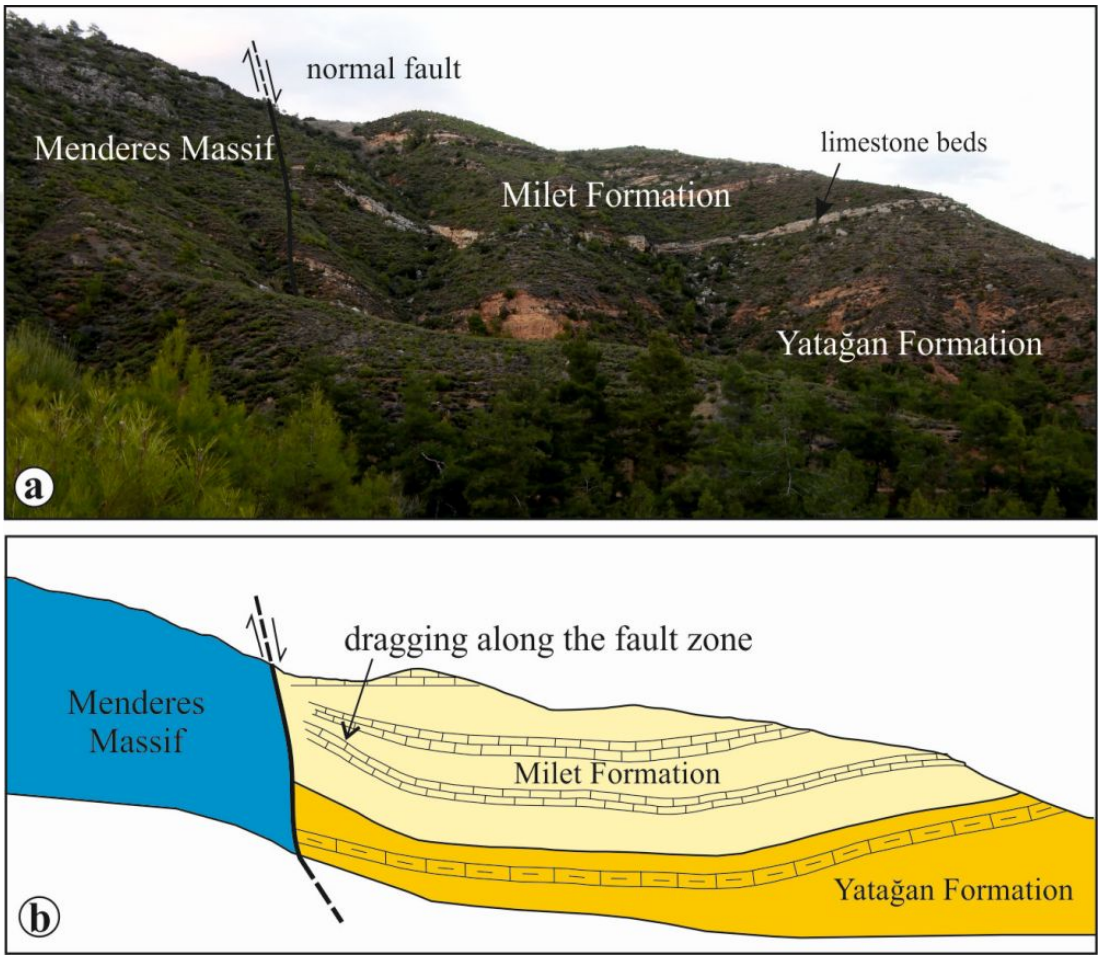


Figure 2.9 Photograph and drawing to show the northern branch of the 2-km-long, NW-SE trending Göktepe Fault. The drag of limestone beds along the fault zone indicates a normal sense of movement. This normal fault put early Miocene - Pleistocene sedimentary units up against a metamorphic basement that is composed of marble and mica-schist (Personal archive, 2015)

The Milet Formation is unconformably overlain by the Sungur Formation.

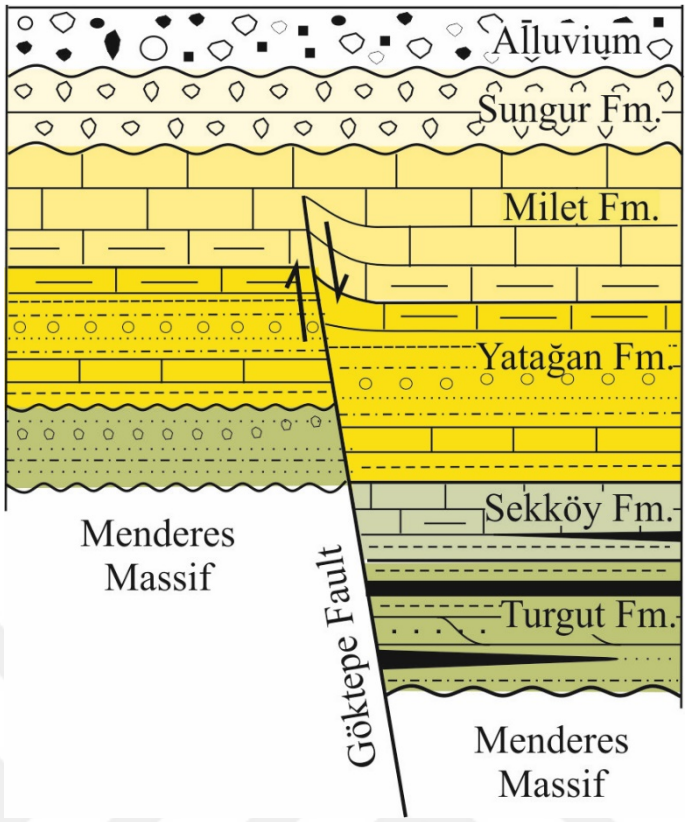


Figure 2.10 Asymmetry in the basin fill indicates that the Göktepe Fault was a growth fault. The formations in the hangingwall are several times thicker than those in the footwall

2.2.5 Sungur Formation

The Sungur Formation exposes in a small area between Göktepe and Sungur villages (Figure 1b). The Sungur Formation consists of brownish-red, matrix-supported, very poorly sorted, poorly lithified conglomerates, and sandstones (Figure 2.11). Conglomerates are made up of angular, pebble- and cobble-sized clasts of schist and marble. The matrix is composed of fine-grained sand and silt.

The alluviums of the Akçay and Sarhoş rivers are the Quaternary deposits of the study area that unconformably overlay the sequence.



Figure 2.11 Field views of the Sungur Formation. a. The formation has the orange color and horizontal beds, b. The formation is composed of poorly sorted conglomerate including angular grains of Menderes metamorphics in a sandy matrix (Personal archive, 2015)

2.3 Paleoenvironmental Evolution

Our stratigraphic, biostratigraphic, and structural data provide a basis to evaluate the depositional environment and the climate conditions of i) late early Miocene–early middle Miocene, ii) middle-late middle Miocene, and iii) Middle Pleistocene terrestrial deposits, which have implications for the paleoenvironmental and tectonic evolution of the Göktepe area.

2.3.1 Late Early Miocene - Early Middle Miocene (MN 4-5)

The oldest deposits of the study area are fluvial clastics (alternation of conglomerates, sandstones, and mudstones) with some lacustrine interbeds (claystone, calcareous mudstone, and marl). These lacustrine layers include some gastropods, Sungur palynomorph assemblages, mammalian bones, and a mandible, which provide an age constraint of late early-early middle Miocene (MN4-5). Moreover, the gastropods and palynomorphs indicate a lacustrine environment that was surrounded by broad-leaved, deciduous forests under a warm subtropical climate. Some of the palynomorphs (e.g., *Botroyococcus, Acacia*, *Calamus*, and *Anemia*) and gastropods tolerant to brackish conditions suggest that this lake may have had brackish characteristics.

The late early–early middle Miocene (Burdigalian (20.44Ma)-Langhian (13.82Ma); MN4-5) corresponds to the deposition period of the lower part of the Turgut Formation in the Yatağan Basin, which should be chronologically correspond with the Eskihisar and the lower part of the Yeni-Eskihisar sporomorph associations (Benda and Meulenkamp, 1990). Studies on the base of the Turgut Formation are very limited and most studies attribute a middle Miocene age for the formation (Atalay, 1980). However, Alçiçek (2010 in fig.2 and fig. 3) suggested an early to middle Miocene (MN4-6) age for the Turgut Formation by using fossil findings of mollusks by Becker-Platen (1970) and vertebrates by Saraç (2003). Our results provide the age constraint of MN4-5 for the deposition time of the lower part of the Turgut Formation.

The early Miocene succession in the Kale-Tavas Basin consists of the Yenidere, Künar, and Kale formations (Hakyemez, 1989) (Figure 2.2). Among these formations, the age of the Künar Formation is the least constrained because it lacks any paleontological findings. Hakyemez (1989) considered the Künar Formation as the fluvial continental equivalent of the marine Kale Formation and therefore suggested its age as Burdigalian. Özcan et al. (2009) described two foraminiferal horizons in the middle part of the Kale Formation and indicated a transgression referring to the Burdigalian age. Büyükmeriç (2017) used stratigraphic relations between the Aquitanian Yenidere Formation and late Burdigalian Kale Formation and proposed the age of the Künar Formation as early Burdigalian. Büyükmeriç (2017) also stated that in the late Burdigalian there was a transgression in the Kale-Tavas Basin characterized by the thick carbonate sequence of the Kale Formation. Moreover, De Graciansky (1972) proposed that a branch of the early Miocene Neotethys Ocean extended towards the Kemer barrage, i.e. the Göktepe area (Figure 2.12). This transgression may have affected the deposition of the Turgut Formation in the Göktepe area and would explain the existence of the brackish tolerant palynomorph assemblage and gastropods.

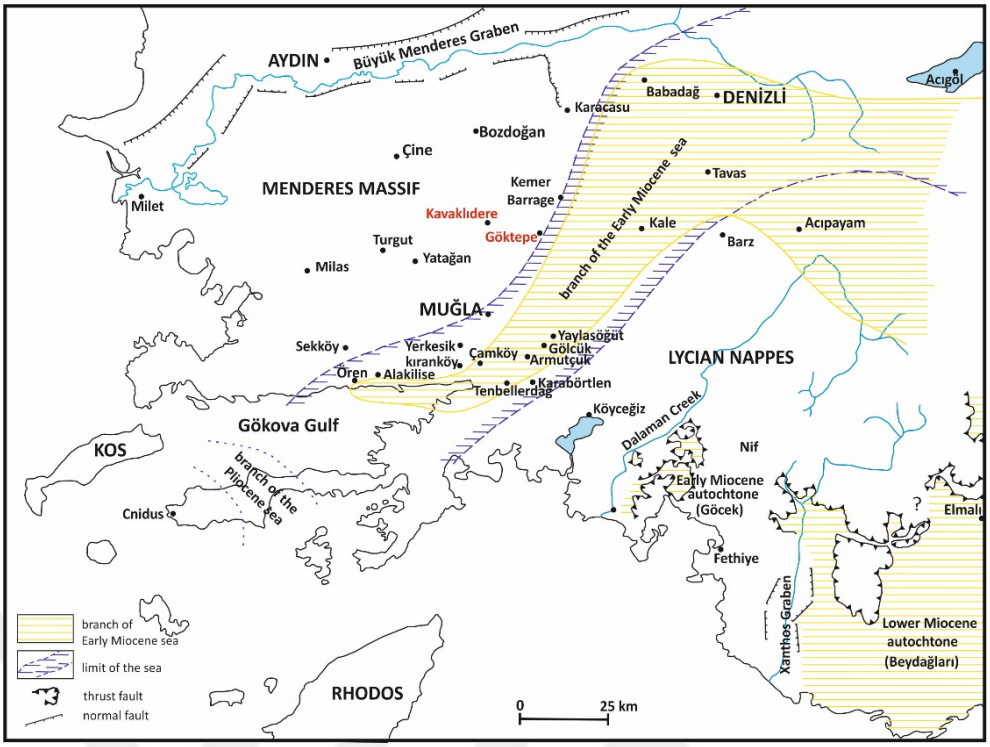


Figure 2.12 The map showing the extension of the early Miocene Sea (redrawn and modified after De Graciansky, 1972)

When the lower part of the Turgut Formation started to deposit in the Yatağan Basin, the Künar/Kale formations were deposited in the Kale-Tavas Basin (Akgün & Sözbilir, 2001) and Kultak Formation was deposited in the Ören Basin (Kayseri-Özer et al, 2014).

2.3.2 Middle-Late Middle Miocene (MN 6-7)

The middle Miocene is characterized by fluvial and lacustrine sediments of the Turgut and Sekköy formations. The debated stratigraphic setting of the lignite in the Yatağan Basin was described in Chapter 1. Our fossil data (mammalian bones, ostracods, and Çamoluk palynomorph assemblage correlated with the upper part of the Eskihisar and Yeni-Eskihisar palynomorph associations (Benda & Meulenkamp, 1990) show that the lignite was deposited during the middle-late middle Miocene (MN6-7) time interval in the freshwater lacustrine environment. Besides coal-bearing sediments of the Turgut Formation were deposited under warm temperate climate

settings. It is considered that there was a cooling in the palaeoclimate conditions (from subtropical to warm temperate) during the deposition of the Turgut Formation.

The lignite stratigraphically forms the uppermost levels of the Turgut Formation as proposed by Atalay (1980) and is followed by the marls of the Sekköy Formation (Bouchal et al., 2017; Güner et al., 2017).

2.3.3 Middle Pleistocene

The Göktepe area is also located in the south of the Bozdoğan Graben. The N-S running Bozdoğan Graben is a product of E-W extension before the late Miocene (Ocakoğlu et al., 2014). The NW-SE striking Göktepe fault lies at the south-eastern end of the graben and may therefore be related to this extension. Moreover, the fault appears to be extinct by ~364 ka (Middle Pleistocene), which is compatible with the direction change of the extension in the Early Pliocene to the NE-SW, and then to N-S extension in the Late Pliocene-Quaternary (Ocakoğlu et al., 2014).

Three models have been suggested for the evolution of the Kale-Tavas Basin: i) a basin due to N-S extension (Seyitoğlu et al., 2004; Sözbilir, 2005; Elmas et al., 2009; ten Veen et al., 2009; Seyitoğlu and Işık, 2015), ii) piggyback basin (Görür et al. 1995; Yılmaz et al. 2000; Gürer and Yılmaz 2002; Alçiçek and ten Veen 2008; Gürer et al., 2013) and iii) molasse basin (Şengör and Yılmaz 1981; Koçyiğit, 1984; Akgün and Sözbilir, 2001; Sözbilir, 2005). The Göktepe fault can be considered as a growth fault that limits the Kale Tavas Basin. The sedimentary sequences on the hanging-wall block of the Göktepe Fault are significantly thicker than those on the footwall block. This may indicate continuous subsidence in the basin until ~364 Ka. Thus we consider that our results are compatible with the extensional model proposed by Seyitoğlu et al., (2004).

CHAPTER 3
MICROFACIES OF THE GÖKTEPE TRAVERTINES

3.1 Introduction

Travertines have unique fabrics, which provide valuable data for the freshwater carbonates and their diagenesis (Chafetz and Folk, 1984).

There are various definitions of travertine in the literature. Chafetz & Folk (1984) describe the travertine as “a "freshwater" carbonate deposited by inorganic and organic processes from spring waters”. Guo & Riding (1998) explained that travertine is a locally restricted and internally complex deposit formed by rapid precipitation in a calcium and bicarbonate rich groundwaters, which emerged from hot springs. Pentecost (2005) established a summary about the definitions of travertine term in the literature and emphasized that they are not precise including his own. Because some of them made a temperature-based definition and some others indicated hydrologic setting or process. Pentecost (2005) suggested a definition that is:

> A chemically-precipitated continental limestone formed around seepages, springs and along streams and rivers, occasionally in lakes and consisting of calcite or aragonite, of low to moderate intercrystalline porosity and often high mouldic or framework porosity within a vadose or occasionally shallow phreatic environment” and he added “Precipitation results primarily through the transfer (evasion or invasion) of carbon dioxide from or to a groundwater source leading to calcium carbonate supersaturation, with nucleation/crystal growth occurring upon a submerged surface.

This definition comprises only inorganic processes. The inorganic process can basically be explained as the precipitation of calcium carbonate because of the loss of carbon dioxide from a calcium-rich bicarbonate solution in a non-marine setting (Pentecost, 2005).

However, travertines may be deposited both inorganic and organic processes. Inorganic processes dominate near the spring orifice where water is hot and acidic, whereas the role of the organic processes increases when the water moves away because bacterial growth tends to become more abundant when the water approaches surface conditions. Bacteria, blue-green algae, bryophytes, and reeds contribute to calcium carbonate precipitation by encrusted with travertine because of their own photosynthetic activity (Pentecost, 2005). Water temperature, amount of dissolved CO_2 per volume of water, pH, salinity, and light intensity controls the relative abundance of organically precipitated carbonates (Chafetz & Folk, 1984).

Besides, the morphology of the accumulation controls the existence of different sub-environments in which the water chemistry determines what organisms can live and grow (Chafetz & Folk, 1984). These physico-chemical conditions influence inorganic precipitation as well as the organic precipitation by affecting the type, abundance, and growth rate of organisms (Chafetz & Folk, 1984). Chafetz & Folk (1984) determined the five categories based on the accumulation morphology; i) waterfall or cascade deposits, ii) lake-fill deposits, iii) steeply sloping mounds, fans, or cones, iv) terraced mounds, v) fissure ridges.

Pedley et al. (1996) suggested climate and temperature as the main controlling factors of the morphology in the freshwater carbonate deposition beside water chemistry and nutrients.

Guo & Riding (1998) recommended some controlling factors for travertine deposition which are spring location and topography, and spring or non-spring water supply. They described travertine lithotypes in Rapolano Terme (Italy) and suggested three depositional environments and related facies of them. These lithotypes are i) crystalline crust, ii) shrub, iii) pisoid, iv) paper-thin raft, v) coated bubble, and vi) reed vii) lithoclast travertines. These are deposited in i) slope depositional system (terrace slope, smooth slope, waterfall facies) ii) depression depositional system (shrub flat, marsh-pool facies), iii) Mound depositional system (reed mound facies). The

morphology and origin of the shrub facies were also described by some researchers (Guo & Riding, 1994; Chafetz & Guidry, 1999).

In this study, terminology and lithotype definitions are based on the Chafetz & Folk (1984), Guo & Riding (1998), and Pentecost (2005). In addition, a parallel method and terminology is used with the studies of the Erdoğan & İşintek (2007), İşintek et al. (2007); Turan (2007), and Yilmaz (2008).

3.2 Carbonate Fabrics, Facies, and Components of the Göktepe Travertines

The carbonate fabrics, facies and components of the Göktepe travertines were studied by two stratigraphic sections located on the Kepez Hill and the Yarılgan Hill. The locations are shown in Figure 1.3 and detailed methodology is given in Section 1.1.2.

The carbonate fabrics referring to textural and structural features of the Göktepe travertines can be classified as 1) micrite fabrics, 2) spar fabrics, 3) zoned algal fabrics 4) shrub fabrics 5) biological components and 6) pores.

1) The micrite fabrics consist of clotted (peloidal) micrite, microbial micrite, encrusted micrite fabrics, and intraclast.
2) The spar fabrics are algal microspar-spar clump, encrusted spar fabrics, macrophytes encrusted spar fabrics, thin macrophytes encrusted spar fabrics, spar carbonate fragments, intra-frame spar fabrics, and inter shrub spar fabrics.
3) Zoned algal fabrics are zoned algal clump fabrics and zoned encrusted algal fabrics.
4) Shrub fabrics are micritic quill-feather shrubs and macrophytes spar quill shrubs.
5) Biological components consist of gastropods, ostracods and charophytes encrusted macrophytes.
6) Pores are fenestral (shrinkage*)* pores, gas escape pores, intra-frame pores and inner organism pores.

These fabrics and components of travertines form the facies, which are classified as i) clotted micrite facies, ii) microbial micrite facies, iii) algal microspar-spar clump facies, iv) zoned algal clump facies, v) micritic quill-feather shrub facies, vi) macrophytes encrusted spar facies, vii) thin macrophytes encrusted spar facies, and viii) fragmented carbonate facies. The entire travertine sequence is composed of the horizontal and vertical alternations of these facies. Each facies represent typical depositional conditions in the lacustrine environment.

3.2.1 Micrite Fabrics and Facies

The micrite is the fine-grained calcite or aragonite crystal that smaller than 4µm in diameter (Folk, 1959). The micrite fabrics of the Göktepe travertines include orthochemical and allochemical components. The orthochemical components consist of i) clotted (peloidal) micrite, ii) microbial micrite, and iii) encrusted micrite. These components directly precipitate from the lake water. The allochemical components that are reworked as a result of sedimentological processes are also represented by iv) intraclasts.

These fabrics and their facies are classified as i) clotted micrite fabrics and facies, ii) microbial micrite fabric and facies, iii) encrusted micrite fabrics, and iv) intraclast.

3.2.1.1 Clotted Micrite Fabrics and Facies (CMF)

The clotted micrite fabrics were characterized by dark, almost opaque small algal micritic clumps or strings (Pentecost, 2005). The clotted micrite fabrics have a regular or irregular, subspherical pellet shape with indeterminate boundaries (Figure 3.1). Their detritic appearance in thin section notwithstanding, they are bonded with each other by micritic ropes and constitute an irregular micritic frame or network. The dark color and bounded textures of clotted micrite may indicate their microbial origin.

The clotted micrite is related to the bacterial colonies (especially cynobacteria) (Pentecost, 2005). Cyanobacterias (the blue-green algaes) consume CO_2 in lake water

by photosynthesis hence pH and alkalinity increase and cause rapid carbonate precipitation. This rapid precipitation led to developing the laminas and thin layers composed of irregular clotted micrites and empty and/or spar filling pores between these fabrics. These regular or irregular laminas and thin layers are named as “clotted micrite facies” (Figure 3.1). In this facies, the pores between the clotted micrite were fully or partly filled by the spar calcite crystals directly precipitated from the water.

The clotted micrite fabrics are sometimes observed as irregular clumps formed by binding of clotted micrites due to prolonged activities of cyanobacterias (Figure 3.1c). Besides, the clotted micrite fabrics may reach microspar size. This is probably due to recrystallization of the micrites (Figure 3.1d).

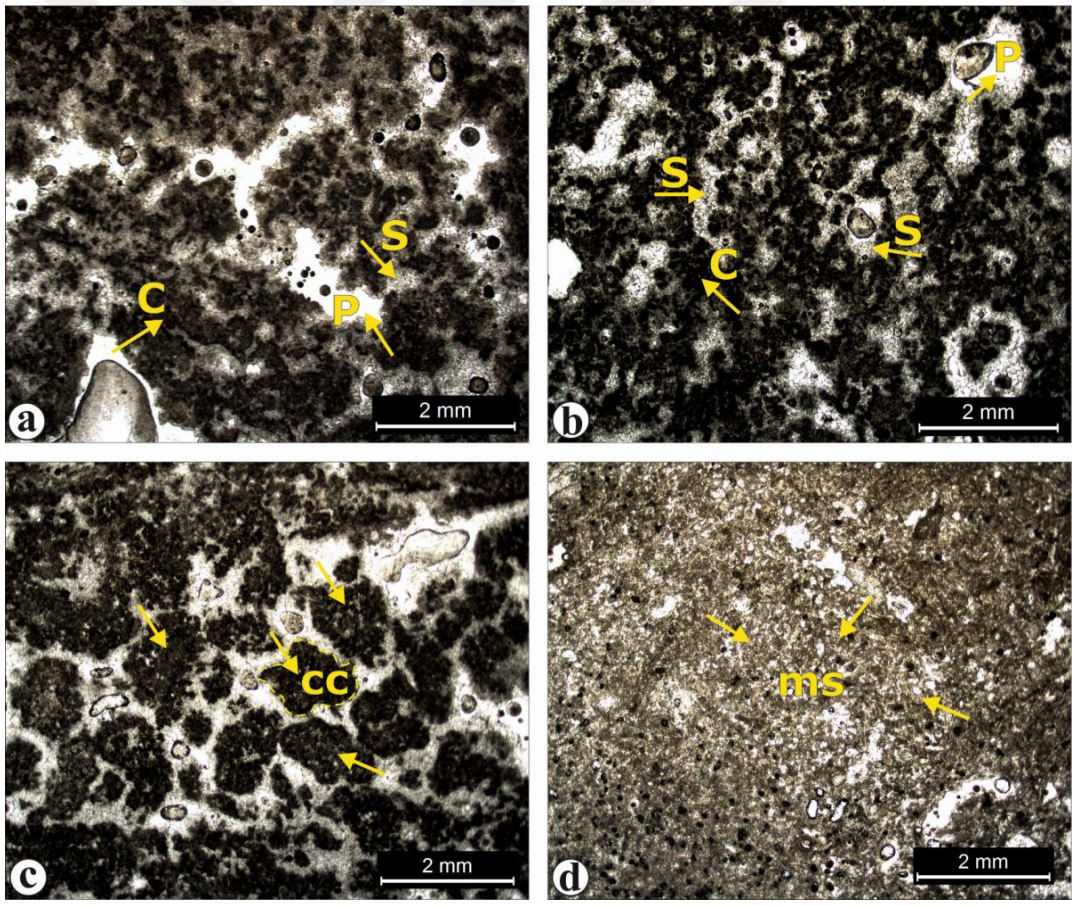


Figure 3.1 The microscope images of clotted micrite facies under plane-polarized light (PPL). a.and b. clotted micrite fabric and facies from sample 77 and 88, respectively c. clotted clumps in a microspar-spar matrix from sample 75, d. clotted microspar from sample 75, (c: clotted micrite fabrics, s: secondary spar fabrics that precipitated in the pores between clotted micrites, p: empty pore. cc: clotted clumps, and ms: microspar size clotted micrite fabrics)

It is considered that the fabrics of these facies were probably deposited in the nearly stagnant, calm, and relatively deep shallow lake environment. This facies is very common in the sequence.

3.2.1.2 Microbial Micrite Fabrics and Facies (MMF)

Microbial micrite is sometimes irregular but generally layered or lamina-shaped micritic structures that are formed by the primary or secondary activities of cyanobacterias (blue-green algae). Microbial micrite fabric, unlike the clotted micrite, has a very dark color (Figure 3.2).

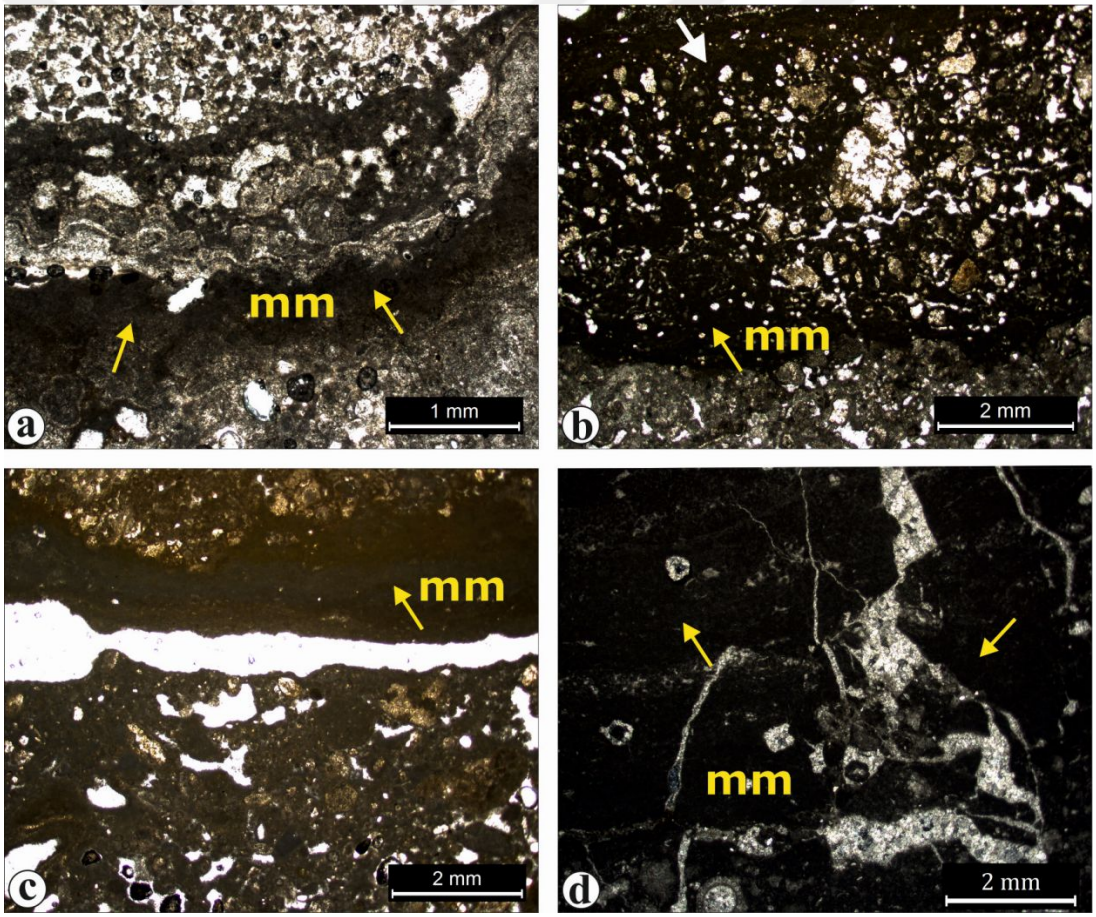


Figure 3.2 The microscope images of very dark-colored, massive microbial micrite facies (yellow arrows) under PPL. a. and c. the layered microbial micrite facies from samples 87 and 58, respectively, b. the microbial micrite between the spar carbonates sample 65, d. very dark microbial micrite fabrics from sample 124

They generally have wavy hues of black and gray colors, and irregular, the small porous structure. This different internal structure and dark color of microbial micrite may be due to the different kinds of cyanobacteria (blue-green algaes) involved in precipitation. These regular or irregular thin layers and laminas are named as “microbial micrite facies”. Due to the restart of cyanobacteria activities, these fabrics may form in existing pores or surround some grains secondarily such as algal microspar clumps or spar carbonate fragments. These facies may probably deposits of a very shallow, calm, and bacteria-rich environment.

3.2.1.3 Encrusted Micrite Fabrics (em)

Encrusted micrites are microbial micrite laminas deposited on the one and/or two sides of the stem or leaves of the reed-like tubular plants (macrophytes) (Figure 3.3).

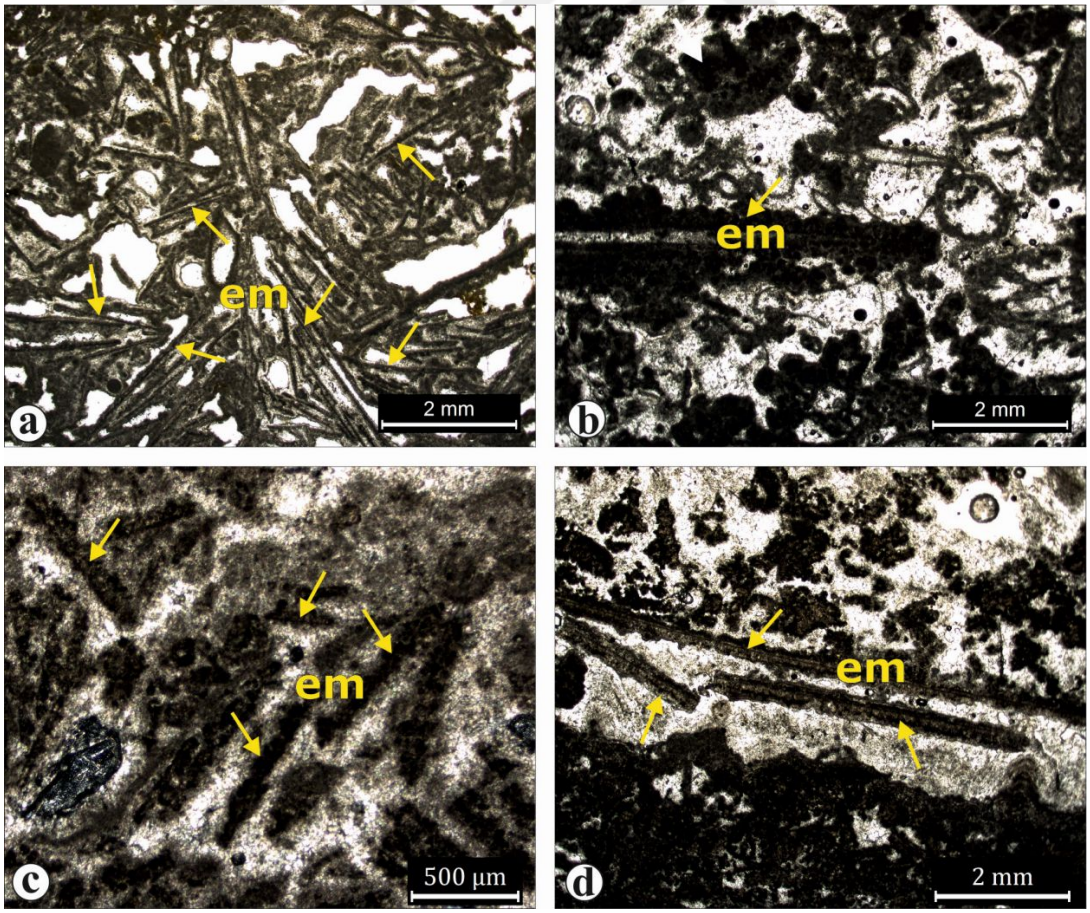


Figure 3.3. The microscopic images of encrusted micrite fabrics (yellow arrows) that surround the reed-like macrophytes under PPL. The images from sample: a. 113, b. 89.2, c.122-c, and d. 137.

The broken fragments of these encrusted micrite fabrics are observed at many levels within the sequence.

3.2.1.4 Intraclast (i)

Intraclasts are micritic, irregular shaped, angular clasts derived from the broken clotted micrite and/or microbial micrite fabrics. They are separated from other grains with their sharp corners and distinct edges. These fabrics take place at different levels of the sequence. It may indicate that the very shallow or dry periods of the lake.

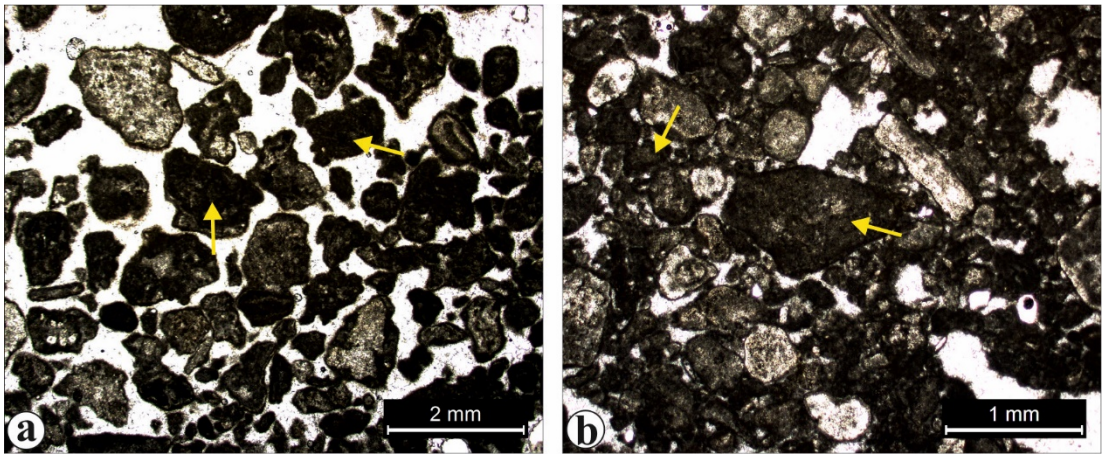


Figure 3.4 The microscopic images of intraclasts (yellow arrows) under PPL from thin sections of a. sample 69 and b. sample 92

3.2.2 Spar Fabrics and Facies

Spar fabrics are distinguished by their transparent crystals in the thin section. In this study, the spar fabric term is used for carbonate fabrics made up of spar calcite crystals ranging from 4µm to 1-1.5 cm and generally show interlocking boundaries. The spar fabrics and facies are classified as i) algal microspar-spar clump fabrics and facies, ii) encrusted spar fabric iii) spar carbonate fragments. Besides, spar fabrics fill the inta-frame pores of the clotted micrite and algal microspar fabrics and pores between the dendrites of shrub fabrics.

3.2.2.1 Algal Microspar-Spar Clump Fabrics and Facies (AMCF)

Algal microspar-spar clumps are initially formed by the biochemical precipitation of calcite or aragonite crystals in water due to cyanobacteria activities (Figure 3.5a, 3.5b). Algal microspar clumps formed by relatively slower precipitation than clotted micrite's deposition. This slower process probably causes the growth of initial micrite crystals and allows them to reach microspar size. Then these microspar clumps reach spar-sized by recrystallization because of the continuing activities of cyanobacterias (Figure 3.5c, 3.5d).

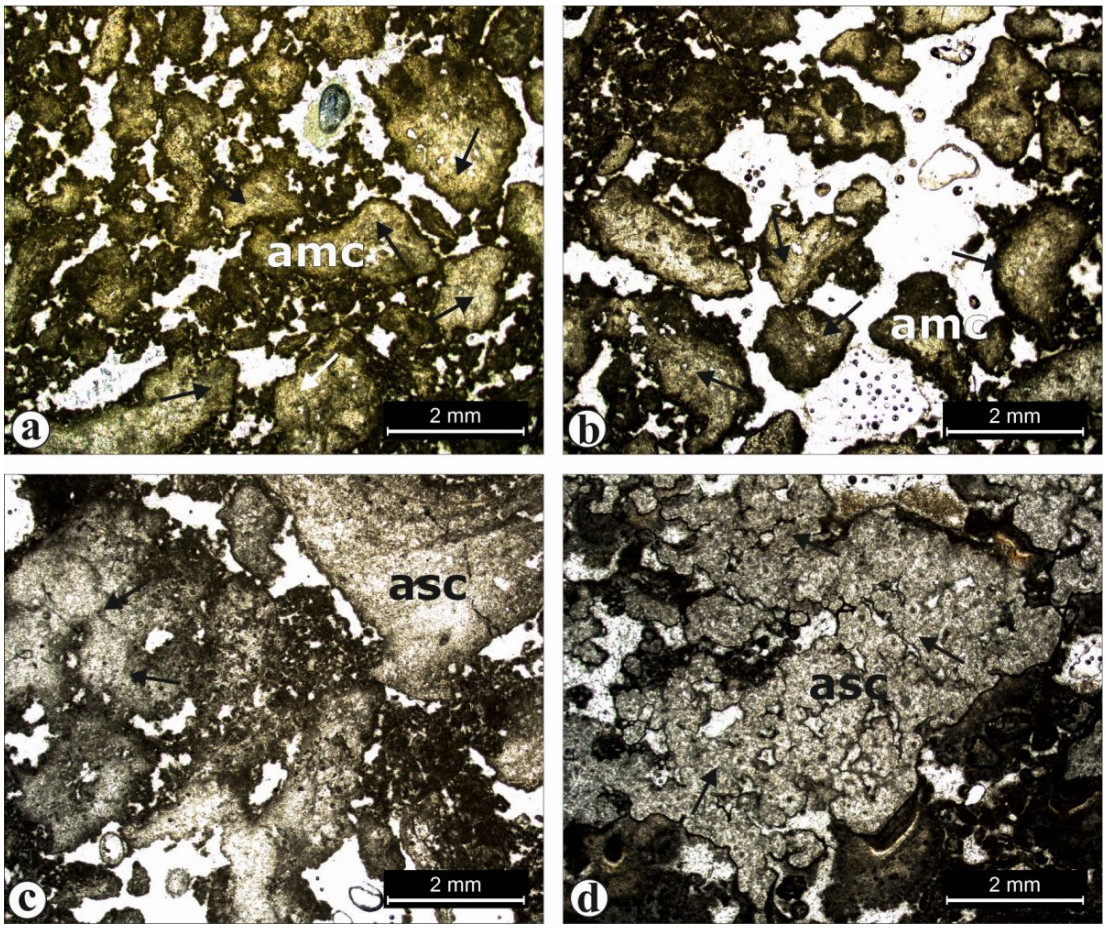


Figure 3.5 The microscopic images of algal microspar clumps (amc,black arrows) and algal spar clumps (ams) from a. sample 180 under cross-polarized light (XPL) b. sample 180 (PPL), c. sample 114 (PPL) and d. sample 128 (PPL). Sometimes the pores between these fabrics are filled by microbial micrite fabric or spar calcite cement secondarily

Due to the secondary activities of cyanobacteria, the pores between these fabrics may fill microbial micrite fabrics. These pores may also be filled the spar calcite cement. The laminas and thin layers composed of algal microspar clumps and empty and/or micrite or spar filling pores are named as “algal microspar clump facies”. These facies may indicate a relatively deep, stagnant, and large shallow lake environment.

3.2.2.2 Encrusted Spar Fabrics (es) and Facies

Encrusted spar fabrics are mostly microspar or spar laminas deposited on the stem or leaves of the reed-like tubular plants, macrophytes or any vegetative surface (Figure 3.6). These laminas may be flat or twisted and generally have teeth like crystals in one and/or two sides on the leaves of the plants.

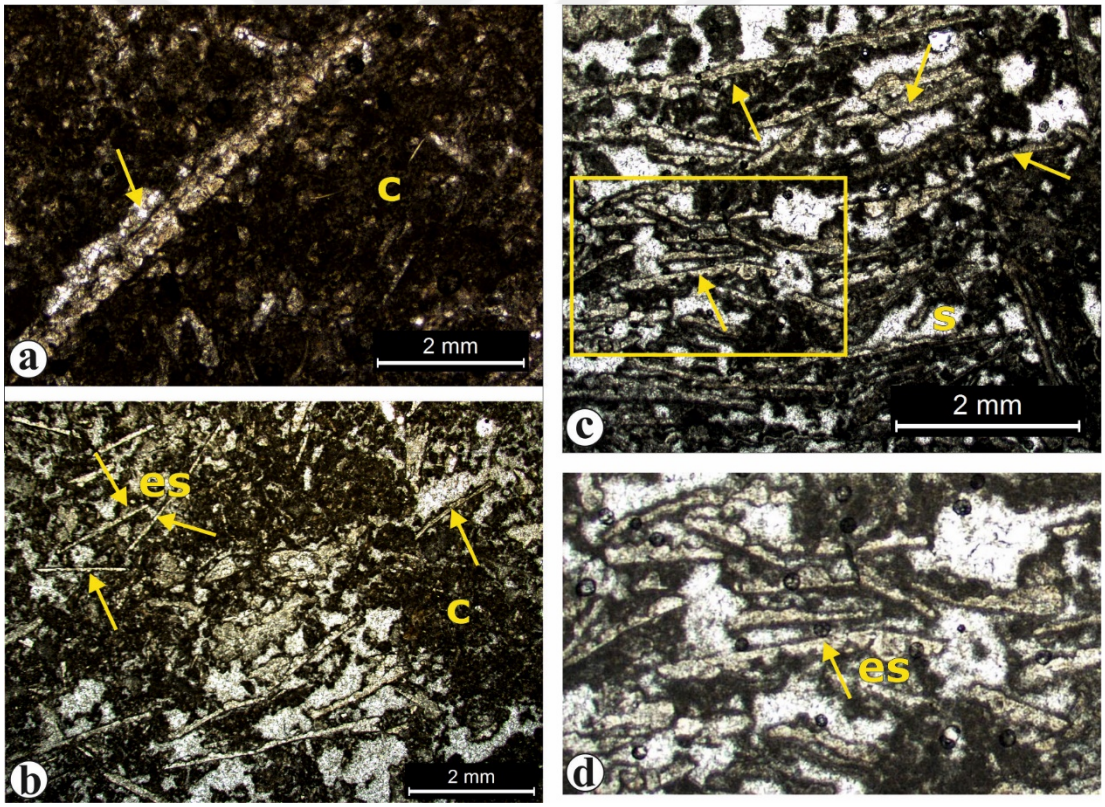


Figure 3.6 The microscopic images of the encrusted spar fabrics (es) (yellow arrows) under PPL from a. sample 159, b. sample 51-2, c. sample 126, and d. closeup view from c (yellow rectangle). c: clotted micrite, s: spar calcite cement

In some thin sections, these microspar fabrics were recrystallized and their lengths up to spar size. The fragments broken from these encrusted spar fabrics are widely observed at many levels within the sequence.

The layer or laminas composed of macrophytes encrusted spar fabrics, and empty or spar calcite filled pores are named as “macrophyte encrusted spar facies” (Figure 3.7). The encrusted spar fabrics are sometimes developed on the thin macrophytes. The layers and laminas composed of these fabrics with spar calcite cement and empty pores are named as “thin macrophyte encrusted spar facies (Figure 3.8).

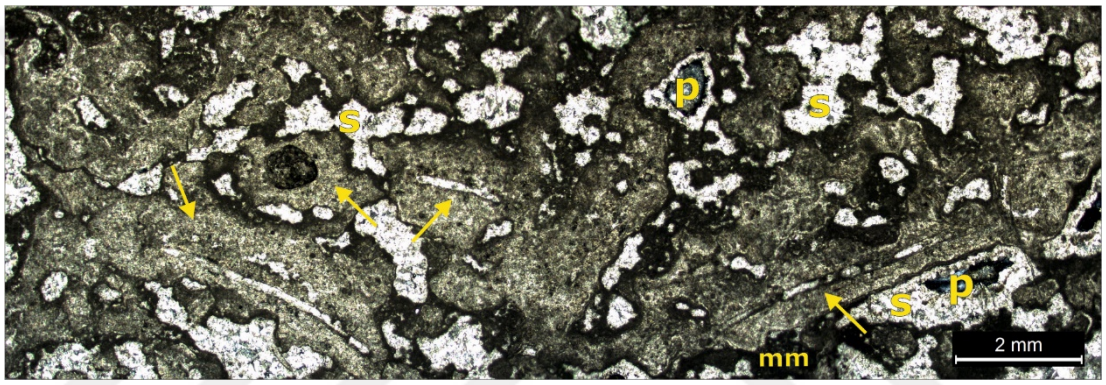


Figure 3.7 The microscopic images of macrophyte encrusted spar facies under XPL from sample 132. These fabrics are surrounded with thin black microbial micrite fabrics (mm). The white areas (s) are secondary spar cement between the macrophyte encrusted spar fabrics. The big pores may sometimes remain empty (p)

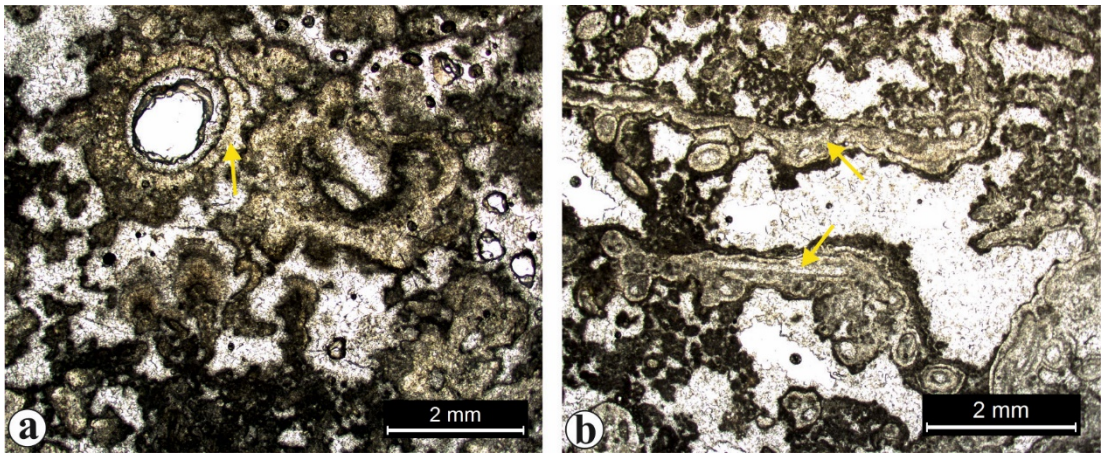


Figure 3.8 The microscopic images of thin macrophyte encrusted spar fabrics (yellow arrows) under XPL from sample 72 (a), sample 175 (b and d), and sample 169 (c)

3.2.2.3 Spar Carbonate Fragments and Fragmented Carbonate Facies (FCF)

The existing spar carbonate fabrics such as shells, shrub fabrics, algal spar clumps, etc. in the environment may break and fragmentize. It may be thought that temporarily drying or excessively shallowness of the lake environment causes this fragmentation. These spar carbonate fragments are surrounded by micritic envelopes (Figure 3.9). Layers and laminas including spar carbonate fragments, intraclast, and empty or spar calcite filled pores between these fabrics are named as fragmented carbonate facies (Figure 3.9). These facies may indicate the dry periods of the lake, this may because of the high evaporation.

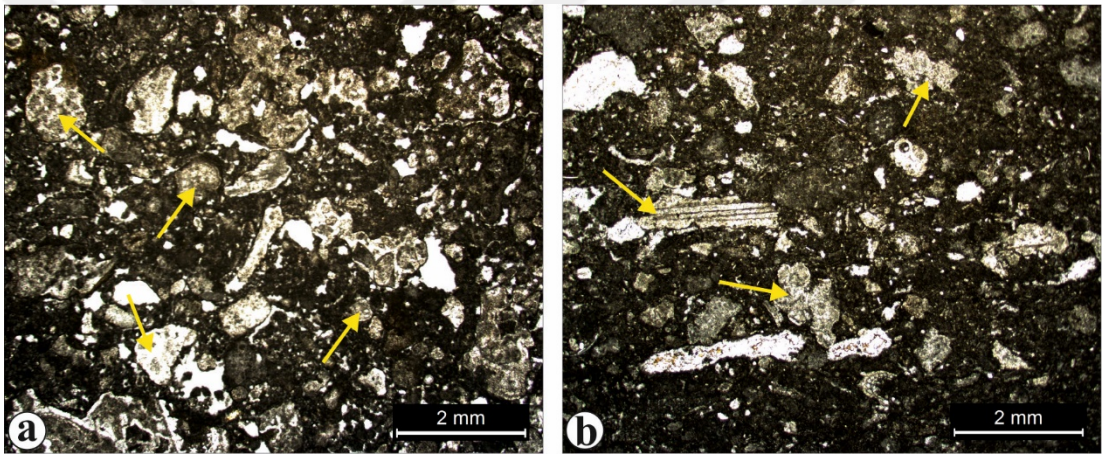


Figure 3.9 The microscopic images of the encrusted microspar-spar fabrics (yellow arrows) under PPL from a. sample 92, and b. sample 66

3.2.2.4 Intra-Frame Spar Fabrics

Intra frame spar fabrics are the spar cement, which was secondarily precipitated from the pore water in the intra-frame pores of the existing fabrics. These spar fabrics are classifed as i) clotted micrite intra-frame spar, ii) algal microspar clump intra-frame spar, iii) encrusted macrophytes intra-frame spar (Figure 3.10).

The spar cement precipitated from the pore waters in the intra-frame pores of the clotted micrite fabrics is named as “clotted micrite intra-frame spar”. While clotted micrite fabrics were being formed, pH droped and sedimentation decelerated because

of the depletion and calcification of the cyanobacterias as time progress. Meanwhile, due to the slow precipitation, spar calcite crystals began to precipitate in the existing pores. Large pores between the clotted micrite fabrics may remain partially empty (Figure 3.10a). Similarly, the secondary spar cement between the algal spar clump fabrics is named as algal spar clump intra-frame spar (Figure 3.10b) and secondary spar cement between macrophytes is named as macrophytes spar intra-frame spar (Figure 3.10c and d).

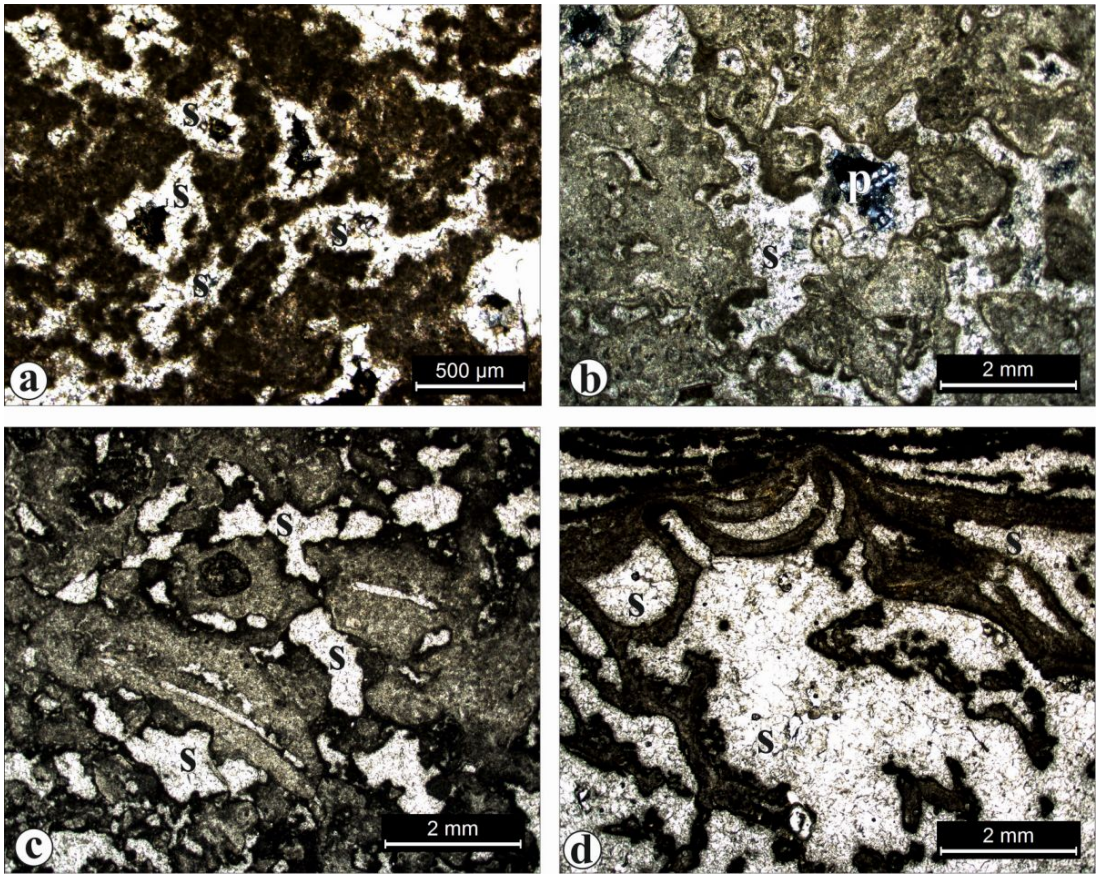


Figure 3.10 The microscopic images of the intra-frame spar fabrics under cross-polarized light (XPL) a. clotted micrite intra-frame spar fabrics from sample 56, b. algal mikrospar clump intra-frame spar fabrics from sample 61, c. and d. encrusted macrophytes intra-frame spar from sample 132, and sample 103, respectively (s: spar calcite cement, p: empty pore)

3.2.2.5 Inter Shrub Spar

The microspar-spar cement precipitated from the pore waters between the dentrites of the micritic shrub fabrics named as inter shrub spar, shown with yellow arrows in Figure 3.13.

3.2.3 Zoned Algal Fabric and Facies

Zoned algal fabric and facies are classified as i) zoned algal clump fabric and facies and ii) zoned encrusted algal fabrics.

3.2.3.1 Zoned Algal Clump Fabrics and Facies (ZAC)

Zoned algal clump fabrics are algal masses consisting of microbial micrite and microspar-spar with very thin laminas (Figure 3.11). These fabrics developed within a certain volume of water due to activities of cyanobacteria forming cluster-shaped colonies.

The layer and laminas consisting of these cluster-shape algal fabrics are named as “zoned algal clump facies”. These fabrics and facies are occasional in the sequence.

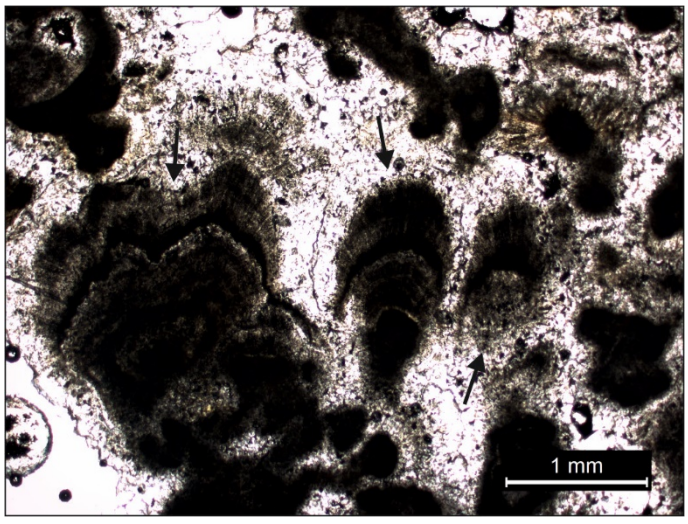


Figure 3.11 The microscopic images of the zoned algal clump fabrics (black arrows) under PPL from sample 80-1

3.2.3.2 Zoned Encrusted Algal Fabrics (ZEA)

Zoned encrusted algal fabrics compose of very thin alternation of microbial micrite and microspar-spar laminas that developed in big intra-frame pores (Figure 3.12). These fabrics are uncommon in the sequence.

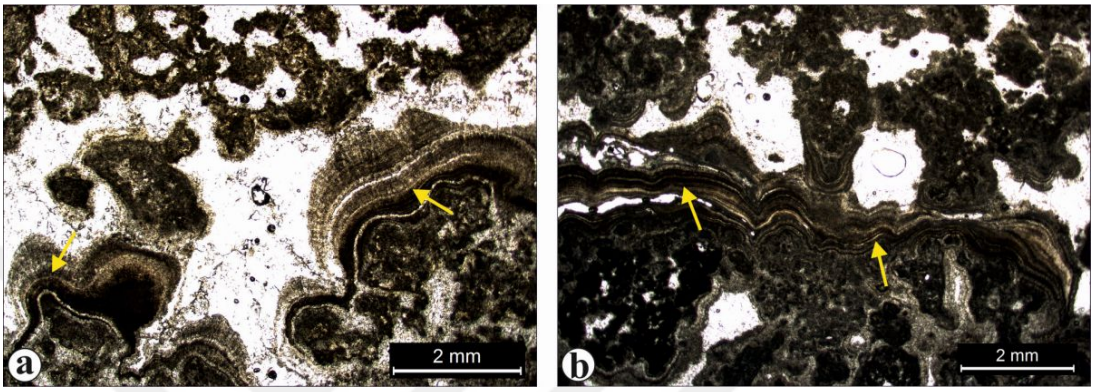


Figure 3.12 The microscopic images of the zoned encrusted algal fabrics (yellow arrows) under PPL from a. sample 54 and b. sample 116

3.2.4 Shrub Fabrics and Facies

The shrub fabrics are generally fanlike shapes or radial fabrics that grew away from the substrates. These fabrics and facies are classified as i) micritic quill-feather shrub fabrics and facies, ii) macrophyte spar quill shrub fabrics and iii) thin macrophyte spar quill shrub fabrics and facies.

3.2.4.1 Micritic quill-feather shrub fabrics and facies (MQFSF)

Micritic quill-feather shrubs are fan or rod shape, branching dendritic crystals formed by shrub-shape cyanobacteria (Figure 3.13). These fabrics have 1-2 mm wide and 2-4 mm in height. These cyanobacteria increase the pH (alkalinity) of the lake water by photosynthesis and cause rapid carbonate precipitation. These shrub fabrics have a porous framework. In this framework, depending on the depletion of the cyanobacteria while their phtosentesis, the precipitaion rate decreases, and spar calcite crystals start to precipitate from pore water. The thin layer or laminas consist of these

micritic shrub-shape fabrics and spar are named as “micritic quill-feather shrub facies”.

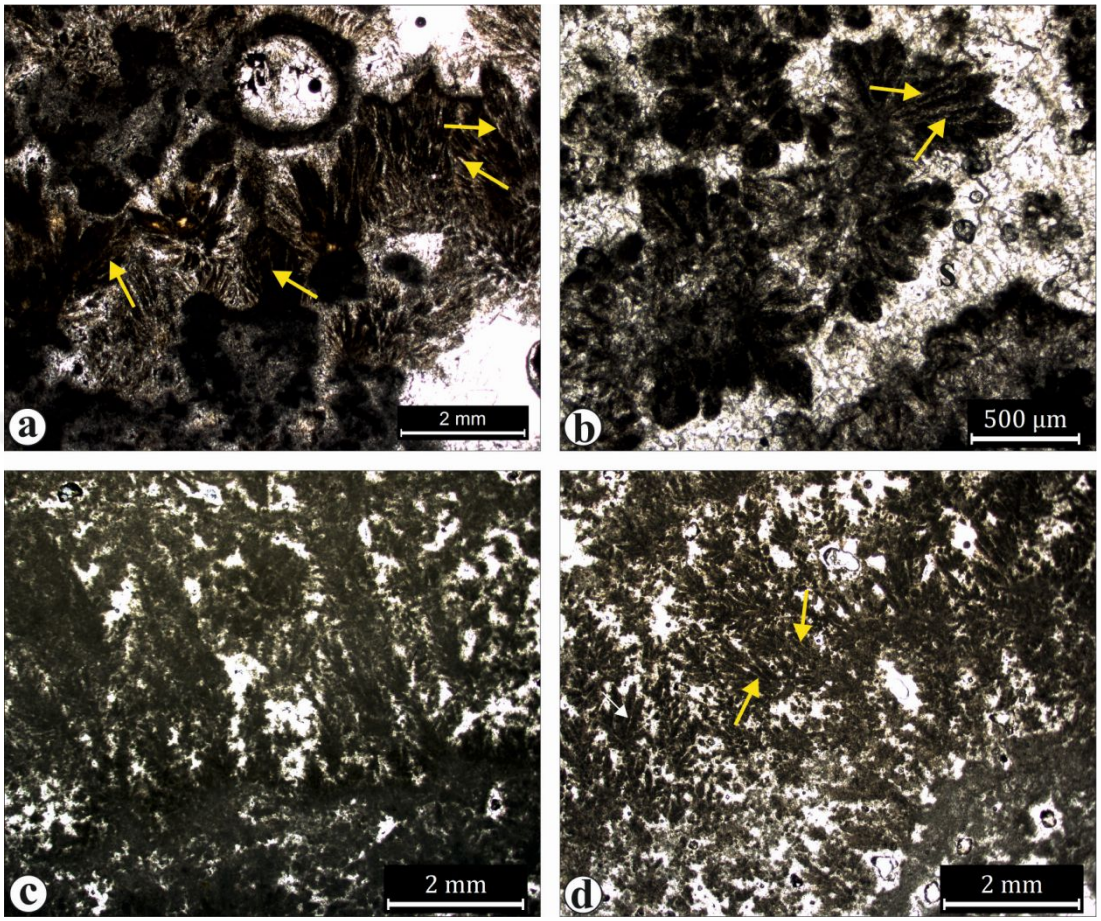


Figure 3.13 The microscopic images of micritic quill-feather shrubs from sample 80-1(a), sample 119 (b), sample 120-2 (c), and sample 121b (d). The micritic shrubs in figure a and figure b are wider and shorter, while others have thinner and taller dendrits. The white areas (s) are spar calcite crystals that secondarily precipitated the pores between these dendritic shrubs. Yellow arrows show the inter shrub microspar-spar fabrics

3.2.4.2 Macrophytes Spar Quill Shrub Fabrics and Facies (MCSQSF)

The macrophytes spar quill shrub fabrics were formed by recrystallization of micritic quill-feather shrub fabrics deposited on macrophytes (Figure 3.14). The layer or laminas including these fabrics are named “macrophytes spar quill shrub facies”. As these shrub fabrics continued to form, depend on their photosyntesis, they depleted over time as a result of their calcification. Then pH decreased and precipitation was

slowdown. Thus, the microspar-spar cement was precipitated from the pore waters between these dendrites.

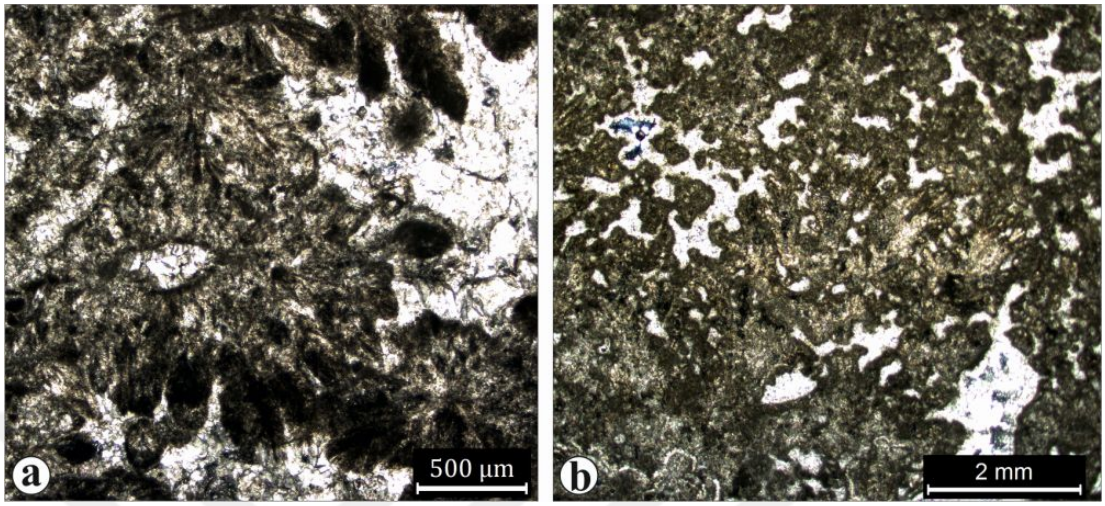


Figure 3.14 The microscopic images of macrophyte spar quill-feather shrubs a. thin section view of the sample 119 (PPL) and b. sample 61 (XPL)

3.2.5 Biological Components

The biological components of the travertine sequence are i) gastropods, ii) ostracods, iii) charophytas, and iv) macrophytes.

The gastropods are easily separated from other biyological components with their single, usually spirally coiled white spar calcite (Figure 3.15). The gastropods are relatively more common in the middle and upper parts of the travertine sequence.

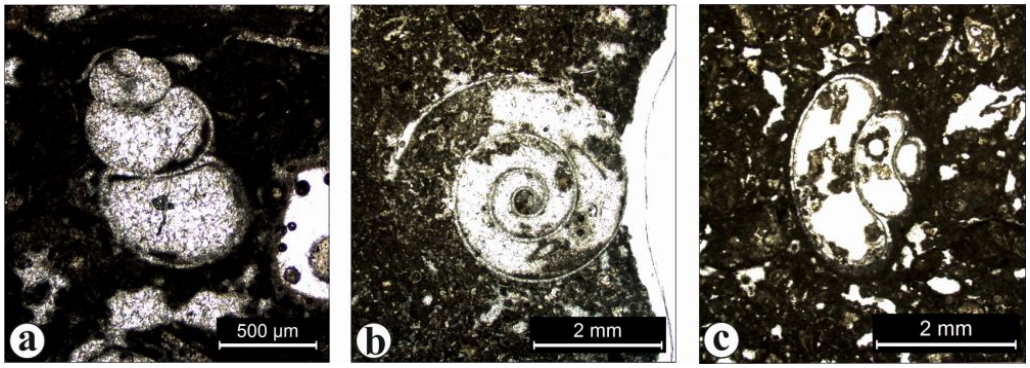


Figure 3.15 The microscopic image of gastropods under plane-polarized light from a.sample 126, b. sample 157, and c.sample 96

The ostracods have lens shape forms in their longituditional section and white calcite crust. Their sizes are generally between 500 µm and 2mm. The ostracods are rarely seen but are mostly observed in the middle and upper parts of the sequence (Figure 3.16).

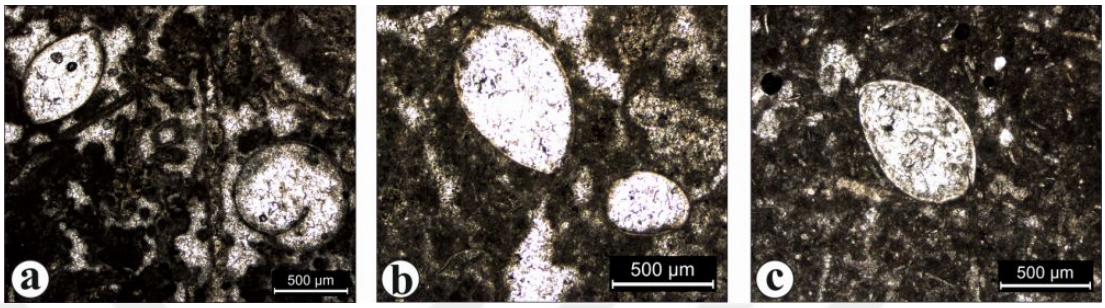


Figure 3.16 The microscopic image of ostracods under XPL from a. sample 126, b. sample 135 and c. sample 154

Charophytes are green algaes indicating freshwater-brackish conditions. They are very rarely seen in the middle-upper parts of the sequence (Figure 3.17).

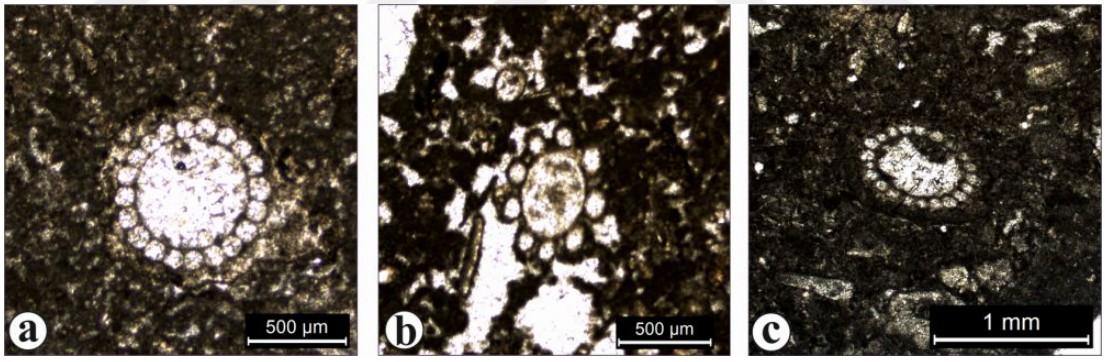


Figure 3.17 The microscopic image of charophytes under PPL from a. sample 62-1, b. sample 51-1, and c. sample 66

The macrophytes are reed-type tubular plants. These are very common, especially in the middle parts (Figure 3.18) and are observed some undefining macrophytes in the Yarılgan Hill section (Figure 3.19).

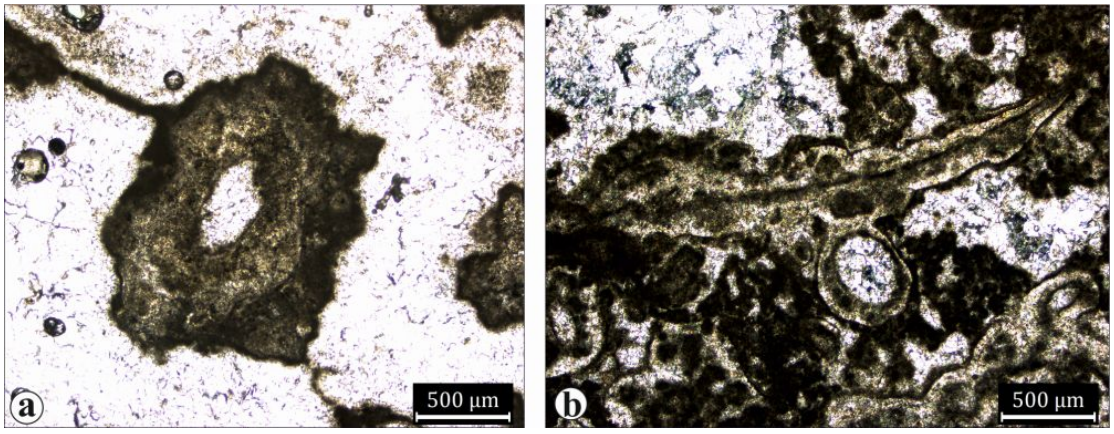


Figure 3.18 The microscopic image of macrophytes under PPL from a. sample 169 and b. sample 175

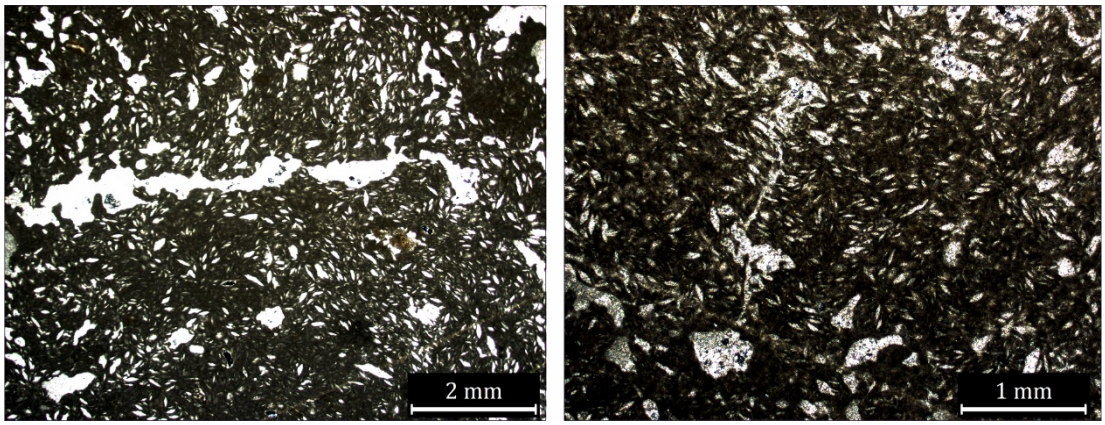


Figure 3.19 The undefining macrophytes from sample 197 under XPL

3.2.6 Cavities and Pores

The travertine sequence has several alternations of porous and non-porous layers in macroscopic scale. These macropores are generally reed-like tubular plants or small-scale cavities (Figure 3.20). The defining pores in the sequence are i) fenestral (shrinkage) pores, ii) gas pores, iii) intra organism pores, iv) intra-frame pores, and v) inter shrub pores.

3.2.6.1 Fenestral Pores

Fenestral pores are generally more or less parallel to the layering and thick at the middle parts and end up thining to the sides (Figure 3.21a). They were formed by the evaporation of the water inside the carbonate due to the fact that the environment was

very shallow or dry and the carbonate has not yet become lithified. These pores may sometimes have partly filled with secondary spar calcite crystals.



Figure 3.20 a. The view from the alternations of porous-non-porous laminas and b. reed-like tubular plants (yellow arrows) (Personal archive, 2014)

3.2.6.2 Gas Pores

Gas pores are generally gas escape pores which rise upward. They are thin at their bottom parts but bulging to the upper parts and end with tapering (Figure 3.21b). They were formed by the degradations of the organic matter in the organicaly rich carbonate mud. If the environment is shallow, these pores may be combined water vapor by evaporation.

3.2.6.3 Intra Organism Pores

The cavities of lacustrine gasttopods and the reed type tubular plants or macrophytes are named “intra-organism pores”. They were partially filled with spar calcite cement, which directly precipitated from pore water (Figure 3.21 c and d).

3.2.6.4 Intra-Frame Pores

These pores are classified as i) clotted micrite intra-frame pores, ii) algal spar clump intra-frame pores, and iii) macrophytes intra-frame pores.

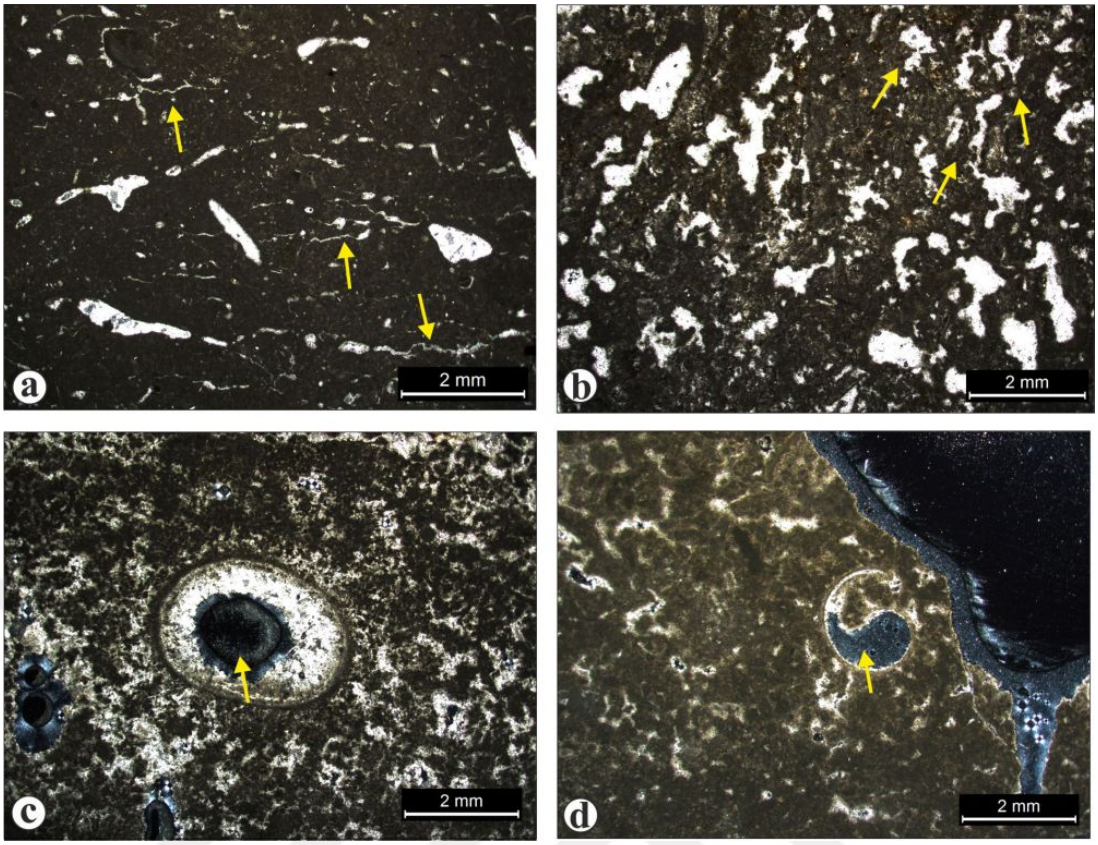


Figure 3.21 The microscopic images of pores. a. fenestral pores from sample 33 (PPL), b. Gas pores from sample 117 (PPL), c. inner pores of the gastropods from sample 90 and 118 (XPL), respectively

While clotted micrite fabrics precipitate directly from the lake water, they form a inter-frame. The pores between the clotted micrite fabrics in this frame are named as “clotted mcirite intra-frame pores” (Figure 3.22a). These pores were partly or fully filled by the secondary spar calcite cement. These spar crystals were directly precipitated from pore water and sometimes have recrystallization.

Similarly, algal spar clump fabrics make a frame when they are precipitated in the lake environment. The pores between the agal clumps in this frame are called as “algal spar clump intra-frame pores” (Figure 3.22b). These pores were partly or fully filled by the calcite cement after the algal clump fabrics deposition.

The shrub fabrics have also porous framework. The pores in this framework are called as “shrub fabrics intra frame pores” (Figure 3.22c). Sometimes, spar calcite crystals secondarily precipitated from pore water.

The stem, branch, and leaf of the reed-like tubular macrophytes form an organic frame in the environment of travertine precipitation. They participate in travertine precipitation and calcified themselves. They have relatively big pores in this frame. These pores are called “macrophyte intra-frame pores” (Figure 3.22d).

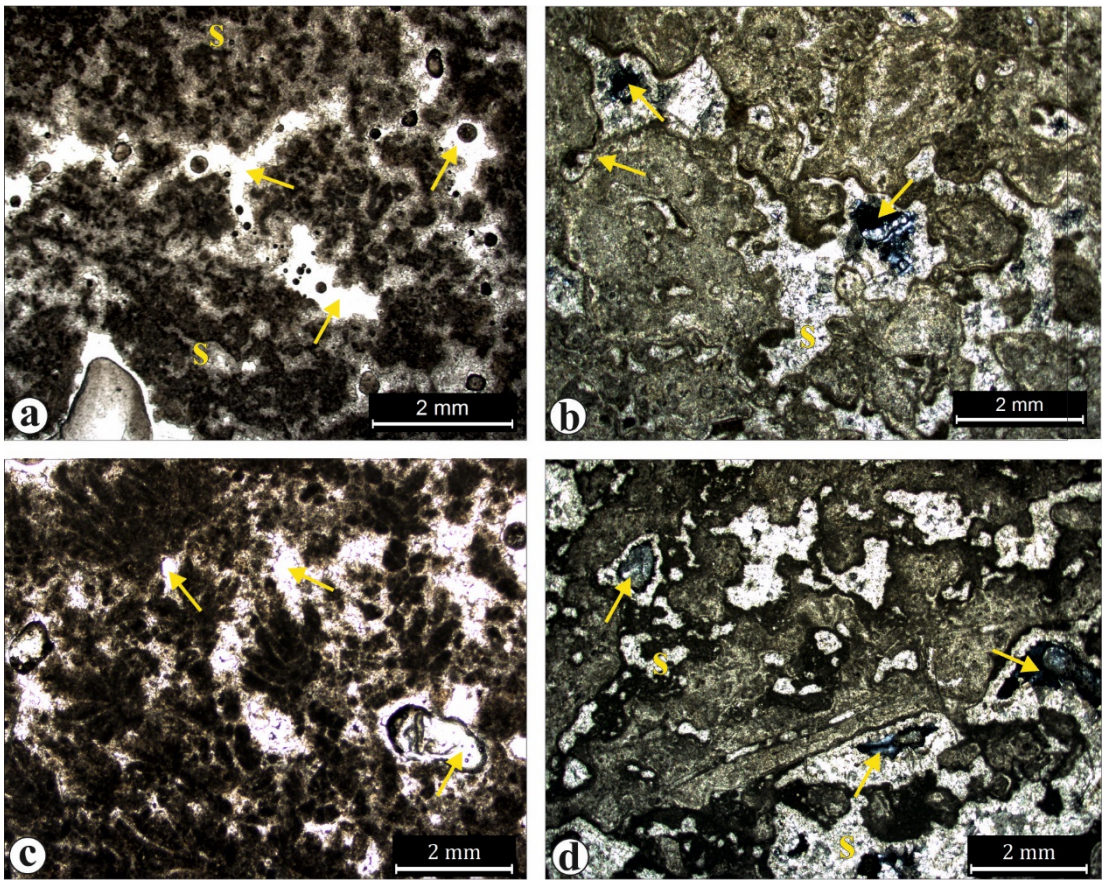


Figure 3.22 The microscopic images of intra frame pores (yellow arrows). a. clotted micrite intra frame pores from sample 77 (PPL), b. algal spar clump intra frame pores from sample 61 (XPL) c. intra frame pores of shrub fabrics from sample 121 (PPL), and d. macrophyte intra-frame pores from sample 132 (XPL)

3.3 Paleoenvironmental Interpretation

The carbonate fabrics, texture, and components made up of the travertine levels indicate that the deposits of this succession were accumulated in a shallow lake environment. The presence of the fossil organisms living in freshwater (lake) environments such as gastropods, ostracods, and charophytes and also reed-like tubular plants supports the lacustrine depositional environment. The fabrics and

components directly precipitated from lake water form the regularly or irregularly alternating facies (Figure 3.23). The entire travertine sequence is composed of the horizontal and vertical alternations of these facies. These alternations are probably related to cyanobacteria variations depending on changes of water thickness and water chemistry. It is considered that the absence of micro and macro terrace formations and slope deposits (inclined laminas) may support this environment.

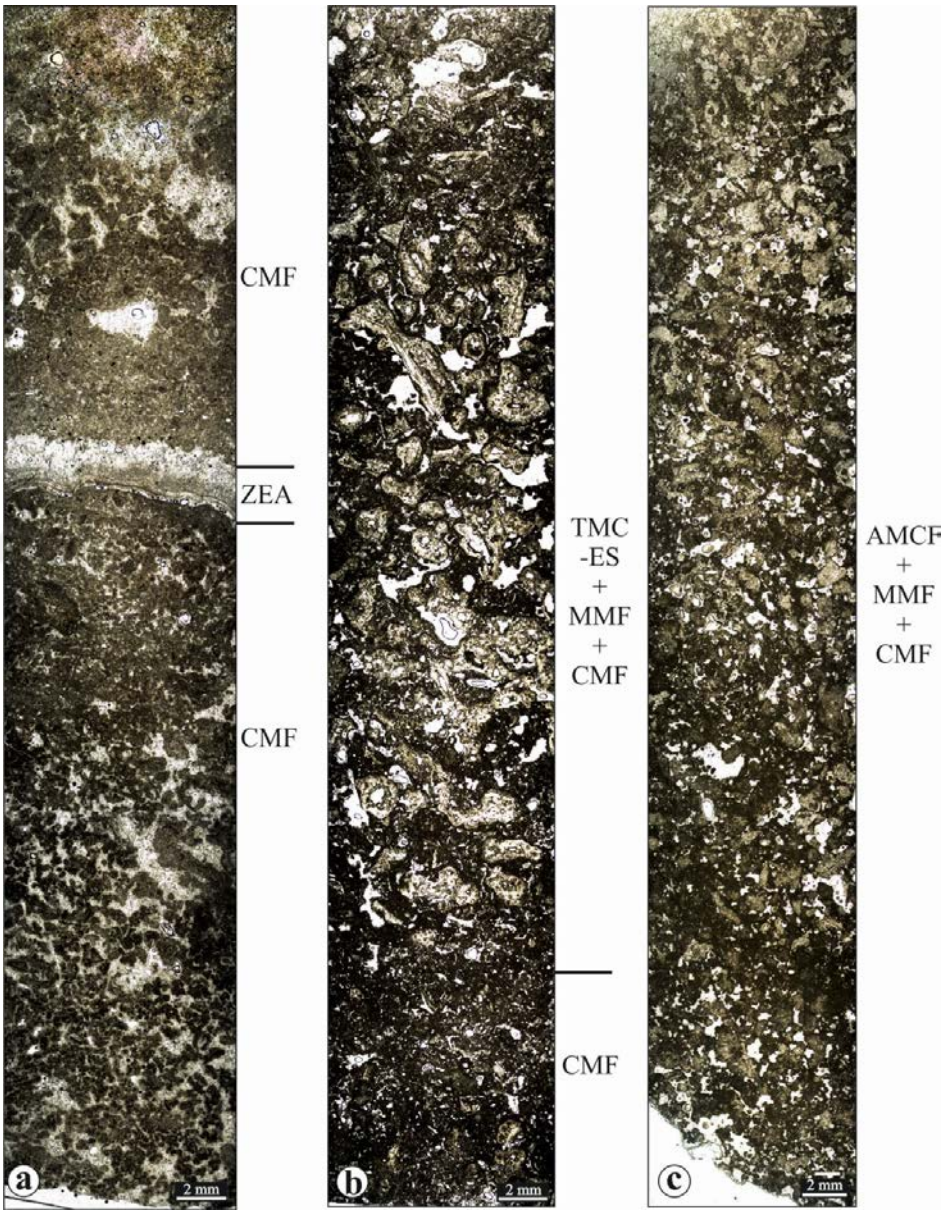


Figure 3.23 The examples of panoramic microscope images under plane-polarized light from a) sample 130, b. sample 93-2, and c. sample 187. CMF: Clotted Micrite Facies, MMF: Microbial Micrite Facies, ZEA: Zoned Encrusted Algal Fabrics, TMC-ES: Thin Macrophyte Encrusted Spar Quill Shrub Facies, AMCF: Algal Microspar Clump Facies.

Each facies represent typical depositional conditions of the lacustrine environments. The clotted micrite facies may indicate shallow lakes or water pools with relatively deep-water levels, the water of which can be warm or hot. The microbial micrite facies reflect a very shallow and calmer, and cyanobacteria rich lake environment, and possibly a hot groundwater inflow. The shrub facies and macrophyte spar quill facies imply a shallow lake, near to shore (litoral) and algal spar clump facies may indicate stagnant, shallow but relatively deeper parts of the shallow lake (sublitoral). The fragmented carbonate facies and fragments of encrusted micrite and encrusted spar fabrics may indicate that the lake water occasionally dried or become very shallow from time to time.

CHAPTER 4
STRATIGRAPHY OF THE GÖKTEPE TRAVERTINES

4.1 Introduction

In this chapter, vertical facies changes of the travertine sequence are interpreted by evaluating the panoramic microscope images and field observations. Detailed methodology was given in Section 1.2. We aim to reveal stratigraphic features of the travertine sequence observed in the Yarılgan Hill and Kepez Hill. We determined their vertical facies changes by panoramic views of the thin sections.

The travertine-type lacustrine carbonates are generally horizontal. The sequence is predominantly yellowish beige, has a light brown-beige and pinkish color at some levels (Figure 4.1). The benches generally consist of micrite fabrics dominated facies. The benches are generally laminated and slightly porous, but in some levels the void ratio increase. The frequency and dimensions of the voids are also variable. The cavities of reed fossils are frequently encountered. Gastropods and charophytes are relatively abundant at some levels but are occasional in general. The four paleosol levels are observed in the sequence. These levels indicate that the travertine precipitation from the lake water decreased or stoped from time to time.

4.2 Yarılgan Hill Section

The sequence measured from the Yarılgan Hill is under the travertines that formed the uppermost part of the sequence (Kepez Hill). Here, a succesion of about 35m was measured with 30 samples (Figure 4.1a). The expansive fractures related to landslide are followed at several parts of the hill (Figure 4.1b and c). The travertines are yellowish beige but some levels have pinkish and light brown-beige color (Figure 4.1d).

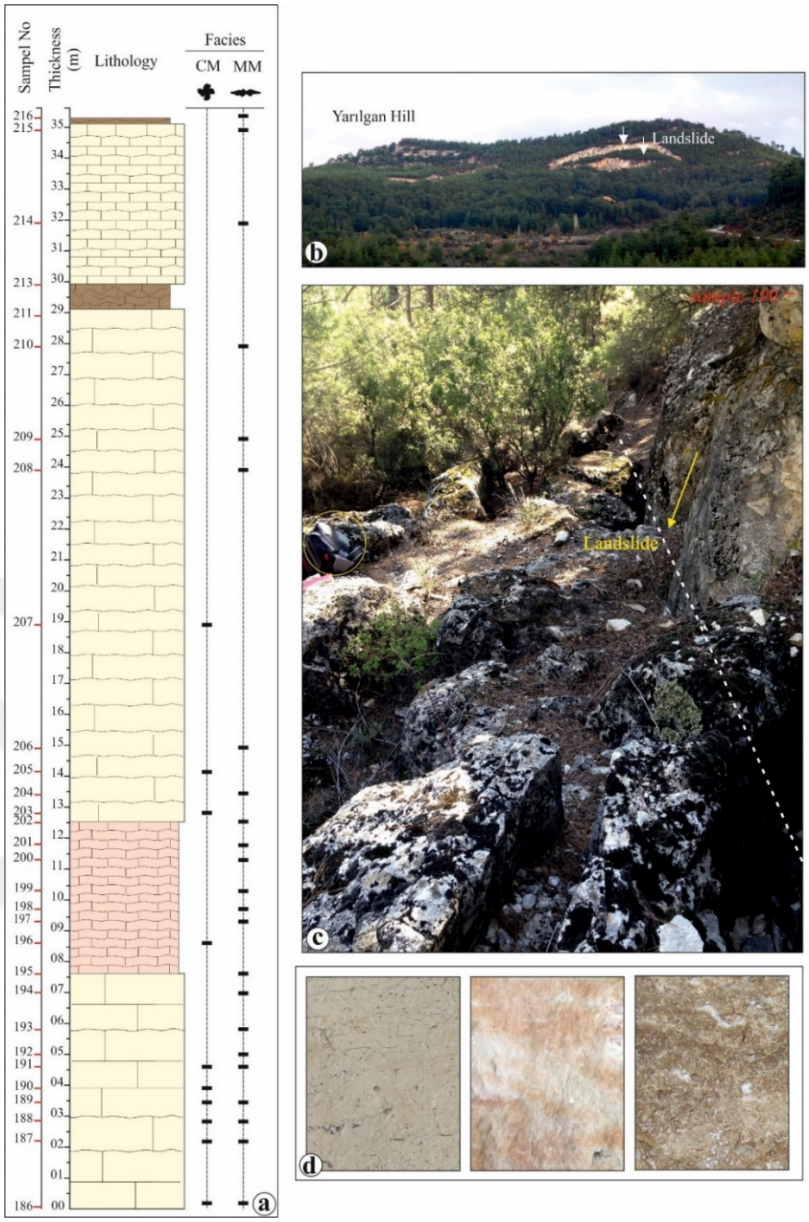


Figure 4.1 a. The measured section of the Yarılgan Hill, b. the view of the Yarılgan Hill and landslides, c. the fractures on the bottom have related the landslides and are seen several parts of the hill. d. examples of beige, pinkish and brown (from left to right) levels of the sequence shown in the measured section (a) (CM: Clotted Micrite, MM: Microbial Micrite) (Personal archive, 2015)

The sequence is composed of clotted micrite and microbial micrite facies (Figure 4.2). Gastropods and charophytes occur at the lowermost and uppermost levels of the sequence. The pore ratio is high at some levels. Geopetal structures are noticeable at almost all levels of the sequence (Figure 4.2).

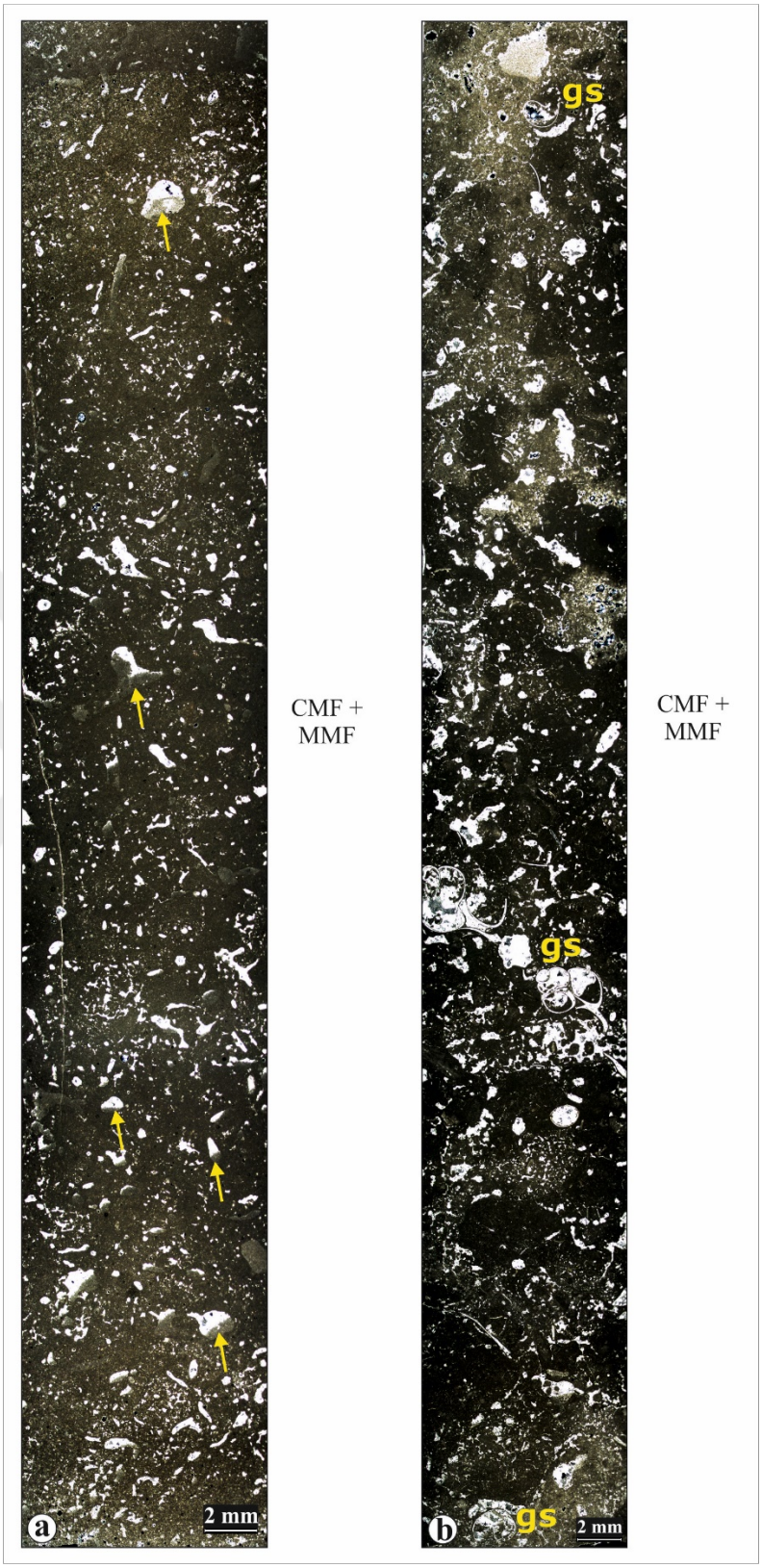


Figure 4.2 The panoramic microscope images under XPL. The images show the clotted micrite facies and microbial micrite facies with geopetal structures (yellow arrows) and gastropods (gs) from a. sample 191 and b. sample 213

The deposits of the first 7 m of the sequence measured on the Yarılgan Hill are yellowish cream-colored. The lower levels of this 7m include gastropods and charophytes. At the middle levels, clotted micrite facies and microbial micrite facies indicating a very shallow lake environment are dominant. There are pinkish-cream non-fossiliferous travertine levels between 7m and 13m of the sequence. In these levels, clotted micrite facies were observed limitedly. Cream travertines are again dominant between 13m and 28m. Fossil contents are limited. The geopetal structures increase through upper parts. Dark-brown travertine levels including gastropods and charophytes are dominant between the 25m-35m, the uppermost part of the sequence. Although this dark color may indicate a microbial effect, it is considered that whole sequence was deposited in a very shallow lake.

4.3 Kepez Hill Section

There is an abondend travertine quarry on the Kepez Hill (Figure 1.3 and 4.3). Travertines up to 80 m thick were quarried in eight benches and the height of each of benches changes from 4 to 10 meters (Figure 4.4).

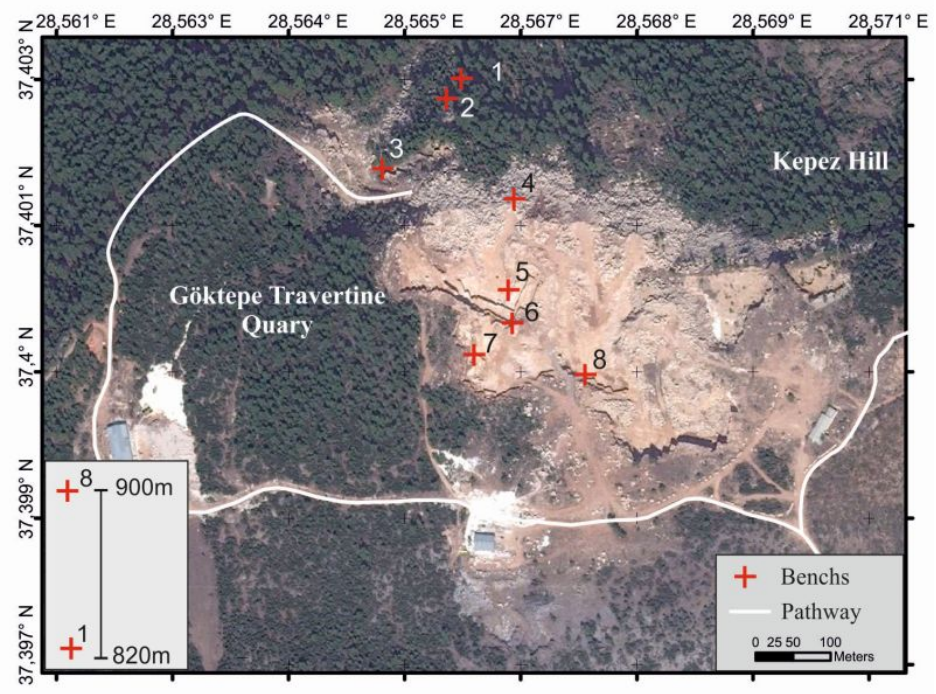


Figure 4.3 The bird-eye view from the 8 benches of the travertine quarry on the Kepez Hill

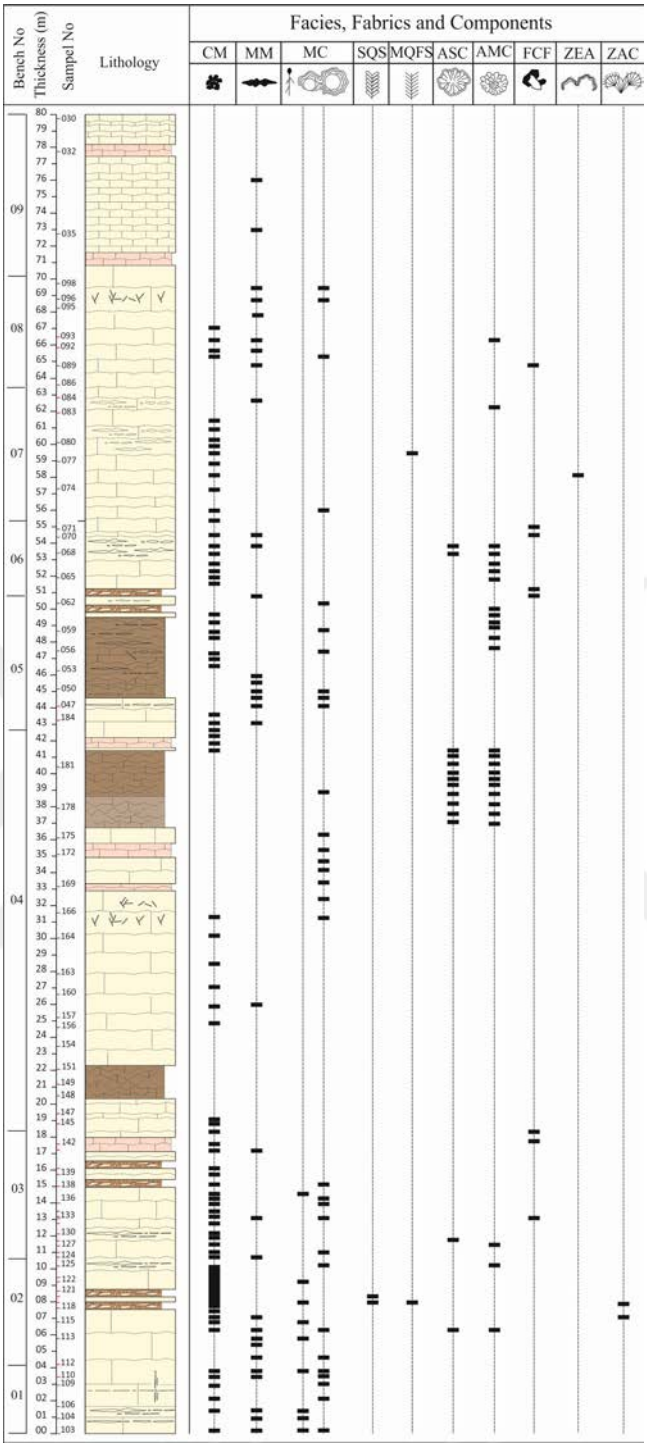


Figure 4.4 The section shows the benches, sample locations and travertines of different colors and textures. Facies, fabrics and the components in related levels of the travertine sequence were also given in columnar section (CM: Clotted Micrite, MM: Microbial Micrite, MC: macrophytes, SQS: Spar Quill Shrub, MQFS: Micritic Quill Feather Shrub, ASC: Algal Spar Clump, AMC: Algal Microspar Clump, FCF: Fragmented Carbonate Facies, ZEA: Zoned Encrusted Algal Fabrics, ZAC: Zoned Algal Clump

The first bench of the the travertines is represented the first 4.20 m of the sequence. (Figure 4.5). The sequence of the bench is generally yellowish cream, parallel or sometimes wavy laminated, and has a few and thin pores. The lower levels of the bench sequence have very few pores but in the middle parts, the pores small and thin in the lower and bigger through the upper parts. The upper levels of the bench sequence relatively have fewer pores and generally look massive. We took 10 samples from this bench (samples 103-112).

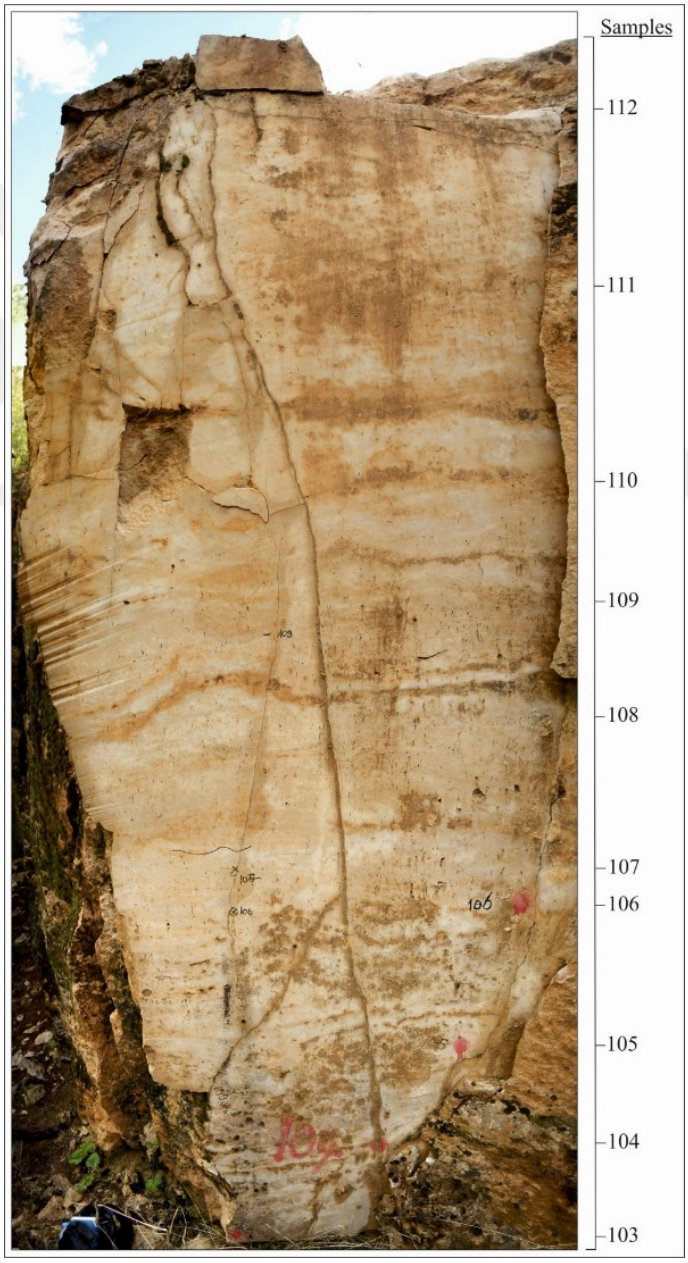


Figure 4.5 The view from the first bench sequence of the quarry and sample locations. The bench thickness is 4.20 m. (Personal archive, 2015)

This bench is dominantly composed of clotted micrite facies. In the middle and upper levels, microbial micrite facies accompany to clotted micrite facies. The macrophyte facies are observed with microbial micrite facies in the lowest and uppermost parts of the bench.

The second bench is represented a 6 m part of the sequence. Here, travertines belonging are generally cream clored and laminated. There are two different paleosol levels (about 20 cm each) in the middle and upper parts of this bench (Figure 4.6). We took 13 samples from this bench.



Figure 4.6 The view of the second bench sequence of the quarry. There are two paleosol levels (black arrows) are seen in the bench. The thickness is 6 m. (Personal archive, 2015)

The dominant facies are clotted micrite and microbial micrite facies. Shrub facies are firstly seen in this part of the sequence. The bottom parts of the bench sequence generally composed of microbial micrite and clotted micrite. Besides, macrophyte facies are appeared in some levels. There is a thick clotted micrite facies level in the middle part, on top of which there is a paleosol level with a thickness of about 30 cm. On top of this paleosol level, microbial micrite facies are dominant but sometimes shrub facies are observed. Another paleosol level overlies these facies. At the top, microbial micrite facies are seen together with macrophyte facies. The bench sequence ends with algal microspar clump and fragmented carbonate facies.

The third bench of the travertines is represented a 8 m part of the sequence (Figure 4.7). We took 23 samples from there. The lower beds of this bench sequence are cream-colored and have few-thin pores, small and medium sized (1- 5mm). However, some levels of upper parts exhibit pinkish colors. The middle levels of the bench there are intercalations of multiporous laminas and thin, few, and small porous laminas. This bench has two main paleosol levels establishing generally parallel but sometimes wavy laminas. Oblique reed pores are occasionally striking.

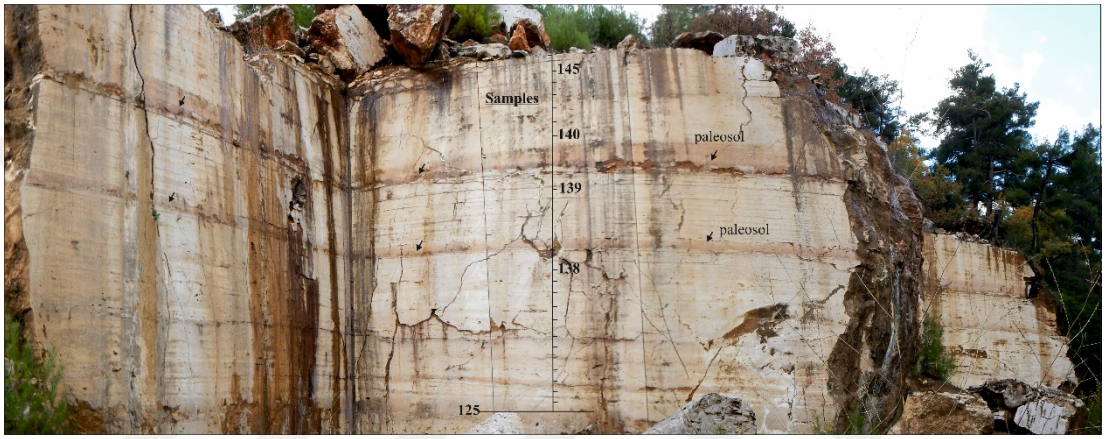


Figure 4.7 The view of the third bench of the quarry and sample locations, paleosol levels (black arrows). The bench thickness is 8 m. (Personal archive, 2015)

The bench sequence generally composed of clotted micrite facies. There are algal microspar clump facies in the lower parts, but they are uncommon. Rare and few quill-feather shrub facies take places in the middle parts. The top of the bench sequence is composed of fragmented carbonate facies. It may indicate another discontinuity of the travertine sequence.

The fourth bench is actually a big waste field located between the upper benches and these three lower benches. The thickness is about 24 m in total (Figure 4.8). 40 samples (samples 145-184) were collected from the waste area below the waste material in which exposures are suitable. Because of the waste materials, we could not do any macroscopic observation. The color of the samples is generally cream but some samples have pinkish color and some of them, unlike the lower benches, have a light brown color. The macrophyte facies start with these color changes and pass to dark brown colors in the upper parts with algal spar clump facies.



Figure 4.8 a. Views from the waste area, b. shows the suitable surfaces (right) that we used for sampling (Personal archive, 2015)

This bench starts with fragmented carbonate facies but predominantly is made up of clotted micrite facies throughout 9 m. The microbial micrite facies are rarely seen at 23-24 meters of the sequence. Subsequently, macrophyte facies are common for the next 4 m. Algal spar clump facies overlay these facies and at the last two meters, thick clotted micrite facies become dominant again.

The fifth bench starts from the 43 meters of the sequence and is represented 7 m of the sequence (Figure 4.8). We took 12 samples from these levels. Two different types of travertine levels are clearly observed (Figure 4.8a). While the lower parts are generally cream, massive, or have thin few porous laminas, after about two meters the color of the travertine darkens to brown and the void ratio greatly increases. This brown level is about 2 m and contains a large number of plant remains. The dark color and plant fossils continue for 3m above it, but the ratio of void decreases. After about 50 m, cream beige travertine starts again with the sixth bench (Figure 4.9).

The first 2 meters of the bench sequence have gray-cream color and slightly thin and small pores with the clotted micrite facies and microbial micrite facies. Along with the macrophyte facies, the sequence pass to dark brown color. The size of the pores of

the plants increases for the next 2m. Microbial micrite facies and macrophyte facies coexist in these levels. Algal microspar clump facies and clotted micrite facies, along with macrophyte facies are dominant over the next 3 m.

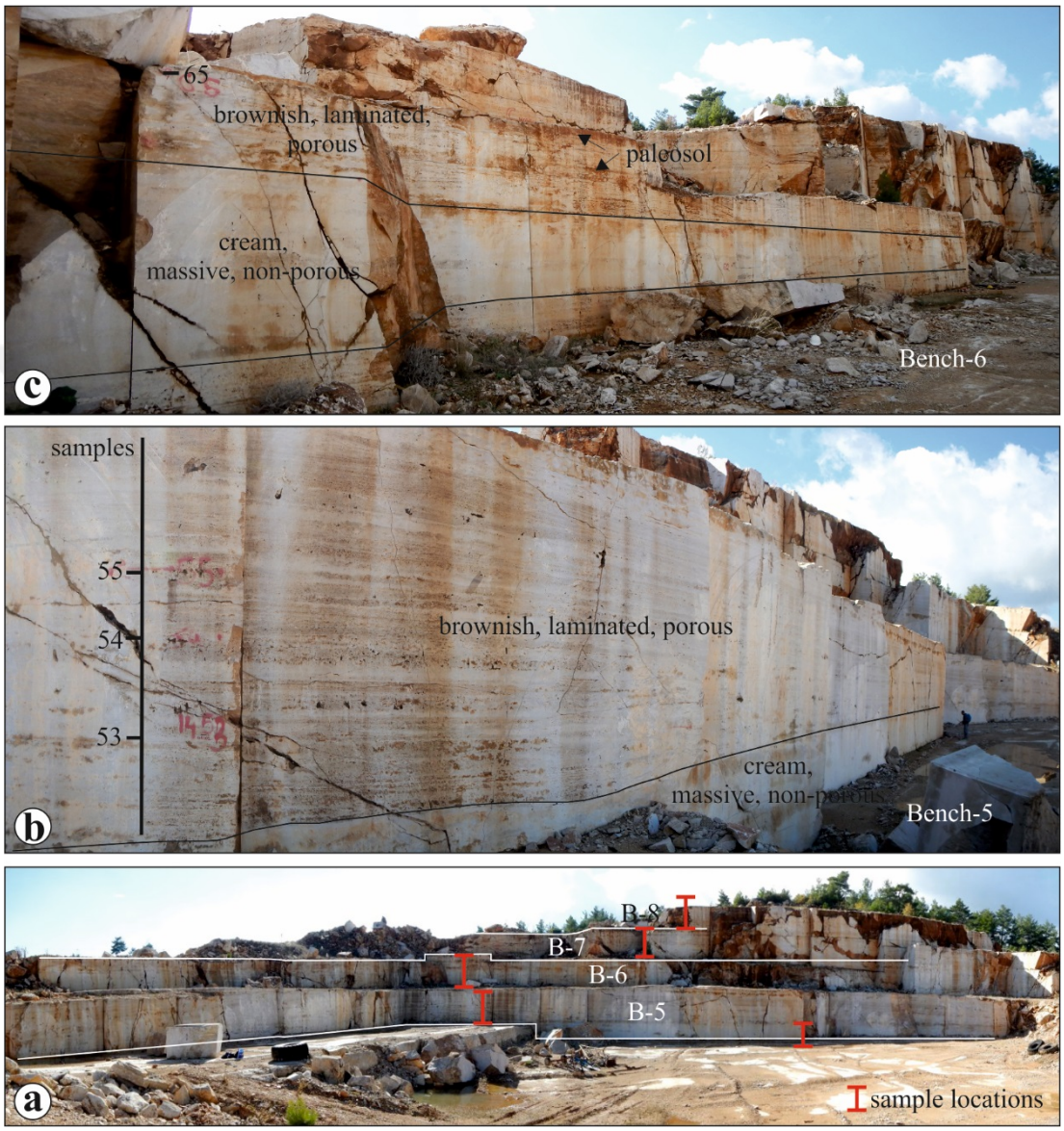


Figure 4.9 a. The general view from the benchs of 5, 6, and 7, b. closer view from the bench-5 c. closer view from the bench-6 (Personal archive, 2015)

After these levels, there are again alternations of massive and medium-sized porous, laminated beige travertine levels with similar microfacies content throughout 2 m in sixth bench (Figure 4.9c). There are two thin paleosol levels in the upper parts of this

bench. On top of these paleosols fragmented carbonated facies and microbial micrite facies occur.

The seventh bench is approximately 4 m thick. This part is represented a 4 m part of the sequence and generally cream and massive but sometimes has few pores (Figure 4.10). There is a 2 m thick porous level at the middle parts of the bench including a medium- and large-sized pores. We took 8 samples (sample: 66-73) from the seventh bench sequence.

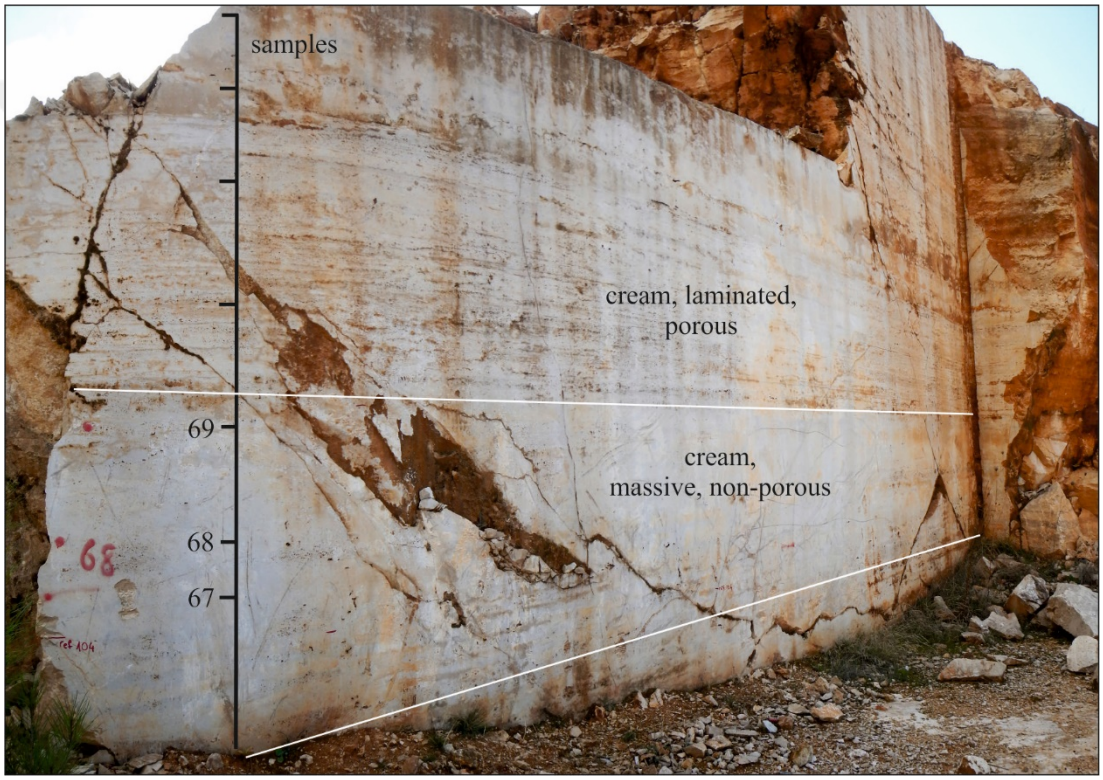


Figure 4.10 View from the seventh bench sequence (Personal archive, 2015)

The bench starts with the fragmented carbonate facies and continues predominantly with clotted micrite facies and algal microspar clump facies in the next 3 m. After these levels, macrophyte facies are seen in one sample. The last meters of the bench exhibit microbial micrite facies, fragmented carbonate facies, and locally algal microspar facies. The top of the bench consists of clotted micrite facies.

The eighth bench is about 9 m thick and generally gray-cream colored, few and small-spaced laminas but the middle and upper parts include fine and dense porous levels. We took 18 samples (sample: 74-91) from these levels. (Figure 4.11).

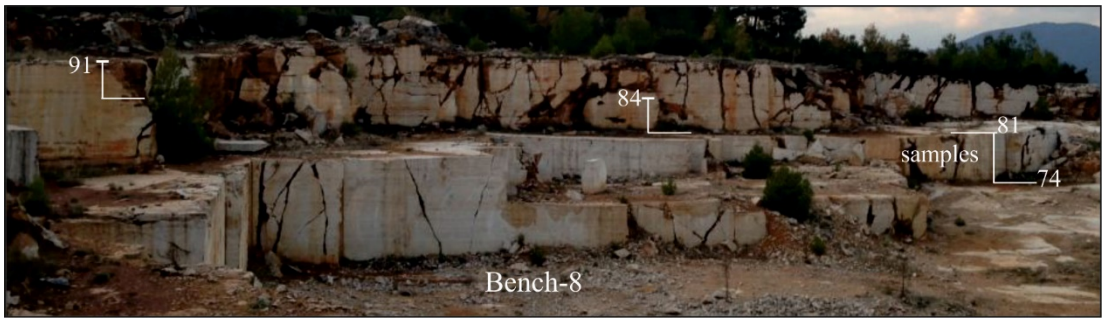


Figure 4.11 View of the eighth bench sequence and sample locations (74-91) (Personal archive, 2015)

The first 6 m of the bench mainly consist of clotted micrite facies. At the bottom parts of the bench macrophytes and zoned algal clump fabrics are rarely seen. Macrophyte spar quill facies are also seen in one sample at the middle levels of the bench. The last 5 m of the bench start with algal microspar clump fabrics and continue predominantly with the clotted micrite fabrics and microbial micrite fabrics.

The ninth bench, which is very thick, corresponds to the uppermost part of the sequence and is located in the eastern part of the Kepez Hill. (Figure 4.11). The lower levels of this part were sampled from the western side of Kepez Hill. Thus, we just sampled upper parts of this level and took 9 samples (sample: 92-100) from this part. Other samples were taken from the highest parts of the Kepez Hill.



Figure 4.12 View from the eastern bench of the Kepez Hill travertine quarry. This bench is at least 15 m in thicknes (Personal archive, 2015)

The bench is generally composed of an alternation of clotted micrite facies, microbial micrite facies, and fragmented carbonate facies. There are macrophytes facies at the uppermost part of the bench. Going further east of the sequence, microbial micrite facies become common on the Kepez Hill.

4.4 Paleoenvironmental Conditions

The preceding descriptions of the microfacies characteristic of the Göktepe travertines and fossil contents allow us evaluate the paleoenvironmental settings in the basin during the Middle Pleistocene.

The first 5 meters of the sequence consist mainly of clotted micrite facies, macrophyte facies, and their fragments and infrequently microbial micrite facies. The shrub facies represent very shallow parts of the lake but clotted micrite facies and algal spar facies indicate the relatively deeper parts of the shallow lake environment and possibly a hot groundwater inflow. These levels indicate very shallow lakeside (littoral) environment.

The 5-20 meters of the sequence contain clotted micrite facies and rarely shrub facies and a small amount of microbial micrite facies. Algal microspar facies appears at some levels as well. These levels may indicate a shallow but relatively deep, offshore facies.

Until these 20 meters of the sequence, there are four paleosol levels. Their distinct reddish color and fragmented texture indicate the excessive decrease of the water level or dry season for the lake environment. Travertine precipitation was disturbed and they were fragmented.

Clotted micrite facies along with a small amount of microbial micrite facies are dominant between 20 m and 30 m of the sequence. This may indicate the shallow lake where the water level was relatively high.

The next 30-35 meters of the sequence macrophyte facies appear again. This shows the littoral part of the lake but at the 35-43 meters of the sequence, algal microspar facies is dominant. These facies indicate a high-water levels, a more stagnant and relatively deep lake environment.

The 43-65m of the sequence starts predominantly with microbial micrite facies but clotted micrite facies is also quite common. Algal microspar facies and macrophyte facies, and their fragments still occur. At the 65-68 meters, fragmented carbonate facies along with some clotted micrite facies become dominant. This may indicate that travertine deposition decreased significantly from time to time due to a change in water chemistry.

The upper parts of the sequence (from 68 m to 80 m) mainly composed of microbial micrite facies and macrophyte facies which may display a stagnant and widespread shallow lake environment.

4.5 Lacustrine Depositional Model

Travertines are horizontal and laterally continuous and deposited in shallow lake environment (Figure 4.13). We consider that vertical facies changes are related to cyanobacteria variations related to fluctuations of water level (due to changes in temperature and rainfall), change in water chemistry, and their joint relationships. A few porous and relatively massive levels of the travertine are generally cream colored but more porous a paralel or wavy laminated levels have more dark color which is related to a high organic content of the lake. Some erosional surfaces cut the sequence in different levels. These several paleosol levels are evident as encrusted micrite-spar fragments and fragmented carbonate facies in the thin section. These indicate that the lake water occasionally dried or become very shallow and deposition stopped time to time. Thus, we conclude this lake may frequently dry up and refilled due to climatic changes (temperature and precipitation).

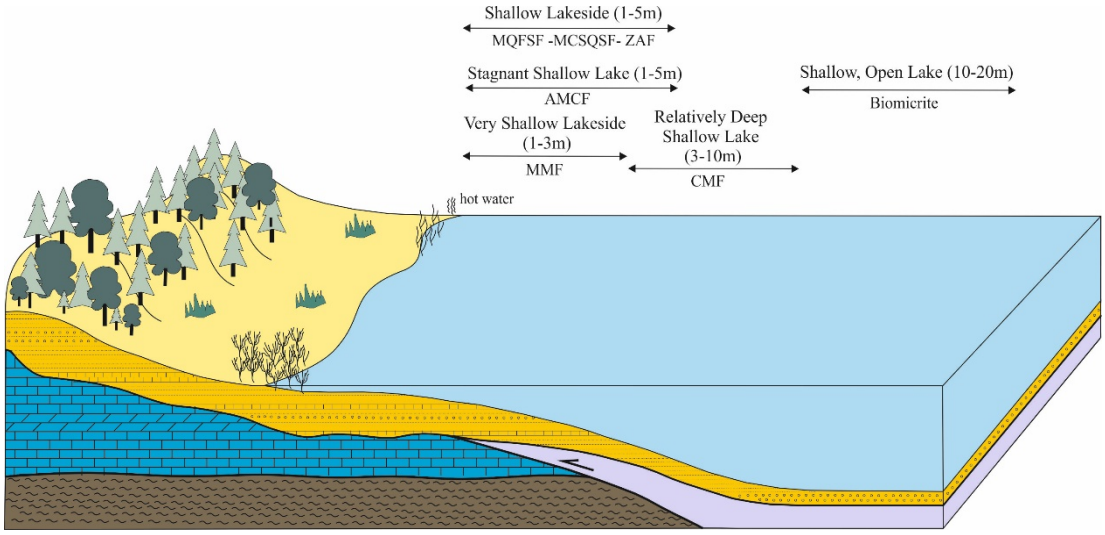


Figure 4.13 The lacustrine environmental model for the depositon of the travertine sequence (CMF: Clotted Micrite Facies, MMF: Microbial Micrite Facies, AMC: Algal Microspar Clump Facies, MCSQSF: Macrophytes Spar Quill Shrub Facies, MQFSF: Micritic Quill Feather Shrub Facies, ZAC: Zoned Algal Facies

CHAPTER 5
STABLE ISOTOPE ANALYSIS OF THE GÖKTEPE TRAVERTINES

5.1 Introduction

Stable isotope analysis of the lacustrine carbonates provides valuable contributions for understanding lacustrine systems and reconstructing their depositional settings (Talbot, 1990; Anadon & Utrilla, 1993, Pentecost, 2005).

The isotopic composition of the lake is controlled by several factors such as temperature changes (cold or warm), humidity (dry or wet), evaporation, precipitation, lake level fluctuation, alkalinity, salinity, productivity of the lake, freshwater input, etc. (Last, 1990; Talbot, 1990; Anadon & Utrilla, 1993; Li & Ku, 1997; Leng & Marshall, 2004; Pentecost, 2005; Roberts et al., 2008).

The $\delta^{18}O$ ratio of the lacustrine carbonates relates the composition of the bottom waters of depositional environment. In the shallow lake carbonates, the low ^{18}O content may reflect the input of ^{16}O-enriched waters of meteoric origin (Anadon & Utrilla, 1993). Pentecost (2005) gave some median values of ^{18}O according to previous studies, such as –7.58 ‰ PDB for epigean meteogene travertines, –6.95 ‰ PDB for thermogene travertines, and –8.79 ‰ PDB for the lake marl samples.

Oxygen isotopes values of meteoric origin reflect to climate and mean annual temperature (Cerling, 1984).

The negative $\delta^{13}C$ values of these carbonates may explain meteoric ground waters that contain isotopically light CO_2 from soils (Anadon & Utrilla, 1993 and references there in).

Photosynthetic activity causes to remove organic carbon, this would lead to increase of lake $\delta^{13}C$. In highly productive lake, $\delta^{13}C$ may reach high values (Li & Ku, 1997).

Strong evaporation raises to pCO_2 of a lake, causing a loss of CO_2 to the atmosphere with lighter carbon isotopes and results an increase of the lake $\delta^{13}C$ (Li & Ku, 1997). Dry conditions cause a decrease in lake level and increase in pH and salinity, thus CO_2 concentration reduced. Photosynthetic plants change use CO_2^- to change their metabolism HCO_3^- and they become relatively enriched in ^{13}C, and this would produce higher $\delta^{13}C$ in the lake. During wetter periods, carbon values of the lake refresh because of a soil-derived CO_2 influx, which cause much lower $\delta^{13}C$ (Leng et al., 2005).

Göktepe travertines are lacustrine carbonates resting on the terrestrial Mio-Pliocene sequence. We sampled nearly every 30 cm of these lacustrine carbonates to perform microfacies and stable isotope analysis. We took 30 samples from ~35 m thick travertine type carbonates on the Yarılgan Hill and 186 samples from ~80 m thick travertine sequence on the Kepez Hill. We studied 211 thin sections (given in Chapter 3) and correlated them with 216 stable isotopes ($\delta^{18}O/\delta^{13}C$) analysis results. These analyses of the travertine sequence and related field observations reveal palaeoclimate and palaeoenvironmental data of the area in the Middle Pleistocene.

5.2 Stable Isotope Values of Göktepe Travertines

Stable isotope values ($\delta^{18}O/\delta^{13}C$) of the Göktepe travertines are studied both on the Yarılgan Hill (lower parts of the sequence) and Kepez Hill sections (upper parts of the sequence).

The $\delta^{18}O$ values of the Yarılgan Hill range from -10.10 to -8.49 ‰ PDB with an average of -9.04 ‰ PDB and $\delta^{13}C$ values range from -0.11 to 1.86 ‰ PDB with an average of 0.91 ‰ PDB (Figure 5.1) (Table 5.1).

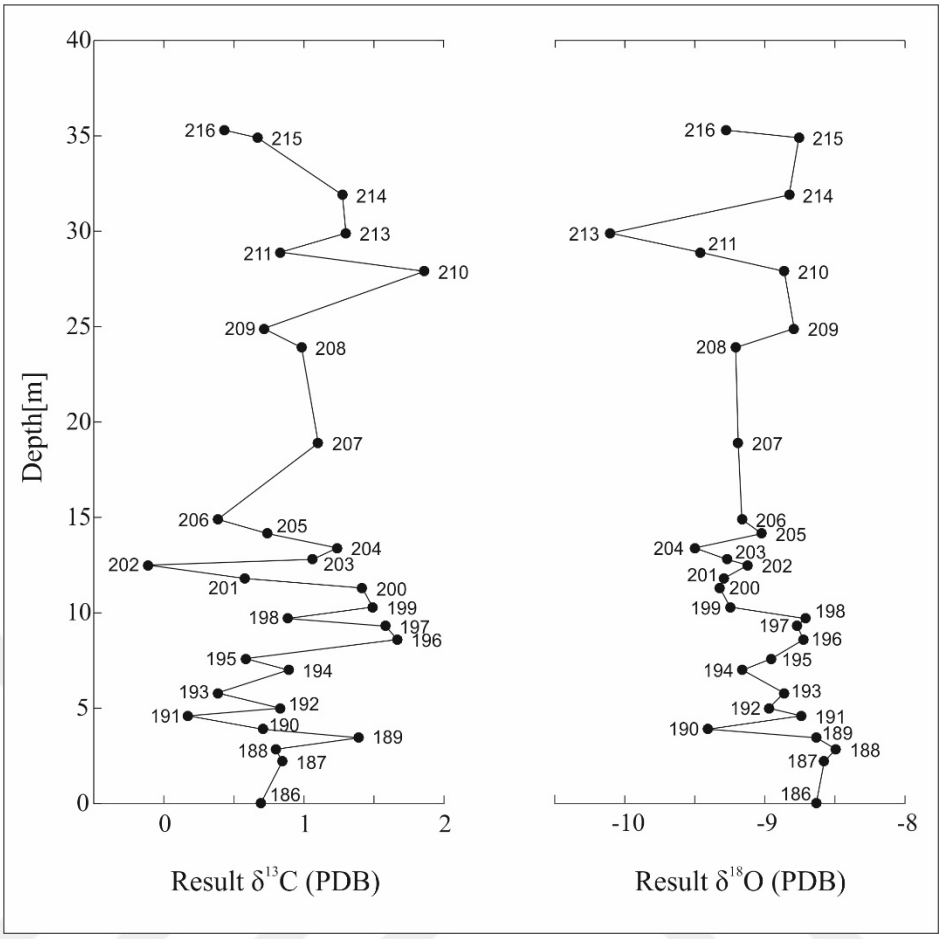


Figure 5.1 The diagram shows the stable isotopes values ($\delta^{18}O/\delta^{13}C$) of the lacustrine carbonate on the Yarılgan Hill section. The number on the blue line with a red circle indicate the sample numbers

Table 5.1 The average, median, minimum, and maximum values of the stable isotopes of the Göktepe travertines

Stable Isotopes	**$\delta^{18}O$ ‰ PDB**		**$\delta^{13}C$ ‰ PDB**	
Sections	**Yarılgan**	**Kepez**	**Yarılgan**	**Kepez**
Average	-9.04	-9.78	0.91	1.52
Median	-9.00	-9.78	0.84	1.46
Min	-10.10	-11.34	-0.11	-4.64
Max	-8.49	-7.93	1.86	3.65

The $\delta^{18}O$ values of the Kepez Hill section range from -11.34 ‰ to -7.93 ‰ PDB with an average of -9.78 ‰ and $\delta^{13}C$ values change from -4.64 ‰ to 3.65 ‰ PDB with an average of 1.52 ‰ PDB (Table 5.1) (Figure 5.2).

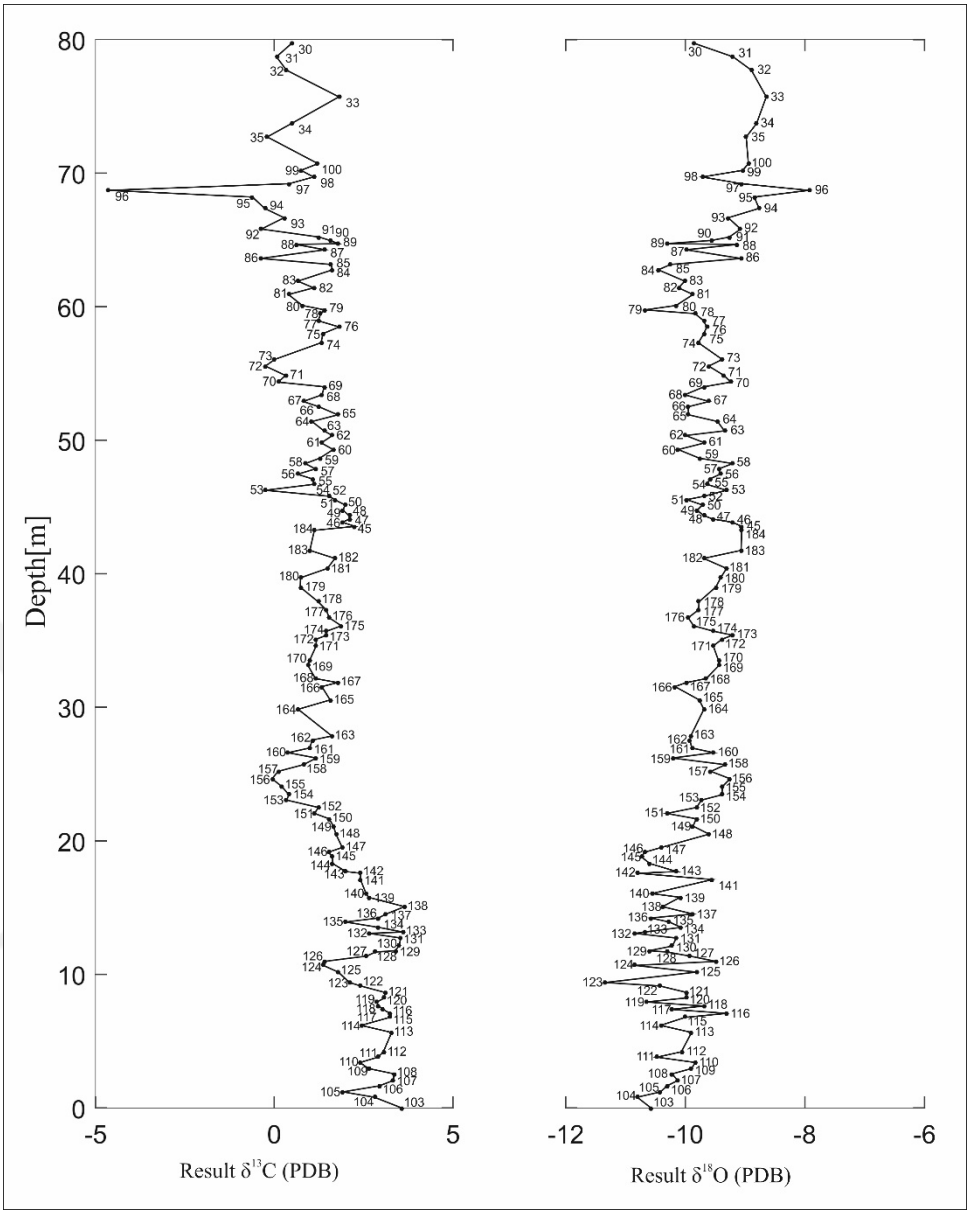


Figure 5.2 The diagram shows the stable isotopes values ($\delta^{18}O/\delta^{13}C$) of the Kepez Hill section. The number on the blue line with a red circle indicate the sample numbers

Our median values of $\delta^{18}O$ are -9.78 ‰ PDB for the Kepez Hill and -9.00 ‰ PDB for the Yarılgan Hil. These values are closer to the values of meteogene travertines and also lake marl deposits (Table 5.1).

The $\delta^{18}O$ values increase upward, whereas, the values for the $\delta^{13}C$ values decrease on the same way of the main travertine succesion (Kepez Hill section). It seems there are two levels where the average of isotopes values distinctly changes (Figure 5.2).

The first part of the sequence (bottom) has minimum $\delta^{18}O$ and maximum $\delta^{13}C$ values according to rest of the sequence. This first part is about 20 m thick and starts with the more arid and colder conditions. Within this 20 m, four discontinuity levels (paleosol) were determined. These levels indicate the periods when the travertine sedimentation nearly stoped and the lake water level droped significantly. Therefore, it may indicate that the lower levels of the sequence by a cold and dry palaeoclimate (i.e. low annual rainfall).

The second part of the sequence shows that generally more humid and warmer conditions began to prevail due to low values of $\delta^{18}O$ and high values of $\delta^{13}C$. This part corresponds approximately to 20-65 meters of the sequence. The warm-humid and cold-arid oscillations continued in this part. Besides, the upper parts of this level have two distinct paleosol levels that are represented the non-depositional process or very low lake level in dry settings.

The third (upper) part of the sequence differs from the lower levels with a sudden increase in δ 18O values and a sudden decrease in δ 13C values. Then these values regress to the previous level and less humid and warmer conditions returned.

5.3 Relation between the Stable Carbon and Oxygen Isotopes

We could not find a correlation on carbon versus oxygen isotope values of the travertines in the Yarılgan Hill section ($r=-0.05$) but they show high negative correlation in the Kepez Hill section ($r=-0.65$) (Figure 5.3 and Figure 5.4).

In hydrologically open lakes, there is little or no correlation between $\delta^{18}O$ and $\delta^{13}C$ whereas they show high positive correlations ($r>0.7$) in closed lakes (Talbot, 1990). Roberts et al. (2008) gave some examples of Mediterranean lake from late Quaternary that contrary to expectation they show no positive covariance. He concluded that co-variance is unreliable indicator of paleo-hydrological closure. Besides, several researchers emphasized some typical conditions about the correlations of stable

isotope values in the lacustrine environment (Li, & Ku, 1997; Leng & Marshall, 2004; Pentecost, 2005).

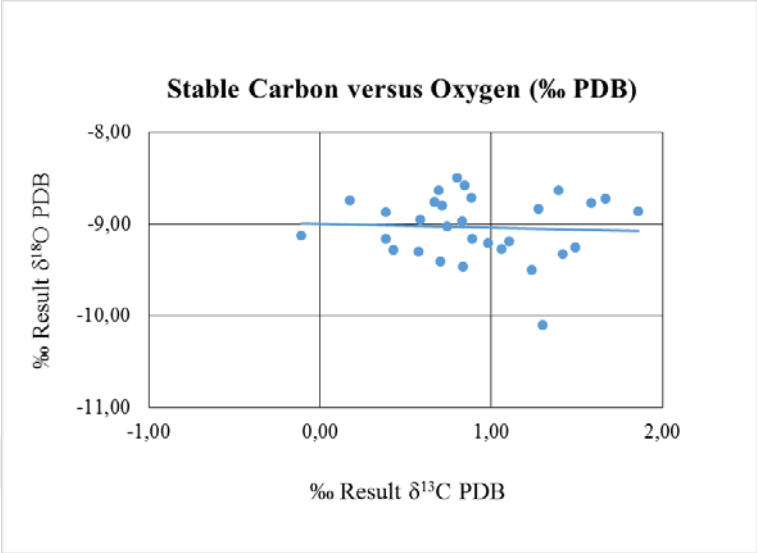


Figure 5.3 The graphics shows the stable carbon and oxygen isotopes of the Yarılgan Hill. There is no specific correlation

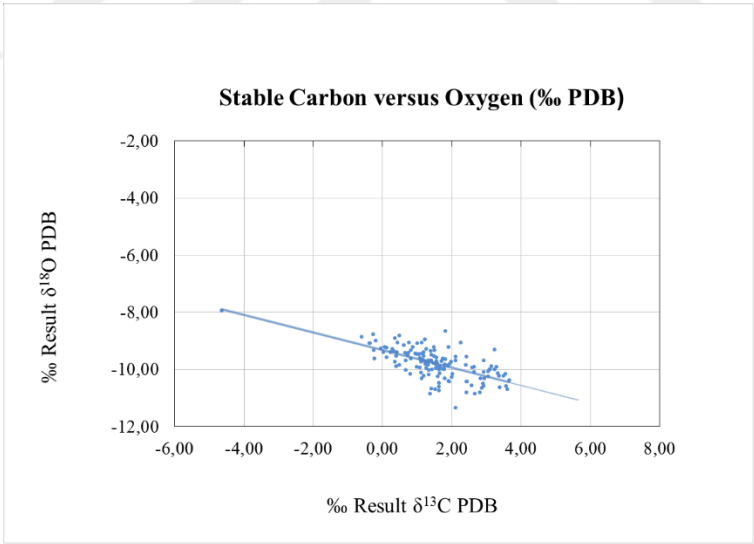


Figure 5.4 The graphics shows the stable carbon and oxygen isotopes. There is a high negative correlation on the stable isotope values

In lake travertines, evaporation is significant because it initially causes to the enrichment of heavier isotopes in the lake water especially at low humidity. For example, both the ^{13}C (of the DIC) and $\delta^{18}O$ is enriched at about 6 ‰ when 80 % of a

surface water evaporates (Pentecost, 2005 and references there in). But there is enough long time that carbon isotopes would be close to atmospheric equilibrium unless it is modified by photosynthetic activities of the lake. In this situation, there should be no correlation between oxygen and carbon (Li & Ku, 1997; Pentecost, 2005).

The vapor exchange and hydrologic balance may also affect this correlation (Li & Ku, 1997). The stable isotopes ($\delta^{18}O$ and $\delta^{13}C$) of the lake approach steady-state values because of the vapor exchange between lake water and the atmosphere. This steady-state value for $\delta\ ^{18}O$ depends on freshwater input, atmospheric oxygen isotopes, humidity, and temperature. (Li & Ku, 1997 and references therein).

If the lake water declines slowly or remain stable and the lake's productivity have a little change $\delta^{18}O$ and $\delta\ ^{13}C$ of the lake should remain relatively constant. In this situation, it is expected $\delta^{18}O$- $\delta^{13}C$ covariance to be weak (Li &Ku, 1997).

When the lake water declines rapidly because of the evaporation, this situation initially causes to the enrichment of heavier isotopes (^{18}O) in the lake water because ^{16}O preferentially pass to the vapor phase. The intense evaporation and the curtailment of freshwater input also result in an increase of the $\delta\ ^{13}C$ for lake DIC (Dissolved Inorganic Carbon). Therefore, $\delta^{18}O$ and $\delta^{13}C$ may be increased and give strong covariance (Li &Ku, 1997).

Cerling, (1984) indicated that ^{18}O values were often 4-8‰ depleted in ^{18}O sparite by recrystallization but ^{13}C values are generally unchanged. The negative correlation in our values may probably because of diagenetic processes.

5.4 Correlation between the Stable Isotope Values and Microfacies of the Göktepe Travertines

The microfacies changes of the sequence are given in the Chapter 3 and stable isotope values have been given above. In this section, we correlate petrographic and

climatic changes of the travertine sequence by using microfacies analysis and stable isotope values (Figure 5.5 and 5.6).

5.4.1 The Yarılgan Hill Section

At about 35m thick travertine sequence was measured on the Yarılgan Hill section. Clotted micrite facies and microbial micrite facies are dominant in this section (Figure 5.5.).

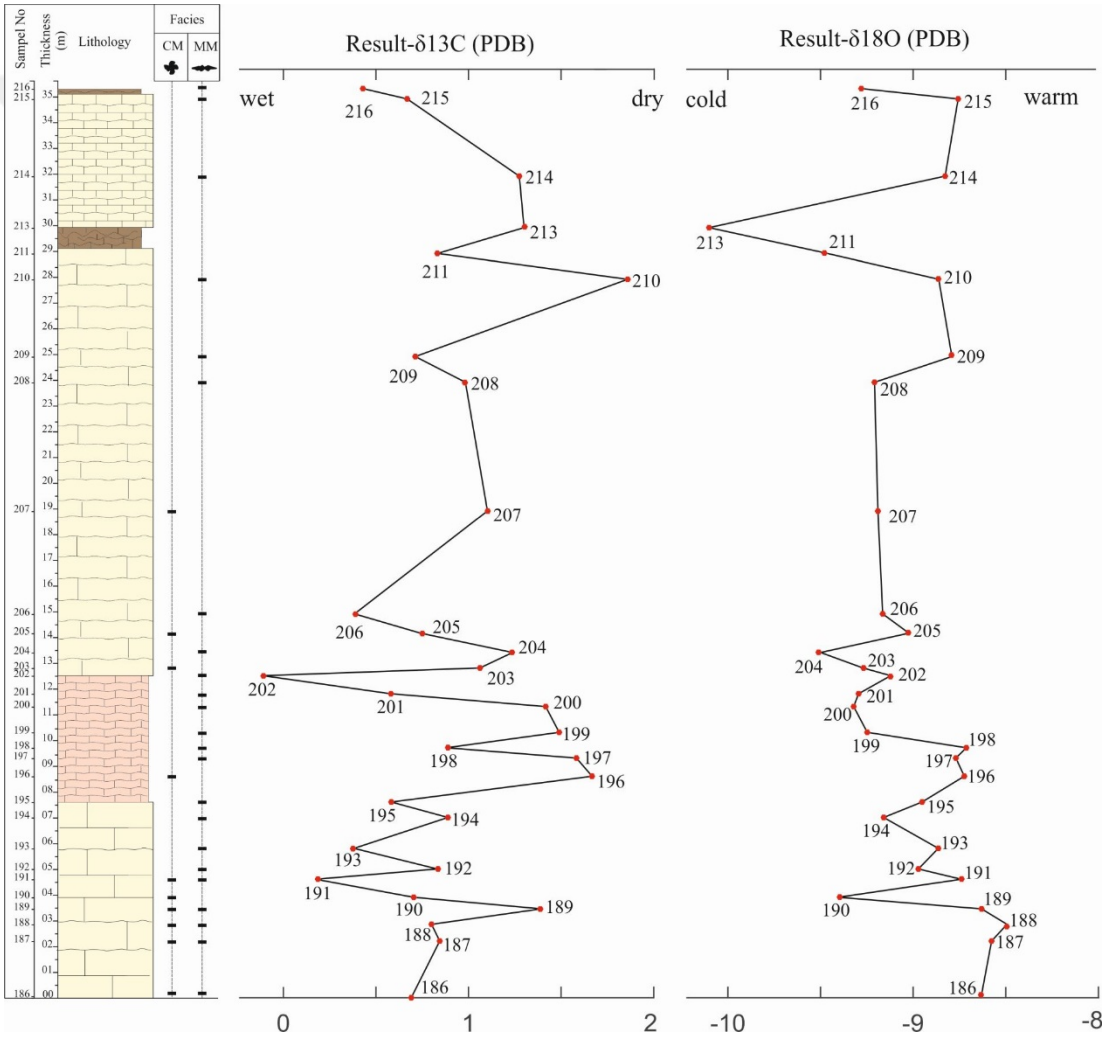


Figure 5.5 The correlation between microfacies and stable isotopes changes of the Yarılgan Hill Section

The first 7 m of the sequence are cream-colored and include gastropods and charophytes. At this level, the average of carbon values is 0.75 ‰ PDB and the average

of oxygen values -8.83 ‰ PDB. Between 7 and 13 meters, the color of the sequence changes from cream to pink. There is no fossil observed these levels. The average of carbon and oxygen values change to 1.04 ‰ PDB and -9.09 ‰ PDB, respectively. There is an increase in the carbon and a decrease in oxygen values. These values may indicate that the conditions become relatively semi-arid and colder. The sream micritic travertines are rewatched between 13 and 28 m. At this level, the average of the carbon values decreases limitedly to 0.95 ‰ PDB and the average of oxygen values are 9.24 ‰ PDB. The brownish travertine levels, which include charophytes and gastropods fossils, overlay the cream-colored travertine levels (Figure 5.5). These levels start with an increase in the carbon values and decrease of the oxygen values. This dark brown color and higher carbon values may be due to rising biochemical productivity of the lake under the dry conditions. At the uppermost part of the sequence, the decreasing carbon and increasing oxygen values may indicate less dry and warmer conditions.

5.4.2 The Kepez Hill Section

As describe above, the isotopic composition of the main travertine sequence of the Milet Formation exhibits some shifts. The climate changed cold-dry conditions to wet-warmer conditions from bottom to top (Figure 5.6).

The first 20 m of the sequence measured in the Kepez Hill mainly consists of clotted micrite facies, macrophyte facies and, also rarely shrub facies and a small amount of microbial micrite facies. Algal microspar clump facies are observed at some levels. These facies correspond to the littoral-sublittoral facies of a shallow lake. This relatively low water level is characterized by the highest $\delta^{13}C$ values and the lowest $\delta^{18}O$ values relative to the rest of the sequence (Figure 5.6). These values correspond to relatively arid and cold conditions in the lacustrine environment.

Four paleosol levels were determined in this bottom part. These paleosol levels may correspond to conditions that evaporation is high and/or lake water level is very low. Because paleosols indicate a breakdown in a travertine deposition.

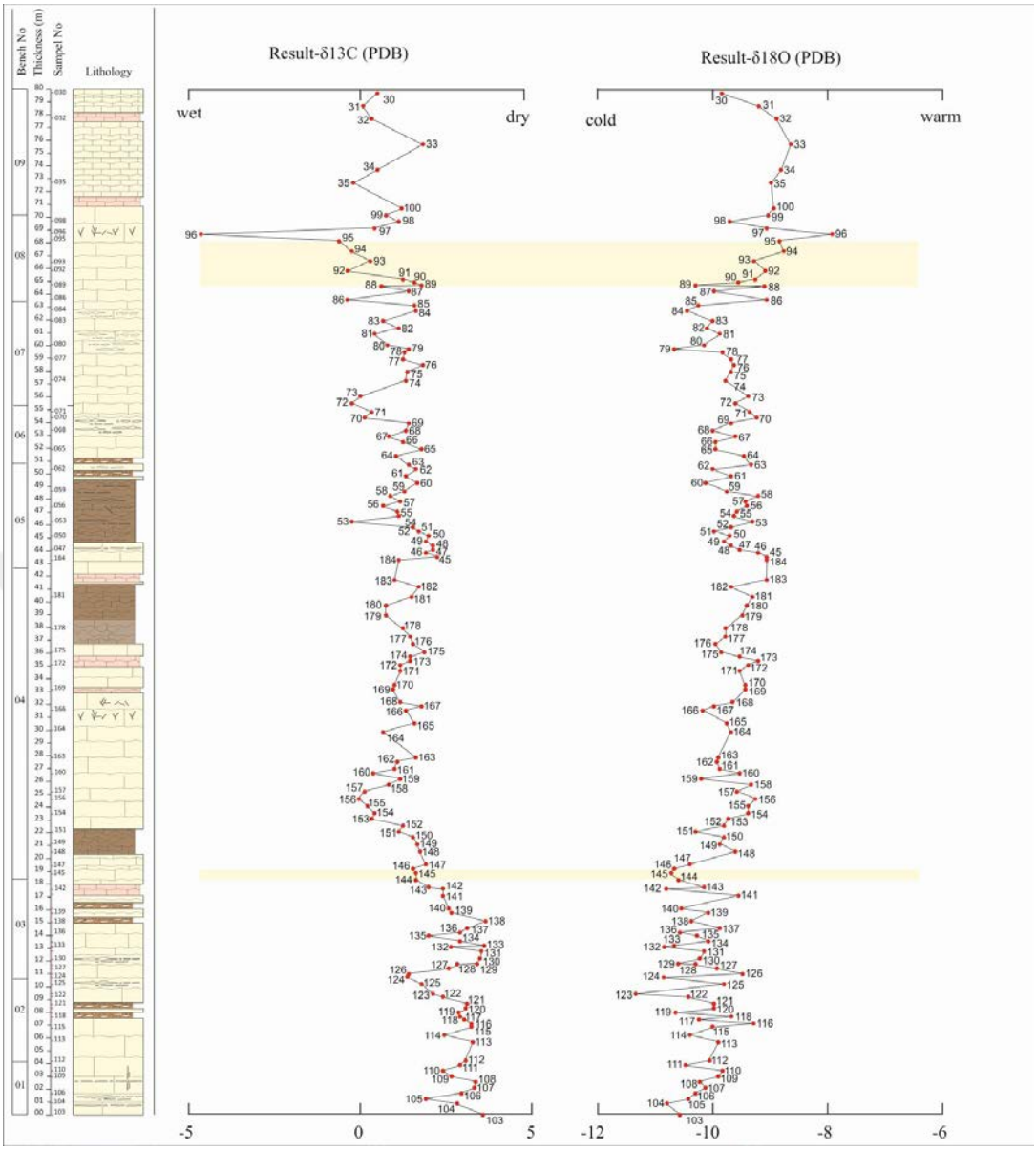


Figure 5.6 The correlation between microfacies and stable isotopes changes of the Kepez Hill Section. The yellow areas show shifting range of the values

At the second (middle) part of the sequence while $\delta^{18}O$ values decrease and $\delta^{13}C$ values increase. Generally, more humid and warmer conditions begin to prevail. This part corresponds approximately to 20-65 meters of the sequence and is represented by different microfacies. The clotted micrite facies are dominant and accompanied by a small amount of microbial micrite facies along the 20-30 meters of the sequence. In the first 5 m, $\delta^{18}O$ values increase and $\delta^{13}C$ values decrease. For the next 5 m, $\delta^{18}O$ and $\delta^{13}C$ values begin to change in the opposite direction. These facies and stable isotope values indicate that a shallow lake environment that has relatively high water

level. The palaeoclimate are more humid and warmer according to the below shore facies of the lake.

The 43-65 meters of the sequence start predominantly with microbial micrite facies, but clotted micrite facies are quite common. Algal microspar clump facies and macrophyte facies and their fragments occur at some levels. The sequence continue with clastic carbonate facies with two distinct paleosol levels, which are represented the non-depositional process. The $\delta^{18}O$ and $\delta^{13}C$ values are generally similar but warm-humid and cold-arid oscillations continued frequently.

The third (upper) part of the sequence differs from the lower levels showing an abrupt increase in $\delta^{18}O$ values, but a sudden decrease in $\delta^{13}C$ values. Then these values regress to the previous level and less humid and warmer conditions returned.

The 65-80 meters of the sequence start with clastic carbonate facies with clotted micrite facies. At the uppermost part of the sequence, it prevailed a stagnant, widespread lacustrine environment where the travertine precipitation decreased.

CHAPTER 6
CONCLUSION

The early middle early Miocene-Pleistocene sedimentary sequences rest unconformably on the tectonic boundary between the Menderes Massif and Lycian Nappes unconformably. These fluvial and lacustrine sedimentary sequences are deposited in the basins between high and rough topographies that were created by the metamorphic basement. The sedimentary sequences are composed of the Turgut, Sekköy, Yatağan, Milet, and Sungur formations, from bottom to top.

The preceding description of the stratigraphy and biostratigraphy allows evaluating the paleoenvironmental conditions in the basin. The fossil evidence of the late early to early middle Miocene indicates a warm, subtropical brackish/freshwater lacustrine environment that was surrounded by broad-leaved deciduous forests that were poor in diversity but rich in conifers. The lacustrine condition implies a transgression caused by tectonic subsidence in the basin. In the case of a brackish lake, the saline conditions could be explained by a marine transgression. The fossil record of the middle-late middle Miocene lignite deposits presents a freshwater lacustrine environment under warm temperate climatic conditions.

Göktepe travertines are lacustrine carbonates of the Milet Formation resting on top of this terrestrial Mio-Pliocene sequence. The age of these travertines was firstly determined with using radiometric dating methods of $^{234}U/^{238}Th$. The results show that the age of the lacustrine travertines of Milet Formation reach 346ka (Middle Pleistocene).

There is a N-S trending, 6 km long normal fault dipping to the east with a high angle, located at the east of the Kale-Tavas Basin. This fault can be considered as a growth fault that limits the Kale Tavas Basin. This fault was active until when it is covered by the the upper layers of the Milet Formation (0.4Ma). The sedimentary sequences on the hanging-wall block of the Göktepe Fault are significantly thicker than those on the footwall block. This may indicate continuous subsidence in the basin

until ~364 Ka. It is compatible with the extensional model proposed by Seyitoğlu et al., (2004).

The carbonate fabrics and facies of the Göktepe travertines are classified as micrite fabrics and facies, spar fabrics and facies, zoned algal fabrics and facies, shrub fabrics and facies, biological components, and pores. The micrite fabrics are clotted (peloidal) micrite, microbial micrite, encrusted micrite fabrics, and intraclast. The spar fabrics are classified as algal microspar-spar clump, encrusted spar fabrics and spar carbonate fragments, intra-frame spar, and intra shrub spar. Zoned algal fabrics, zoned algal clump fabrics and zoned encrusted algal fabrics. Shrub fabrics are micritic quill-feather shrubs and macrophytes quill-feather shrubs. Biological components consist of encrusted macrophytes, gastropods, ostracods and charophytes. Pores are fenestral (shrinkage) pores, gas escape pores, intra-frame pores and inner organism pores.

The carbonate fabrics, facies, and components (fossil content) of the Göktepe travertines indicate a depositional environment that was a littoral and sublittoral shallow lake. The vertical facies changes are related to cyanobacteria variations related to changes of water levels and chemistry. The clotted micrite facies may indicate shallow lakes or water pools with relatively deep-water levels, the water of which can be warm or hot. The microbial micrite facies reflect a very shallow and stagnant, and cyanobacteria rich lake environment, and possibly a hot groundwater inflow. The shrub facies and macrophyte spar quill facies represent a very shallow lake environment, near to shore (littoral) and algal spar clump facies may indicate relatively deeper parts of the shallow lake (sublittoral). The fragmented carbonate facies and fragments of encrusted micrite and encrusted spar fabrics may indicate that the lake water occasionally dried or become very shallow from time to time. The existence of thin paleosol levels confirms this assumption frequently dry up and refill conditions in the lake due to climatic changes (temperature and precipitation).

Our microfacies analysis of the travertine sequence and related field observation revealed several findings; such as limited plant fossil (reed) content, fluctuation of the lake water level due to climatic changes (due to the changes of temperature and

rainfall), deficiency and low variety of fauna and flora due to the changes of water chemistry.

The stable isotope values of the Göktepe travertines were measured in two section. The $\delta^{18}O$ values of the Yarılgan Hill range from -10.10 to -8.49 ‰ PDB with an average of -9.04 ‰ PDB and $\delta^{13}C$ values range from -0.11 to 1.86 ‰ PDB with an average of 0.91 ‰ PDB. We could not find a correlation on carbon versus oxygen isotope values of the travertines in the Yarılgan Hill section (r = -0.05)

The $\delta^{18}O$ values of the Kepez Hill section range from -11.34 ‰ to -7.93 ‰ PDB with an average of -9.78 ‰ and $\delta^{13}C$ values change from -4.64 ‰ to 3.65 ‰ PDB with an average of 1.52 ‰ PDB. The carbon versus oxygen isotope values show high negative correlation (r=-0.65). This negative correlation may probably because of diagenetic processes. The carbon values decrease upward, whereas, oxygen values increase on the same way. There are two main shifts in these values. These shifts on the stable istopes values may reflect the changes on the climate from cold-dry conditions to warm-wet conditions.

When the oscillations in isotope values are evaluated together with petrographic changes, it is seen that the climatic conditions change frequently. The lower parts of the sequence start dominantly with macrophyte facies, encrusted micrite facies and continue with clotted micrit facies. This show relatively low water level and is characterized by the highest $\delta^{13}C$ values and the lowest $\delta^{18}O$ values relative to the rest of the sequence. These values correspond to relatively arid and cold conditions in the lacustrine environment. The middle parts are the thickest part of the sequence and have several alternations of the facies. Hovewer, algal microspar clump facies and clotted micrite facies are dominant in some level of this part. These facies indicate a shallow lake environment, relatively high-water level. The stable isotope values give moderate values. The climatic conditions were more humid and warmer according to the below shore facies of the lake. The third (upper) part of the sequence differs from the lower levels with a sudden increase in $\delta^{18}O$ values and a sudden decrease in $\delta^{13}C$ values then these values regress to the previous level and semiarid conditions return. Our

microfacies analysis and stable isotope results contribute with further evidence for the climatic conditions of the MIS 11 interglacial periods for the Aegean region. However, additional age analysis is needed for the travertines to be able to interpret paleoclimate conditions and relate them to other basins.

REFERENCES

Akgün, F., Olgun, E., Kuşçu, İ., Toprak, V., & Göncüoğlu, M. C. (1995). Orta Anadolu kristalen kompleksinin "Oligo-Miyosen" örtüsünün stratigrafisi, çökelme ortamı ve gerçek yaşına ilişkin yeni bulgular. *Turkish Association of Petroleum Geologists Bulletin, 6*, 51-68.

Akgün, F., & Akyol, E. (1999). Palynostratigraphy of the coal-bearing Neogene deposits graben in Büyük Menderes Western Anatolia. *Geobios, 32*, 367-383.

Akgün, F., & Sözbilir, H. (2001). A palynostratigraphic approach to the SW Anatolian molasse basin: Kale–Tavas molasse and Denizli molasse. *Geodinamica Acta, 14*, 71-93.

Akgün, F. (2002). Stratigraphic and Paleoenvironmental Significance of Eocene Paynomorphs of the Çorum-Amasya Area in the Central Anatolia, Turkey. *Acta Palaeontologica Sinica, 41,* 576-591.

Akgün, F., Akay, E., & Erdoğan, B. (2002). Terrestrial to shallow marine deposition in Central Anatolia: A palynological approach. *Turkish Journal of Earth Sciences, 11*, 1-27.

Akgün, F., Kayseri M. S., & Akkiraz, M. S. (2007). Paleoclimatic evolution and vegetational changes during the Late Oligocene–Miocene period in Western and Central Anatolia (Turkey). P*alaeogeography, Palaeoclimatology, Palaeoecology 253*, 56-90.

Akgün, F., Akkiraz, M. S., Üçbaş S. D., Bozcu M., Kapan Yeşilyurt S., & Bozcu, A. (2013). Oligocene vegetation and climate characteristics in north-west Turkey: Data from the South-western part of the Thrace Basin. *Turkish Journal of Earth Sciences, 22*, 277-303.

Akkiraz, M. S., Kayseri, M. S., & Akgün, F. (2008). Palaeoecology of Coal-Bearing Eocene Sediments in Central Anatolia (Turkey) Based on Quantitative Palynological Data. *Turkish Journal of Earth Sciences, 17*, 317-360.

Akkiraz, M. S., Akgün, F., & Örçen, S. (2011). Stratigraphy and palaeoenvironment of the lower-“middle” Oligocene units in the northern part of the Western Taurides (İncesu area, Isparta, Turkey). *Journal of Asian Earth Sciences, 40*, 452-474.

Akyol, E. (1971). Microflore de l’Oligocene inférieur récoltée dans un sondage prés d’ Avcıkoru, Şile-İstanbul [Microflora Oligocene collected in a survey near Avcıkoru, Şile-Istanbul]. *Pollen et Spores, 13*, 117-133.

Alçiçek, C. M., & ten Veen J. H. (2008). The late Early Miocene Acıpayam piggy-back basin: Refining the last stages of Lycian nappe emplacement in SW Turkey. *Sedimentary Geology, 208*, 101-113.

Alçiçek, H. (2010). Stratigraphic correlation of the Neogene basins in southwestern Anatolia: Regional palaeogeographical, paleoclimatic, and tectonic implications. *Palaeogeography, Palaeoclimatology, Palaeoecology, 291*, 297-318.

Anadon P. & Utrilla, R (1993). Sedimentology and isotope geochemistry of lacustrine carbonates of the Oligocene Campins Basin, north-east Spain. *Sedimentology, 40,* 669-720.

Atalay, Z. (1980). Muğla - Yatağan ve yakın dolayı karasal Neojen'inin stratigrafi araştırması. *Türkiye Jeoloji Kurumu Bülteni, 23*, 93-99.

Batı, Z., & Sancay, R. H. (2007). Palynostratigraphy of Rupelian sediments in the Muş Basin, Eastern Anatolia, Turkey. *Micropaleontology, 53*, 244-283.

Batten, D. J. (1999). Small palynomorphs. In Jones, TP., Rowe, NP. (Eds.), Fossil plants and spores: modern techniques. *Geological Society, London, 15*, 19.

Becker-Platen, J. D. (1970). Lithostratigraphische Unterschungen im Kanozoikum Sudwest Anatoliens (Turkei) – Kanozoikum und Braunkohlen der Turkei. *Beihhefte zum Geologischen Jahrbuch, 97*, 1-244.

Benda, L. (1971). Grundzüge einer pollenanalytischen Gliederung des türkischen Jungtertiärs (Känozoikum und Braunkohle der Türkei. 4). *Beihhefte zum Geologischen Jahrbuch, 113*, 1- 46

Benda, L, & Muelenkamp, J.E. (1990). Biostratigraphic correlations in the Eastern Mediterranean Neogene 9. Sporomorph associations and event stratigraphy of the Eastern Mediterranean Neogene. *Newsletter Stratigraphy, 23* (1), 1-10.

Bergounioux, F. M., Zbyszewski, G., & Crouzel, F. (1953). Les Mastodontes Miocènes de Portugal. Memoires dos Serviços Geologicos de Portugal, Lisboa, *Nouvelle Serie, 1*, 1-140.

Bouchal, J. M., Zetter, R., Grimsson, F., & Denk, T. (2016). The middle Miocene palynoflora and paleoenvironments of Eskihisar (Yatağan Basin, south-western Anatolia): a combined LM and SEM investigation. *Botanical Journal of the Linnean Society, 182*, 14-79.

Bouchal, J. M., Mayda, S., Zetter, R., Grimsson, F., Akgün, F. & Denk, T. (2017). Miocene palynofloras of the Tınaz lignite mine, Muğla, southwest Anatolia: Taxonomy, paleoecology and local vegetation change. *Review of Paleobotany and Palynology, 243*, 1-36.

Brongniart, A. (1822) Sur la classification et la distribution des végétaux fossiles en général et sur ceux des terrains de sédiment supérieur en particuliére. *Mémoire du Museum Nationale d'Histoire Naturelle, Paris, 8,* 203-240.

Büyükmeriç, Y. (2017). Molluscan biostratigraphy of early Miocene deposits of the Kale-Tavas and Acıpayam basins (Denizli, SW Turkey). *Bulletin of the Mineral Research and Exploration, 155*, 49-73.

Cavagnetto, C., & Anadón, P. (1996). Preliminary palynological data on floristic and climatic changes during the Middle Eocene- Early Oligocene of the eastern Ebro Basin, northeast Spain. *Review of Palaeobotany and Palynology, 92*, 281-305.

Cerling, T. E. (1984). The stable isotopic composition of modern soil carbonate and its relationship to climate. *Earth and Planetary Science Letters, 71*, 229-240.

Chafetz, H. S., & Folk, R. L. (1984). Travertines: depositional morphology and the bacterially constructed constituents, constructed constituents. *Journal of Sedimentary Petrology, 54*, 289-316.

Chafetz, H. S. & Guidry, S. A. (1999). Bacterial shrubs, crystal shrubs, and ray-crystal shrubs: bacterial vs. abiotic precipitation. *Sedimentary Geology, 126*, 57-74.

Collins, A. S, & Robertson, A. H. F. (1998). Processes of Late Cretaceous to Late Miocene episodic thrust-sheet translations in the Lycian Taurides, SW Turkey. *Journal of the Geological Society of London, 155*, 759-772.

Coplen, T. B., Kendall, C., & Hopple, J. (1983) Comparison of stable isotope reference samples. *Nature 302*, 236-238.

De Graciansky, P. C. (1972). *Recherches géologiques' dans le Taurus lycien occidental.* PhD Thesis, University Paris-Sud (Orsay), France.

Deschamps, P., Hillaire-Marcel, C., Michelot, J. L, Doucelance, R., Ghaleb, B., & Stephane B. (2004). $^{234}U/^{238}U$ Diesqulibrium along stylolitic discontinuities in deep Mesozoic limestone formations of the Eastern Paris basin: evidence for discrete uranium mobility over the last 1-2 million years. *Hydrology and Earth System Sciences, 8* (1), 35-46.

Ediger, V. Ş., Batı, Z., & Alişan, C. (1990). Paleopalynology and paleoecology of Calamus-like disulcate pollen grains. *Review of Paleobotany and Palynology, 62*, 97-105.

Elmas, G., Seyitoğlu, G., Kazancı, N., & Işık, V. (2019). Syn-sedimentary tectonic markings in the Oligocene Datça-Kale-Acı Göl Basin, Western Anatolia. *Bulletin of The Mineral Research Exploration, 160,* 1-20.

Erdei, B., Yavuz, N., Akgün, F., & Hably, L. (2002). Some data to the Miocene flora of Western Turkey. *6th European Palaebotany Palynology Conference Athens. Abstract Book,* 79-80.

Erdoğan, B., & Güngör, T. (2004). The problem of the core-cover boundary of the Menderes Massif and an emplacement mechanism for regionally extensive gneissic granites, Western Anatolia (Turkey). *Turkish Journal of Earth Science, 13,* 15-36.

Erdoğan, B., & İşintek İ. (2007). Traverten çökellerin aranmasında karbonat fasiyes analizleri, 61. *Türkiye Jeoloji Kurultayı Bildiri Özleri*. 44.

Freels, D. (1980). Limnische Ostrakoden aus Jungtertiar und Quartar der Turkei. *Geologisches Jahrbuch, 39*, 3-169.

Folk, R. L. (1959) Practical petrographic classification of limestones: *American Association of Petroleum Geologists Bulletin, 43*, 1-38.

Fortelius, M. (1990). Rhinocerotidae from Paşalar, middle Miocene of Anatolia (Turkey). *Journal of Human Evlolution, 19* (4-5), 489-508.

Geraads, D., & Miller, E. (2013). Brachypotherium minor n. sp., and other Rhinocerotidae from the Early Miocene of Buluk, Northern Kenya. *Geodiversitas, 35* (2), 359-375.

Geyh, M. A., & Schleicher, H. (1990). *Absolute age determination. Physical and chemical dating methods and their application*. Verlag, Berlin, Heidelberg: Springer.

Ghaleb, B., Falguères, C., Carlut, J., Pozzi, J. P, Mahieux, G., Boudad, L. et al. (2019). Timing of the Brunhes-Matuyama transition constrained by U-series disequilibrium, *Scientific Reports, 9*, 6039.

Görür, N., Şengör, A. M. C, Sakınç, M., Tüysüz O., Akkök, R., Yiğitbaş, E. et al. (1995). Rift formation in the Gökova region, southwest Anatolia: Implications for the opening of the Aegean Sea. *Geological Magazine, 132*, 637-650.

Gruas-Cavagnetto, C. (1977). *Etude palynologique de l'Eocene du Bassin Anglo–Parisien*. These de Doctorate d'Etat es Sciences Naturelles, Universite de Pierre Marie Curie VI, Paris.

Guo, L. & Riding, R. (1994). Origin and diagenesis of Quaternary travertine shrub fabrics, Rapolano Terme, central Italy. *Sedimentology, 41*, 499-520

Guo, L. & Riding, R. (1998). Hot-spring travertine facies and sequences, Late Pleistocene, Rapolano Terme, Italy. *Sedimentology, 45*, 163-180.

Güner, T. H, Bouchal, J.M., Köse, N., Göktaş, F., Mayda, S., & Denk, T. (2017). Landscape heterogeneity in the Yatağan Basin (southwestern Turkey) during the middle Miocene inferred from plant macrofossils. *Palaeontographica, Abteilung B, Palaophytologie, 296*, (1-6), 113-171.

Gürer, Ö. F. & Yılmaz, Y. (2002). Geology of the Ören and surrounding areas, SW Anatolia. *Turkish Journal of Earth Science, 11*, 1-13.

Gürer, Ö. F., Sangu, E., Özburan, M., Gürbüz, A., & Sarıca-Filoreau, N. (2013). Complex basin evolution in the Gökova Region: implications on the Late Cenozoic tectonics of southwest Turkey. *International Journal of Earth Science, 102*, 2199-222.

Hakyemez, H. Y. (1989). Kale –Kurbalık (GB Denizli) bölgesindeki Senozoyik yaşlı çökel kayaların jeolojisi ve stratigrafisi. *Bulletin of the Mineral Research and Exploration, 109*, 9-21.

Harzhauser, M., Kowalke, T., & Mandic, O. (2002). Late Miocene (Pannonian) gastropods of Lake Pannon with special emphasis on early ontogenetic development. *Annalen des Naturhistorischen Museums in Wien, 103*, 75-141.

Harzhauser M. & Mandic, O. (2008). Neogene lake systems of Central and South-Eastern Europe: Faunal diversity, gradients and interrelations. *Palaeogeography Palaeoclimatology Palaeoecology, 260*, 417-434.

Harzhauser M., Daxner Höck, G., Göhlich, U. B., & Nagel, D. (2011). Complex faunal mixing in the early Pannonian palaeo-Danube Delta (Late Miocene, Gaweinstal, Lower Austria). *Annalen des Naturhistorischen Museums in Wien, 113*, 167-208.

Harzhauser, M., Mandic, O., Büyükmeriç, Y., Neubauer, T. A., Kadolsky, D., Landau, B. M. et al. (2016). A Rupelian mangrove swamp mollusc fauna from the Thrace Basin in Turkey, *Archiv für Molluskenkunde, 145* (1), 23-58.

Howard, W. (1997). Awarm future in the past. *Nature, 388*, 418– 419.

Inaner, H., Nakoman, E., & Karayiğit, A. I. (2008). Coal resource estimation in the Bayir Field, Yatağan–Muğla, SW Turkey; *Energy Sources, 30*, 1000-1015.

Iso Anaytical Laboratory Report, Retrived, March, 26, 2015, Carbonate isotope analysis, reference no: 150227-2. http://www.iso-analytical.co.uk/quality.html

İşintek, İ., Turhan, E., & Erdoğan, B. (2007). Killik düzeyi traverten tipi karbonatlarının (Denizli- Kaklık, Batı Türkiye) fasiyes özellikleri ve yapıtası üretimiyle ilişkisi. 61. *Türkiye Jeoloji Kurultayı Bildiri Özleri*, 303-304.

Karayiğit, A.İ., Akgün, F., Gayer, R. A., & Temel, A. (1999). Quality, Palynology, and palaeoenvironmental interpretation of the Ilgin lignite, Turkey. *International Journal of Coal Geology, 38*, 219-236.

Kayseri, M. S. & Akgün, F. (2008). Palynostratigraphic, Palaeovegetational and Palaeoclimatic Investigations on the Miocene Deposits in Central Anatolia (Çorum Region and Sivas Basin). *Turkish Journal of Earth Sciences, 17*, 361-403.

Kayseri, M. S. (2010). *Oligo-Miocene palynology, palaeobotany, vertebrate, marine faunas, palaeoclimatology and palaeovegetation of the Ören Basin (North of the Gökova Gulf), Western Anatolia*. PhD Thesis, Dokuz Eylül University, İzmir.

Kayseri-Özer, M. S. (2014). Spatial distribution of climatic conditions from the Middle Eocene to Late Miocene based on palynoflora in Central, Eastern and Western Anatolia. *Geodinamica Acta, 26* (1-2), 122-157.

Kayseri-Özer, M. S, Akgün F, Mayda S, & Kaya T (2014). Palynofloras and vertebrates from Muğla-Ören region (SW Turkey) and palaeoclimate of the Middle Burdigalian–Langhian period in Turkey. *Bulletin of Geosciences, 89*, 137–162.

Koçyiğit, A. (1984). Güneybatı Türkiye ve yakın dolayında levha içi yeni tektonik gelişim. *Türkiye Jeoloji Kurumu Bülteni, 27*, 1-17.

Konak, N., Akdeniz, N., & Öztürk, E. N. (1987). Geology of the South of Menderes Massif. IGCP Proj. 5: Guide Book field excursion Western Anatolia, Turkey. *Mineral Research and Exploration Institute of Turkey Publication*, 42-53.

Last, W. M. (1990). Lacustrine dolomite – an overview of modern, Holocene, and Pleistocene occurences. *Earth-Science Reviews, 27*, 221-263.

Leng, M. J, & Marshall, J. D. (2004). Palaeoclimate interpretation of stable isotope data from lake sediment archives. *Quaternary Science Reviews, 23*, 811-831.

Leng M. J., Lamb, A. L., Heaton, T. H. E., Marshall, J. D., Wolfe, B. B., Jones, M. D. et al. (2005). Isotopes in lake sediments. In M. J. Leng, (Ed). *Isotopes in paleoenvironmental research* (147-184). Netherlands: Springer.

Li, H. C., & Ku, T. L. (1997). $\delta^{13}C$-$\delta^{18}O$ covariance as a paleohydrological indicator for closed-basin lakes. *Palaeogeography, Palaeoclimatology, Palaeoecology, 133*, 69-80.

Loutre, M. F. & Berger, A. (2003) Marine Isotope Stage 11 as an analogue for the present interglacial. *Global and Planetary Change, 36*, 209-217

Ludwig, K.R, & Paces, J. B. (2002). Uranium-series dating of pedogenic silica and carbonate, Crater Flat, Nevada. *Geochimica et Cosmochimica Acta, 66* (3), 487-506.

Ludwig, K.R. (2012). User's Manual for Isoplot 3.75, a Geochronological Toolkit for Microsoft Excel, *Berkeley Geochronology Center Special Publication, 5*, 1-72.

Maldonado, E., Mazo, A.V., & Alferez, F. (1983). Los mastodontes (Proboscidea, Mammalia) del Orleaniense medio de Corcoles (Guadalajara). *Estudios Geologicos (Madrid), 39* (5-6), 431-449.

Markov G. N. & Vergiev, S. (2010). First report of cf. Protanancus (Mammalia, Proboscidea, Amebelodontidae) from Europe. *Geodiversitas, 32* (3), 493-500.

Matheron, P. (1843). Catalogue méthodique et descriptif des corps organisés fossiles du département des Bouches-du-Rhône et lieux circonvoisins précedé d'un Mémoire sur les terrains supérieurs au grès bigarré du S.E. de la France: *Répertoire des travaux de la Société de Statistique de Marseille, 6*, 81-341.

Matzke-Karasz R. & Witt, W. (2005). Ostracods of the Paratethyan Neogene Kılıç and Yalakdere formations near Yalova (İzmit Province, Turkey). *Zitteliana, A* (45), 115-133.

Mikuz, V. & Pavsic, J. (2000). Brotia (Tinnyea) escheri (Brongniart) iz miocenskih plastipiri tunjicah (Brotia (Tinnyea) escheri (Brongniart) from Miocene beds at Tunjice, Central Slovenia), *Geologija, 43* (1), 43-53.

Mazo, A. V (1977). *Revision de los mastodontes de España*. PhD Thesis, Universidad Complutense; Madrid.

Mazo, A.V. (1996). Gomphotheres and Mammutids from the Iberian Peninsula. In Shoshani, J, Tassy, P (eds.): *The Proboscidea. Evolution and Palaeoecology of Elephants and Their Relatives* (2nd edition, 1997) (136-142). New York: Oxford University.

Morkhoven van, F. P. C. M. (1963). Post-paleozoic Ostracoda. Their Morphology. Taxonomy and Economic Use. *Elsevier Publishing Company, Amsterdam* (2), 478.

Nakoman, E (1966). Palynological Contribution of Tertiary formations in the Thrace Basin. I. *Qualitative Study. Annales de la Société Géologique du Nord, 86*, 65-107.

Nakoman E (1978). Linyit içeren Soma Neojen bölgesi. Batı Anadolu. *Maden Tetkik Arama Enstitüsü Dergisi, 90*, 20-70.

Nakoman, E. & İnaner, H. (1996). Turgut Bayır ve Karacahisar Linyit Sektörlerinin Ekonomik Jeoloji Yönünden Değerlendirilmesi, Scientific Project, No: 0908-95-06-04, Dokuz Eylül University, İzmir, 107.

Nebert, K. (1956). Denizli–Acıgöl merkezinin Jeolojisi, 1/100.000 ölçekli Denizli 105/1, 105/2 ve Isparta 106/1 paftalarının sahası içinde yapılan jeolojik harita

çalışmaları hakkında rapor. *Mineral Research and Exploration Institute (MTA)*, Report No: 2509.

Ocakoğlu F., Açıkalın, S., Özsayın, E., & Dirik, R. K. (2014). Tectonosedimentary evolution of the Karacasu and Bozdoğan basins in the Central Menderes Massif, W Anatolia. *Turkish Journal of Earth Sciences, 23*, 361-385.

Okay, A. I. (2001). Stratigraphic and metamorphic inversions in the central Menderes Massif: a new structural model. *International Journal of Earth Sciences, 89*, 709-727.

Önay, T.Ş. (1949). Über die Smirgelgesteine Südwest-Anatoliens. *Schweizerische Mineralogische und Petrographische Mitteilungen, 29*, 357-491.

Özcan, E., Less, G., Beke-Baldi, M., Kollanyi, K., & Acar, F. (2009). Oligo-Miocene foraminiferal record (Miogypsinidae, Lepidocyclinidae and Nummulitidae) from the Western Taurides (SW Turkey): Biometry and implications for the regional geology. *Journal of Asian Earth Science, 34* (2009), 740-760.

Özer, S. & Sözbilir, H. (2003). Presence and tectonic significance of Cretaceous rudist species in the so-called Permo-Carboniferous Göktepe Formation, central Menderes Massif, western Turkey. *International Journal of Earth Sciences, 92*, 397-404.

Pedley, M., Andrews, J., Ordonez, S., Garcia del Cura, M. A., Martin, J. A. G., & Taylor, D. (1996). Does climate control the morphological fabric of freshwater carbonates? A comparative study of Holocene barrage tufas from Spain and Britain. *Paleogeography, Paleoclimatology, Paleoecology, 121*, 239-257.

Pentecost, A. (2005). *Travertine*. Netherlands: Springer.

Pickford, M., & Ertürk, C. (1979). Suidae and Tayassuidae from Turkey. *Bulletin of the Geological Society of Turkey, 22*, 141-154.

Pickford, M. (2001). Intérêt biochronologique des Kubanochoerinae (Mammalia, Suidae) et étude de nouveaux restes de Megalochoerus khinzikebirus et

Libycochoerus massai du Kenya. *Comptes Rendus de l'Académie des Sciences, Series IIA 332,* 193-200.

Pickford, M. & Morales, J. (2003). New Listriodontinae (Mammalia, Suidae) from Europe and a review of listriodont evolution, biostratigraphy and biogeography. *Geodiversitas, 25* (2), 347-404.

Plaziat, J. C., Cavagnetto, C., Koeniguer, J. C., & Baltzer, F. (2001). History and biogeography of the mangrove ecosystem, based on a critical reassessment of the paleontological record. *Wetlands Ecology and Management, 9*, 161-179.

Querol, X., Alastuey, A., Plana, F., Lopez-Soler, A., Tuncali, E. Toprak, S. et al. (1999). Coal geology and coal quality of the Miocene Mugla Basin, southwestern Anatolia, Turkey. *International Journal of Coal Geology, 41*, 311–332.

Riegel, W., Bode, T., Hammer, J., Hammer-Schiemann, G., Lenz, O., & V. Wilde. (1999). The Palaeoecology of the Lower and Middle Eocene at Helmstedt, Northern Germany-A Study in Contrasts. *Acta Palaeobotanica Supplement, 2*, 349-358.

Ring, U., Johnson, C., Hetzel, R., & Gessner, K. (2003). Tectonic denudation of a Late Cretaceous-Tertiary collisional belt-regionally symmetric cooling patterns and their relation to extensional faults in the Anatolide belt of western Turkey. *Geological Magazine, 140*, 1-21.

Roberts, N., Jones, M. D., Benkaddour, A., Eastwood, W. J., Filippi, M. L., Frogley, M. R. et al. (2008). Stable isotope records of Late Quaternary climate and hydrology from Mediterranen lakes: the ISOMED synthesis. *Quaternary Sciense Reviews, 27*, 2426-2441.

Sancay, R.H., Batı, Z., Işık, U., Kırıcı, S., & Akça, N. (2006). Palynomorph, foraminifera, and calcareous nanoplankton biostratigraphy of Oligo–Miocene sediments in the Muş Basin, Eastern Anatolia, Turkey. *Turkish Journal of Earth Science, 15*, 259-319.

Saraç, G. (2003). Mammal Fossil Findings in Turkey, General Directorate of the Mineral Research and Exploration Institute (MTA). Scientific Report No: 10609208p.

Seyitoğlu, G., & Scott, B. (1991). Late Cenozoic crustal extension and basin formation in west Turkey. *Geological Magazine, 128,* 155–166.

Seyitoğlu, G., Işık, V., & Çemen, İ. (2004). Complete Tertiary exhumation history of the Menderes Massif, western Turkey: an alternative working hypothesis. *Terra Nova 16,* 358–363.

Seyitoğlu, G., & Işık, V. (2015). Late Cenozoic extensional tectonics in Western Anatolia: exhumation of the Menderes core complex and formation of related basins. *Bulletin of The Mineral Research Exploration, 151*, 47-106.

Sözbilir, H. (2005). Oligo-Miocene extension in the Lycian Orogen: evidence from the Lycian molasse basin, SW Turkey. *Geodinamica Acta, 18,* 255-282.

Şengör, A. M. C. & Yılmaz, Y. (1981). Tethyan evolution of Turkey: A plate tectonic approach. *Tectonophysics, 75,* 181-241.

Talbot, M.R. (1990). A review of the palaeohydrological interpretation of carbon and oxygen isotopic ratios in primary lacustrine carbonates. *Chemical Geology* (Isotope Geoscience Section), 80, 26l-279.

Tassy, P. (1985). *La place des mastodontes miocènes de l'Ancien Monde dans la phylogénie des Proboscidea (Mammalia): hypothèses et conjectures.* Thèse Dr. ès Sc. Mémoires des Sciences de la Terre Université Curie, Paris.

Tassy, P. (2014). L'odontologie de Gomphotherium angustidens (Cuvier, 1817) (Proboscidea, Mammalia): données issues du gisement d'En Péjouan (Miocène moyen du Gers, France*). Geodiversitas, 36* (1), 35-115.

Ten Veen, J. H., Boulton, S. J., & Alçiçek, M.C. (2009). From palaeotectonics to neotectonics in the Neotethys realm: the importance of kinematic decoupling and inherited structural grain in SW Anatolia (Turkey). *Tectonophysics, 473,* 261–281.

Turhan, E. (2007). *Denizli yöresi (Batı Anadolu) traverten tipi karbonatların fasiyes Özellikleri*. Master Thesis, Dokuz Eylül University, İzmir.

Ünal, D. (1988). Geology of Muğla-Milas-Ören-Alatepe Fields; Report No: KÖ 86, Mineral Research and Exploration Institute, MTA.

Van Der Made, J. (1996). Listriodontinae (Suidae, Mammalia), their evolution, systematics and distribution in time and space. *Contributions to Tertiary and Quaternary Geology, 33*, 3-254.

Witt, W. (2003). Freshwater ostracods from Neogene deposits of Develiköy (Manisa Turkey). *Zittelina, A 43*, 93-108.

Yılmaz, Y., Genç¸ S. C., Gürer, O. F., Bozcu, M., Yılmaz, K. Karacık, Z. et al. (2000) When did the western Anatolian grabens begin to develop? In Bozkurt E, Winchester JA, Piper JDA (eds) *Tectonics and Magmatism in Turkey and the Surrounding Area.* Geological Society of London (353-384), Special Publication, 173.

Yılmaz Ö. (2008). *Salihli yöresi traverten yataklarının fasiyes analizi ve ekonomik potansiyeli*. Master Thesis, Dokuz Eylül University, İzmir.

Yılmaz, Ö., İşintek, İ, Kayseri-Özer, M.S., & Güngör, T. (2016). Correlation of microfacies changes and stable isotope values on travertine type carbonates: a case study of Göktepe (Mugla)-Preliminary results. 7. Quaternary Symposium of Turkey, Symposium Proceedings, 154.

Yılmaz, Ö., Güngör, T., Kayseri-Özer, M.S., Akgün, F., Mayda, S., Kaya, T., Nazik, A., & Büyükmeriç, Y. (2020). Stratigraphy of the Mio-Pleistocene sequence in the Göktepe region based on the fossil record (Muğla, SW Turkey). *Turkish Journal of Earth Science, 29*, 501-520.

APPENDICES

APPENDIX-1: The microfacies of Yarilgan Hill section. The numbers in the first column are given to show from top to bottom of the sequence, 1 – 30 (CMF: clotted micrite facies, MMF: microbial micrite facies)

No	Thin Section No	Microfacies
1	216	MMF
2	215	MMF
3	214	MMF
4	213	MMF+PMF
5	211	MMF+PMF
6	210	MMF+PMF
7	209	MMF+PMF
8	208	MMF+PMF
9	207	MMF+PMF
10	206	MMF
11	205	PMF+MF
12	204	MMF+PMF
13	203	PMF+MF
14	202	MMF
15	201	MMF+PMF
16	200	MMF+PMF
17	199	MMF+PMF
18	198	MMF
19	197	MMF
20	196	MMF+PMF
21	195	MMF+PMF
22	194	MMF+PMF
23	193	MMF
24	192	MMF+PMF
25	191	MMF+PMF
26	190	MMF+PMF
27	189	MMF+PMF
28	188	MMF+PMF
29	187	MMF+PMF
30	186	MMF+PMF

APPENDIX-2: The microfacies of Kepez Hill section. The numbers in the first column are given to show from top to bottom of the sequence, 1 to 154 (CMF: clotted micrite facies, MMF: microbial micrite facies, MC-ES: macrophytes encrusted spar, EM: encrusted micrite, MCSQSF: macrophytes spar quill shrub facies, MQFSF: micritic quill feather shrub facies, AMCF: algal microspar-spar clump facies, FCF: fragmented carbonate facies, ZEA: zoned encrusted algal fabrics, ZAC: zoned algal clump fabrics)

No	Thin Section No	Microfacies
1	30	MMF
2	31	CMF
3	32	CMF+MMF
4	33	CMF+MMF
5	34	MMF
6	35	CMF+MMF
7	100	MC-ES+AMKF+MMF
8	99	AMKF-MC-ES+MMF
9	98	MMF
10	97	CMF+MMF
11	96	FCF+MMF+CMF
12	95	FCF+MMF+CMF
13	94-2	CMF+MMF
14	94-1	CMF+MMF
15	93-2	MC-ES+MMF
16	93-1	CMF
17	92	FCF+MMF
18	91	CMF
19	90	CMF
20	89	CMF
21	88	CMF
22	87	CMF
23		MMF
24	86	CMF+MMF
25	85	CMF
		AMCF+CMF
26	84	CMF
27	83	CMF
28	82	CMF
29	81	CMF
30	80-2	CMF+MQFSF
31	80-1	CMF+MQFSF
32	79	CMF
33	78	CMF
		ZAF
34	77	CMF
35	76	MMF+CMF+ZAC

No	Thin Section No	Microfacies
36	75	CMSF
37	74	MC-ES+MMF+CMF
38	73	CMF
39	72	CMF+AMKF
40	67	AMCF+CMF+MMF
		FCF+CMF
41	65	FCF+MMF
		CMF+MMF
42	64	FCF+MMF
		MC-ES+CMF
43	63	FCF+CMF+MMF+AMCF
44	62	CMF
45	61	CMF+AMCF
46	60	CMF+AMCF
47	59	MMF+CMF+AMCF
48	58b	CMF+MMF+AMCF+MC
49	58a	AMCF+MMF+CMF
		MMF
50	57	CMF
51	56	CMF
		MC+MMF
52	55	CMF
53	54	CMF
		MC-ES+MMF
54	53	AMKF+CMF+MMF
		MMF+CMF
55	52	MC-ES+MMF
56	51	MC-ES+MMF
57	50b	MC-ES+AMCF+MMF
58	50a	MCF+AMCF+ MMF
59	49	CMF
60	48	CMF
61	47	MMF+CMF
62	46	MMF+CMF
63	45	MMF+CMF
64	184	CMF
65	183	CMF

APPENDIX-2 continues

No	Thin Section No	Microfacies
66	182	AMCF+MMF+CMF
67	181	AMCF+MC-ES+MMF
68	180	AMCF+MMF+CMF
69	179	AMCF+CMF
70	178	AMCF+MMF+CMF
71	177	AMCF+MMF+CMF
72	176	AMCF+MMF+CMF
73	175	MCF+CMF
74	174	AMCF+CMF
75	173	AMCF+CMF+FCF
76	172	AMCF+MMF+CMF
77	171	AMCF+PMF
		CMF+MCMS
78	170	MC-ES+CMF+MMF
79	169	MC-ES+CMF+MMF
80	168	MC-ES+CMF+MMF
81	167	MC-ES+CMF+MMF
82	166	AMKF+CMF+MMF
83	165	MC-ES+MMF
84	164	CMF
85	163	CMF
86	162	CMF
87	161	CMF
88	160	CMF
89	159	CMSF
90	158	CMF
91	157	CMSF
92	156	CMF
93	155	MMF
94	154	MMF
95	153	CMSF
96	152	CMF
97	151	CMF
98	150	CMF
99	149	MMF+CMF
100	148	CMF
		MMF+CMF+MC-ES
101	147	MC-ES
		FCF+MMF
102	146	CMF+FCF
103	145	CMF
104	144	FCF+CMF
105	143	FCF
106	142-2	CMF
107	142-1	CMF
108	141	MMF+CMF

No	Thin Section No	Microfacies
109	140	CMF
110	139	CMF
111	138	MC-ES
		CMF
112	137	CMF+ZAC
113	136	MC-ES+CMF
114	135-2	CMSF+es
115	135-1	CMF
116	134	CMF
117	133	CMF+CMF
118	132	MMF+ZAC+FCF
		MC-ES+MMF
119	131	CMF
		MQFSF
		CMF
120	130	CMF+ZAC+CMSF
121	129	MC-ES
		FCF+CMF+ZAC
122	128	ASCF+MMF+ZAC
123	127	CMF+MMF+MC-ES
124	126	MC-ES +CMF+MMF
125	124	MMF
		FCF+CMF
126	125	AMCF
		CMF
127	123	CMSF
128	122c	CMF+MC-EM
129	122b	CMF
130	122a	CMF+MMF+ZAC
131	121b	CMF
		MQFSF
		CMF
132	121a	CMF
133	120-2	MMF+CMF
		QFSF
		MMF+CMF
134	120-1	CMF
135	119	MCSQSF
136	118b	CMF
137	118a	CMF
138	117b	CMF
139	117a	CMF
140	116b	ZAC+MMF+CMF
141	116a	MMF+CMF+ZAC
142	115	CMF+MMF
		MC-EM+MMF

APPENDIX-2 continues

No	Thin Section No	Microfacies
143	114	AMCF+MMF+CMF
		CMF
144	113	MC-MM+MMF
145	111	MMF+MC-ES+MC-MM
146	110	CMF+MMF+MC-ES
147	109	CMF+MC-ES
148	108	CMF+MC-ES
149	107	CMF+MMF+Thin MC
150	106-2	MC-MM+CMSF
151	106-1	MMF+MC-EM
152	105	MC-MM+CMF+MMF
153	104	MC-MM+MMF
154	103	CMSF+MC-MM+ES

APPENDIX-3: Cross-Sections

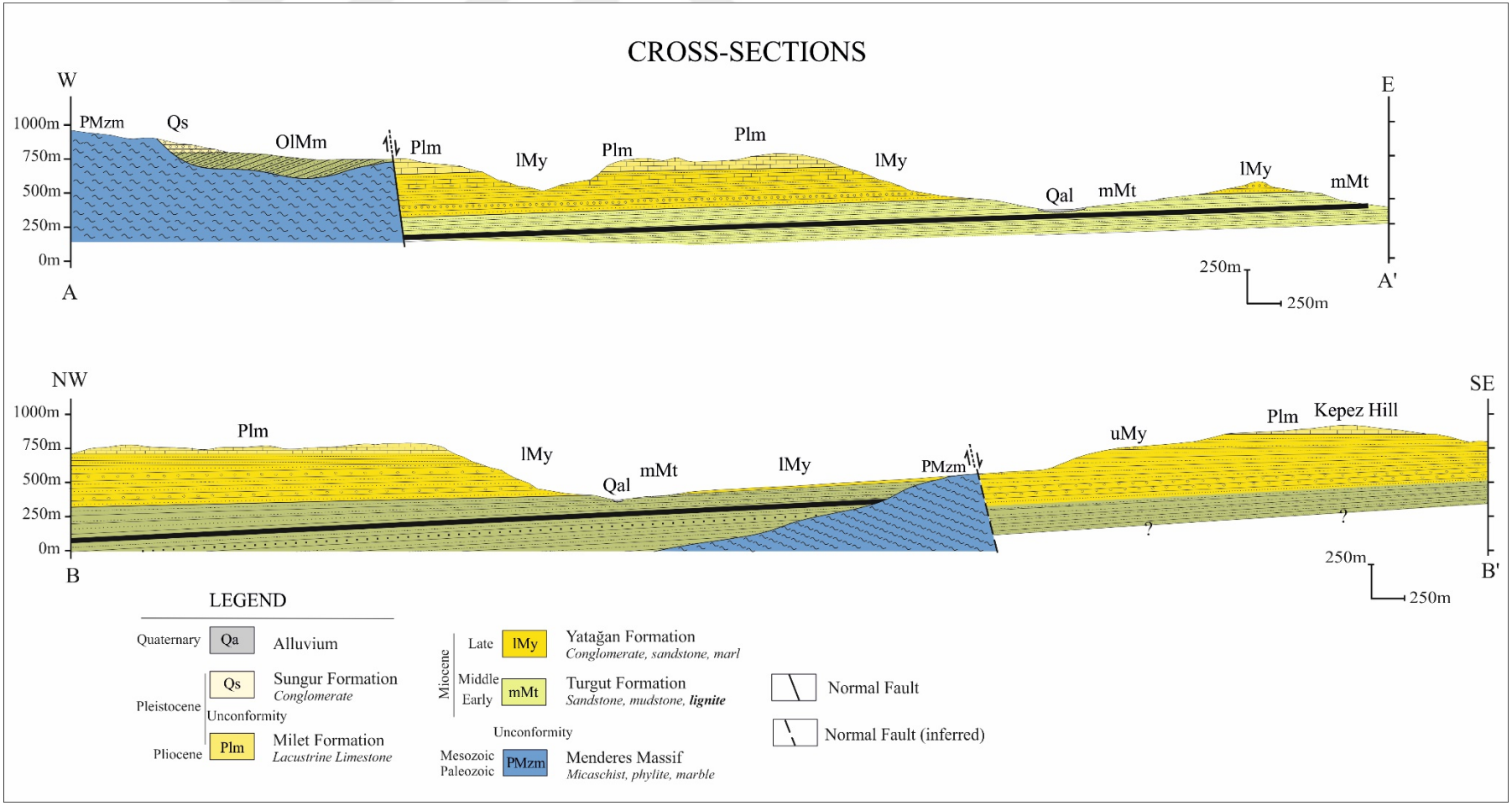


Figure A.1 Cross-Sections